Session V

Measurements of nuclear data

Chairs: Nicolae Marginean, Yosef Eisen

Systematic study of activation cross-sections of deuteron induced reactions used in accelerator applications

F. Tarkanyi,[1] **A. Hermanne,**[2] **F. Ditroi,**[1] **S. Takacs,**[1] **B. Kiraly,**[1] **J. Csikai,**[1]
M. Baba,[3] **H. Yamazaki,**[3] **M.S. Uddin,**[3] **A.V. Ignatyuk,**[4] **S.M. Qaim**[5]
[1]Institute of Nuclear Research of the Hungarian Academy of Sciences (ATOMKI), Debrecen, Hungary
[2]Vrije Universiteit Brussel (VUB), Brussels, Belgium
[3]Cyclotron and Radioisotope Center (CYRIC), Tohoku University, Sendai, Japan
[4]Institute of Physics and Power Engineering (IPPE), Obninsk, Russian Federation
[5]Institut fur Nuklearchemie, Forschungszentrum Julich, Julich, Germany

Abstract

Integral excitation functions for the production of residual nuclides through light charged particle activation constitute basic data for various applications. Nowadays, deuteron induced reactions start to play an important role as the stripping process generates high production yields and the stopping power for deuterons is relatively low.

Some years ago, to meet requirements of practical applications, we started to establish an experimental activation database by performing new experiments and a systematic survey of existing data of deuteron induced cross-sections up to 50 MeV. Today, this study involves around five hundred reactions taking place on the following 40 target elements: B, N, Ne, Al, Sc, Ti, V, Cr, Mn, Fe, Co, Ni, Cu, Zn, Kr, Y, Zr, Nb, Mo, Rh, Pd, Ag, Cd, In, Sn, Te, Xe, La, Ce, Pr, Nd, Ho, Er, Tm, Yb, Lu, Hf, Ta, W, Re, Os, Ir, Pt, Au, Tl, Pb.

The measured excitation functions are compared with experimental data found in the literature and with the results of the nuclear reaction model codes ALICE-IPPE, EMPIRE-II, GNASH, PHITS and TALYS (from the TENDL-2009 and EAF-2007 data libraries). These comparisons can show the present predictivity of the codes and contribute to their development e.g. in used potentials, reaction parameters, reaction mechanism and phenomenological corrections, resulting in better description of for instance (d,p) and (d,2n) reactions.

Introduction

It is essential to prepare a deuteron-induced activation cross-section database for various applications:

- Accelerator and target technology to produce high-energy, high-intensity neutron fluxes for nuclear waste transmutation (ADS);
- Intensive neutron sources (SNS, ESS, EVADA/IFMIF, ARC neutron activators);
- Radioactive ion beam (RIB) production with neutrons (EURISOL, RIA, SPIRAL-2, etc.);
- Future controlled fusion experiments and reactors (ITER, DEMO, etc.);
- Space applications (resistance of electronics, shielding, etc.);
- Intensive deuteron beams play an important role in the field of medical radioisotope production as well. High yields of some radioisotopes can be produced only with deuterons (^{15}O, ^{57}Co, etc.);
- The (d,2n) reaction is more productive than the (p,n) reaction on the same target material (^{186}Re, ^{103}Pd, etc.) in case of some important medium- and high-Z radioisotopes;
- When irradiating with an accelerator, not only the target itself but its backing, covering layer or holder and accelerator parts (gases, transport tubes, energy degraders and collimators, target windows, window supports and grids) is bombarded.

Unlike proton induced reactions, the status of the experimental data for deuteron induced reactions is rather poor, especially above 15-20 MeV: no systematic study has been performed earlier, the published data show large discrepancies (except for a few monitor and medically important reactions), the values collected in the EXFOR database are incomplete and contain mistakes. Confirmation of excitation functions by experimental assessment of integral yield or other benchmarks is also missing. Moreover, the reliability of presently used theoretical codes for deuteron induced reactions is low, compared to proton and alpha particle induced reactions, due to the modelling problems of the deuteron stripping and pickup.

With the aim of generating a recommended database, the IAEA launched several Coordinated Research Projects with our participation, including deuteron induced reactions, by performing a systematic compilation and evaluation of literature, by gathering experimental data from new measurements and by a comparison with different theoretical codes.

The subsequent CRP's concerned:

- Thin layer activation method and its applications in industry (1992-1996);
- Charged particle cross-section database for medical radioisotope production: Diagnostic radioisotopes and monitor reactions (1995-1999);
- Cross-section database for medical radioisotope production: Production of therapeutic radionuclides (2003-2007);
- Nuclear Data Libraries for Advanced Systems: Fusion Devices: Fusion Evaluated Nuclear Data Library FENDL 3.0 (2008-2011).

In the frame of the above mentioned projects, for the everyday applications in the participating institutes and for basic research, we performed a systematic experimental study on deuteron induced reaction cross-sections for a large variety of elements during the last two decades.

We present here the used methods and some examples of the results, the status of the investigations and future plans.

Earlier investigations

As it was mentioned in the introduction, the activation cross-section database of deuteron induced nuclear reactions is very scarce, especially when compared to that of proton induced reactions.

The available data were gathered in four types of experiments:

- At era of low energy nuclear physics, measurements were done mostly on elements having only one stable isotope to investigate basic nuclear reaction mechanisms. The effect of the secondary neutrons was neglected. Only very few cross-section measurements used solid state detectors for spectrum analysis; some of them are obviously erroneous.
- A more systematic study on thick (and thin) target yields for many targets was done up to/at 22 MeV at IPPE (in Obninsk) for practical applications.
- Recently, some groups (from Japan and Czech Republic) made a few irradiations specifically for accelerator technology (focused on IFMIF).
- By recognizing the importance of deuterons in medical radioisotope production, new data were measured on some highly enriched targets.

In these studies, only very few data were reported above 20 MeV deuteron energy but fortunately, as exception, reliable experimental data were measured in Julich, Karlsruhe and Kiev on some metallic targets with higher energy beam.

Experimental method

Here we present the most important features of the experimental techniques used in our investigations in the last 20 years.

The standard single target or stacked target irradiation method was used to measure cross-sections [1]. Solid targets or gas cells were stacked with interleaved beam monitor foils. The target stacks were inserted into a Faraday-cup like target holder, equipped with a collimator and secondary electron suppressor. The monitor foils were used as recoil catchers as well as for exact determination of beam intensity and energy by re-measuring the well known excitation function of the monitor reaction in the covered energy range.

Most of the metal targets were commercially available high purity foils; other targets were prepared by electro-deposition, vacuum-deposition, pressing or sedimentation from natural or enriched metals or oxides; high purity gases were filled in gascells. The irradiation setups are shown in Figure 1a and 1b.

Figure 1: Irradiation setup; stacked foils (a) and stacked gas cells (b)

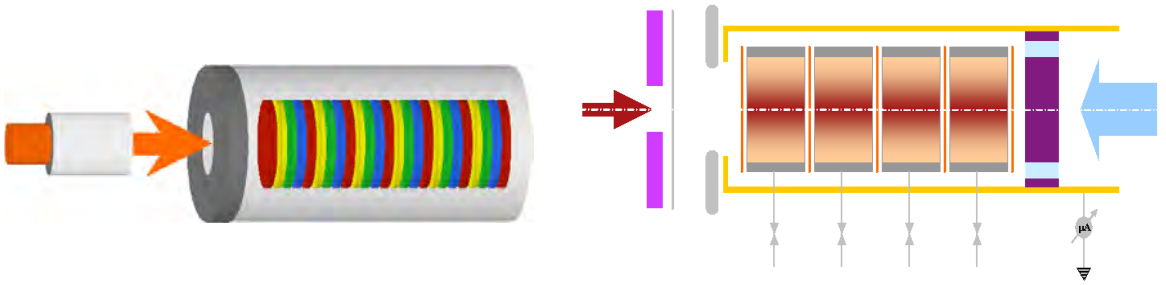

The irradiations were performed using external beams of the cyclotrons given in Table 1, at low beam intensity to avoid target damage (outgassing, evaporation, melting). Typical irradiation intensities varied between 30-200 nA. The irradiation time was chosen between 3-120 min depending on the half life of the investigated radionuclide. As in most cases short- and long-lived activation products are produced simultaneously, a compromise has to be reached.

Data acquisition started shortly after end of bombardment in case of low energy irradiations (below 20 MeV) while in case of high energy irradiations a cooling time of at least 3-4 h was introduced because of the high activity induced and/or the transport from the irradiation place to the detector. Spectra were measured by means of standard or extended-range HPGe detectors (γ-ray or X- and low energy γ-ray, respectively) and Si surface barrier detectors (α-particles).

Table 1: Accelerators used in our experiments

Accelerator	k-value	Laboratory, City	Beam
Cyclone	110	UCL, Louvain La Neuve (BE)	p, d, ^{3}He, α, HI
AVF	110	CYRIC, Sendai (JP)	p,d, ^{3}He, α, HI
CGR 560	40	VUB, Brussels (BE)	p, d, α
CV 28 JULIC	28 45	FZ Julich, Julich (DE)	p, d, ^{3}He, α
MGC 20	20	Abo Akademi, Turku (FI)	p, d, ^{3}He, α
MGC 20	20	ATOMKI, Debrecen (HU)	p, d, ^{3}He, α

In most cases, no chemical separation was done, except for investigations of a dedicated medical radioisotope production route. The measurements were repeated several times for months, allowing more accurate determination of long lived activation products as well. Suitable large detector-sample distances (5-70 cm) guaranteed low dead times and no pile-up effects. For activities derived from X-ray or low energy γ-ray measurements, a correction for self-absorption in the metal foils was applied. As the gamma spectra were very complex, an interactive spectrum analysis and iterative data evaluation (corrections for contribution of contaminating signals) were used to separate and identify different activation products. In case of any contradiction, the spectrum unfolding and the data evaluation were repeated, taking into account systematic trends, parent-daughter relationships, etc.

Difficulties and drawbacks of the used experimental method

- Too ambitious program: large number of targets and wide energy range in one irradiation. In many cases, no dedicated activation product is looked for (except for medical applications, TLA and monitor).
- Cumulative effects due to the stacked target technique: uncertainties in energy degradation and particle number throughout the stack.
- High activities at end of bombardment, delayed start of gamma spectra measurement, hence lost of the shorter lived isotopes.
- Numerous targets and limited detector capacity: lost of information on the short and very long lived isotopes. Problem with following the cumulative effects and with measuring the decay curve. In some cases poor statistics.
- Various targets (having different thicknesses) are stacked together and various reactions take place. It is difficult to use the available beam time optimally and to optimize the irradiation parameters.

Data processing

In case of a monoisotopic (or enriched) target, so called isotopic cross-sections were determined; in case of target elements with natural isotopic composition, so called elemental cross-sections were deduced considering as if the target were monoisotopic. The cross-sections were calculated from the well known activation formula using measured activity, particle beam and number of target nuclei as input parameters. In some cases, cumulative processes occur *i.e.* decay of metastable states or decay of parent nuclides contribute to the production of the given radioisotope. The decay characteristics were taken from the NuDat database [2].

The number of incident particles was initially derived from the total charge on target, measured by a Faraday cup-like target holder using a digital integrator. The incident beam energy was determined from the accelerator settings; the mean energy in each foil was calculated by means of the polynomial approximation of Andersen and Ziegler [3] or with the help of the SRIM code [4].

The beam energy and intensity were further adapted by comparing the excitation function of monitor reactions re-measured over the whole energy region studied with the recommended values given in IAEA-TECDOC-1211 or its updated version [5] (Figure 2). Depending on the irradiation energy and on the stack composition, the monitor reactions may be as follows: ^{27}Al(d,x)^{22,24}Na, ^{nat}Ti(d,x)^{48}V,

$^{nat}Fe(d,x)^{56,57}Co$, $^{nat}Cu(d,x)^{62,63,65}Zn$, $^{nat}Ni(d,x)^{61}Cu$. After monitoring, the incident energy on the first foil was usually confirmed, *i.e.* it was equal to that determined from the accelerator settings with uncertainty of ±0.3 MeV. Taking into account the cumulative effects on variation of possible incident energy and target thicknesses, the uncertainty on the median energy in the last foil of a stack may reach ±0.8-1.5 MeV.

Figure 2: Example of a recommended monitor reaction and the adjusted re-measured values (series 1-4)

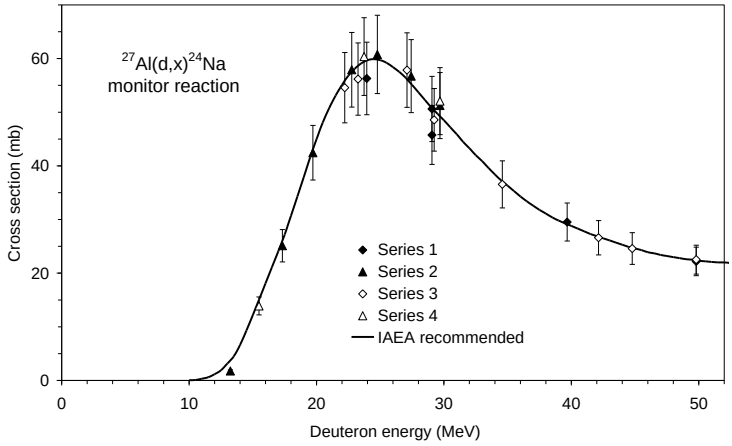

The cross-section uncertainties were estimated in the standard way [6]: by taking the square root of the sum in quadrature of all individual linear contributions, supposing equal sensitivities for the parameters appearing in the formula. The following uncertainties were taken into account in the propagated error calculation: intensity of the detected radiation (4-20%), peak area determination including statistical errors (mostly <5%), number of target nuclei including non-uniformity (5%), detector efficiency (10%) and incident particle intensity (7%). Typical cross-section uncertainties were evaluated to be approximately 11-14%. The strongly non-linear (exponential) effect of half life and time was not taken into account.

Experimental results

The overview of the target materials studied and the related publications or status of the evaluation is given in Table 2.

Table 2: Overview of our work

Target	E (MeV)	Application			Reference (journal, volume, year, page)
		Medical	Monitor	TLA	
^{nat}B	10			^{7}Be	NIMB 103 (1995) 389
^{nat}N	15	^{15}O, ^{13}N, ^{11}C			RA 80 (1998) 59
^{nat}Ne	8.6	^{18}F			IPS 59 (1997) 1707
^{27}Al	50		$^{22,24}Na$		NIMB 174 (2001) 235
^{45}Sc	50	^{44g}Sc		^{46}Sc	measured, data evaluation in progress
^{nat}Ti	50		^{48}V	^{48}V	ARI 48 (1997) 657 NIMB 161-163 (2000) 178 NIMB 174 (2001) 235 NIMB 262 (2007) 7
^{nat}V	40	^{51}Cr		^{51}Cr	submitted
^{nat}Cr	50	^{52m}Mn		^{54}Mn	measured, data evaluation in progress
^{55}Mn	40			^{54}Mn, ^{51}Cr	measured, data evaluation in progress

Table 2: Overview of our work *(continued)*

Target	E (MeV)	Application			Reference (journal, volume, year, page)
		Medical	Monitor	TLA	
^{nat}Fe	50	^{52,54}Mn, ^{51}Cr	^{56,57}Co	^{57}Co	AIP 392 (1997) 659 NIMB 161-163 (2000) 178 NIMB 174 (2001) 235 NIMB 267 (2009) 15
^{59}Co	40			^{60}Co	NIMB 268 (2010) 17
^{64,nat}Ni	50	^{60,61,64}Cu, ^{52}Mn, ^{51}Cr	^{61}Cu	^{56,57}Co	IPS 59 (1997) 1262 RA 76 (1997) 15 IPS 59 (1997) 1262 NIMB 174 (2001) 235 IRRMA-6 (2005) NIMB 258 (2007) 308 Proc. ND2007 (2008) 1354
^{nat}Cu	50	^{64}Cu	^{65}Cu	^{65}Cu	AIP 392 (1997) 659 NIMB 174 (2001) 235 IRRMA-6 (2005) NIMB 251 (2006) 56 NIMB 260 (2007) 495
^{nat}Zn	50	^{66,67}Ga, ^{61,64,67}Cu		^{65}Zn	NIMB 217 (2004) 531
^{78,80,nat}Kr	13	^{81}Rb/^{81}Kr generator			RA 88 (2000) 135 RA 92 (2004) 203
^{89}Y	40	^{88}Y		^{88}Zr, ^{88}Y	AIP 769 (2005) 1658 Proc. ARCEBS 06 (2006) 69 RA 95 (2007) 187
^{nat}Zr	50	^{88}Y		^{91m,92m,95}Nb, ^{95}Zr	NIMB 217 (2004) 373 AIP 769 (2005) 1658
^{93}Nb	40			^{93}Mo	NIMB 161 (2000) 172 JLCR 255 (2007) 297
^{nat,100}Mo	50	^{94}Tc, ^{99}Mo, ^{99m}Tc	^{96m}Tc	^{95m,95g}Tc	IPS 59 (1997) 1637 AIP 475 (1999) 987 AIP 769 (2005) 1658 Proc. ND2007 (2008)1354 Proc. ENC 2010 ARI (2010) in print
^{103}Rh	21	^{103}Pd		^{102g}Rh	NIMB 187 (2002) 3 JNST Suppl. 2 (2002) 1286 ARI 67 (2009) 1574
^{nat}Pd	40	^{104,110,111}Ag		^{105mg}Ag, ^{110,111}Ag	RA 92 (2004) 215 NIMB 217 (2004) 193 Ann. Univ. Turkuensis Ser. D 499 (2002) 14
^{nat}Ag	40	^{110}Ag		^{110m}Ag, ^{109}Cd	ARI 64 (2006) 1013
^{nat,114,116}Cd	40	^{110,111,114m}In		^{114m}In	AIP 769 (2005) 1662 RA 93 (2005) 561 NIMB 259 (2007) 817
^{nat}In	40	^{113}Sn/^{113m}In generator		^{113}Sn	ARI (2010) in print
^{nat}Sn	40	^{119}Sb		^{120,124}Sb, ^{117m}Sn	AIP 769 (2005) 1662 will be submitted
^{122,123}Te	20	^{123,124}I			ARI 48 (1997) 267 ARI 50 (1999) 535
^{nat}Xe	44	^{123,124}I			RA 47 (1989) 25 RA 47 (1989) 169
^{nat}La	50	^{139}Ce			measured, data evaluation in progress
^{nat}Ce	50	^{141}Ce			measured, data evaluation in progress

Table 2: Overview of our work *(continued)*

Target	E (MeV)	Application			Reference (journal, volume, year, page)
		Medical	Monitor	TLA	
^{141}Pr	40	^{140}Nd/^{140}Pr, ^{139m}Nd/^{139}Pr generator			JLCR Suppl. 50 (2007) 102 NIMB 267 (2009) 727
^{nat}Nd	40	^{140}Nd/^{140}Pr generator			measured, data evaluation in progress
^{nat}Gd	50	^{161}Tb			measured, data evaluation in progress
^{159}Tb	50	^{157}Dy			measured, data evaluation in progress
^{165}Ho	40	^{165}Er			JLCR Suppl. 50 (2007) 99 NIMB 266 (2008) 3529
^{167,nat}Er	40	^{167,170}Tm			JLCR Suppl. 50 (2007) 487 NIMB 259 (2007) 829
^{169}Tm	40	^{169}Yb			ARI 65 (2007) 663 JLCR Suppl. 50 (2007) 99 NIMB 267 (2009) 727 ARI (2010) in print
^{nat}Yb	40	^{177g}Lu, ^{167}Tm			NIMB 247 (2006) 223 Proc. ND2007 (2008)1354
^{nat}Lu	50	^{169}Yb			
^{nat}Hf	50	^{177g}Lu			NIMB (2010) in print
^{nat}Ta	40			^{182g}Ta	NIMB 267 (2009) 19:3293
^{nat}W	50	^{186}Re		^{183,184m,184g}Re	JLRC Suppl. 42 (1998) 912 Proc. 6th ILC (1997) 761 NIMB 211 (2003) 319
^{nat}Re	40	^{186}Re		^{185}Os	measured, data evaluation in progress
^{192,nat}Os	50	^{192}Ir, ^{186}Re		^{189,190,192}Ir	ARI 65 (2007) 1215
^{nat}Ir	40	^{191,193m,195m}Pt, ^{192g}Ir		^{190,192}Ir	5ICI Brussels (2005) NIMB 247 (2006) 210
^{nat}Pt	40	^{198,199}Au, ^{191,195m}Pt, ^{192}Ir		^{188,191}Pt, ^{192}Ir	NIMB 226 (2004) 490 RA 92 (2004) 223 AIP 769 (2005) 1015 NIMB 243 (2006) 20
^{197}Au	40	^{198g}Au		^{196g,198g}Au	
^{nat}Tl	50	^{201}Tl			Proc. ND2010 in print
^{nat}Pb	40	^{206}Bi		^{205,206}Bi	JRNC 276 (2008) 835

Theoretical calculations

Why model calculations were performed for our investigated reactions?

- To check the predictivity of model codes with a priori calculations.
- To have preliminary knowledge on the behaviour of the excitation functions, before the experiment and during the data evaluation.
- To select among contradicting experimental data found in the literature (energy shifts, significant differences in absolute values).
- To estimate the contributions of reactions taking place on the stable isotopes of the target element and the contributions of decays in case of cumulative processes.
- To estimate radionuclide impurities from residual nuclei having unfavourable decay characteristics (very long half life, no gamma, etc.).
- To prepare recommended curves by adjusting the theoretical result to the experimental data.

- A variety of codes have been developed on the basis of equilibrium and pre-equilibrium reaction mechanisms. These codes have similar physics with different degrees of complexity in input preparation and require different computing times. Some of them are used when detailed properties of nuclear reactions are needed, including population of discrete levels. On the other hand, when the number of open channels is large and it is impossible or very time consuming to provide all the required input data with sufficient accuracy, the advantages of these detailed codes may be reduced.

We have found at the beginning and during long period that in such a case, the faster codes with less effort in input preparation are often more practical choices. The situation, however, is more complex. The used codes also depend significantly on many other factors, like availability of proper expert for using dedicated codes and development of computer technology and the automation of recommended input parameters, which make easier the use of more detailed codes. Therefore, at the beginning, taking into account our aim with model calculations, we have tried to make calculations with the simpler codes in all cases.

Only when more detailed calculation promised the solution, we used more complex codes (isomeric yields, recommended data) to solve the large discrepancy in case of simple code. The calculations have always been carried out without any parameter adjustment to see the general tendencies. In the last decade, we systematically performed detailed calculations by using more sophisticated codes and by comparing the results of the different approaches.

The cross-sections of the investigated reactions were calculated using the pre-compound model codes ALICE-IPPE [7], EMPIRE-II [8], GNASH [9], TALYS [10] and PHITS [11]. The experimental data are also compared with the cross-section data in the TENDL-2009 [12] and the EAF-2007 [13] nuclear reaction data library. In recent years the ALICE-IPPE-D and EMPIRE-II-D versions ALICE-D and EMPIRE-D for simplicity), modified for better description of deuteron induced reactions, were used.

While ALICE-IPPE gives only the total cross-section of the concerned reaction channels, the TALYS and EMPIRE codes permit to calculate a population of different low-lying levels and can thus estimate the isomeric ratios for these levels. Knowledge of isomeric ratios is important for all cases where only a part of the integral reaction cross-section can be measured in the corresponding experiment.

In our previous works, ALICE-IPPE and EMPIRE-II were used successfully for the description of a large amount of reaction cross-sections induced by light charged particles. However, during the recent analyses of the (d,p) reactions on the isotopes ^{114}Cd [14], ^{169}Tm [15], ^{192}Os [16] and some others, we were confronted with a large underestimation of the measured cross-sections.

It is well known that for the (d,p) reactions at low energies, the direct stripping process play a very important role [17] so we tried to estimate a possible contribution of the neutron stripping process on the basis of the standard distorted wave born approximation (DWBA). The simplified DWBA approximation gives a rather reasonable description of the observed cross-sections for the (d,p) reaction only at energies of about 20 MeV. To improve the description of experimental data at lower energies by analyzing more carefully the schemes of neutron single-particle levels, as well as the optical model parameters for the incident deuteron and emitted proton, are in progress.

To achieve now a better description of (d,p) reactions with the theoretical codes, statistical blocks of a phenomenological simulation of direct (d,p) and (d,t) transitions based on the general relations for nucleon transfer reactions in the continuum, considered by Walker [18], were introduced. A phenomenological enhancement factor K in these relations was taken as energy dependent and estimated to describe the whole set of the observed (d,p) cross-sections for medium and heavy nuclei.

By this improvement, in the ALICE- D and EMPIRE- D code versions, the direct (d,p) channel is increased strongly and this is reflected in changes for all other reaction channels. As ALICE-IPPE calculates only the total cross-section, for estimation of isomeric states, isomeric ratios calculated by EMPIRE-D were applied to ALICE-D total cross-sections.

Examples

Some preliminary unpublished results as examples are shown in Figures 3-8 to see the status of the experimental data and the predictivity of the theoretical codes.

Figure 3: Excitation function of $^{nat}V(d,x)^{51}Cr$ reaction

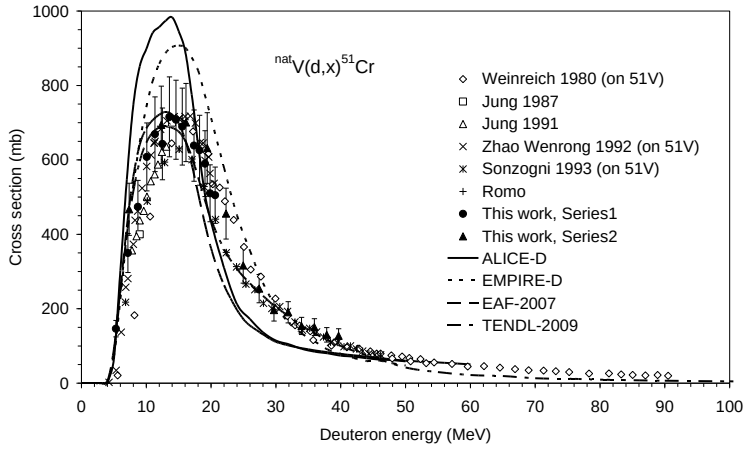

Figure 4: Excitation function of $^{nat}Mo(d,x)^{96}Tc$ reaction

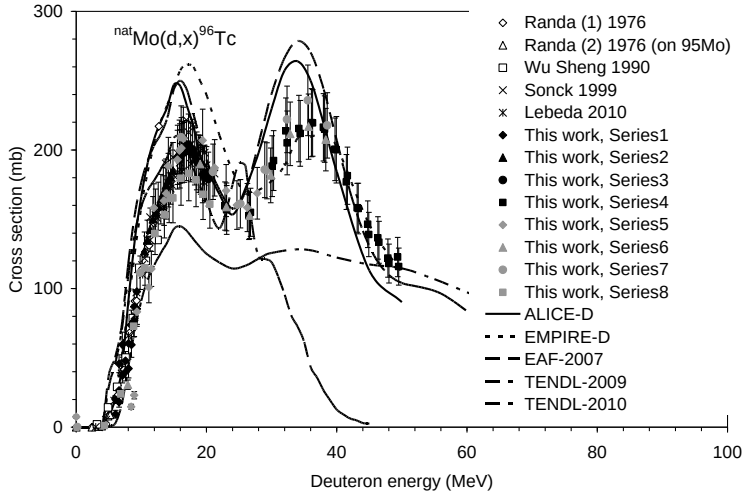

Figure 5: Excitation function of $^{nat}In(d,x)^{113mg}Sn$ reaction

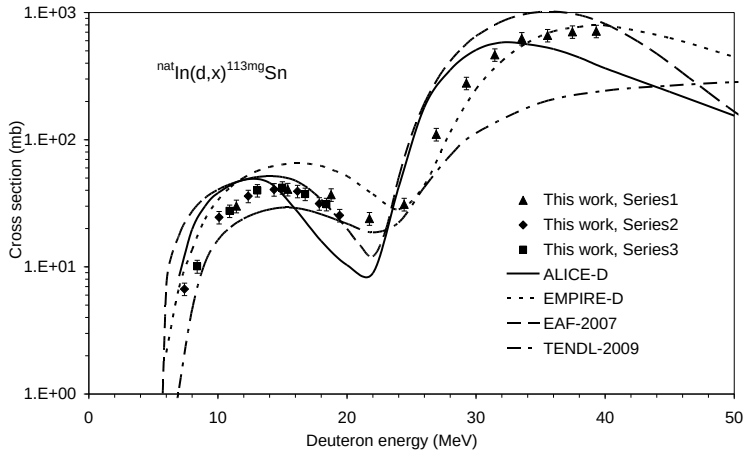

Figure 6: Excitation function of $^{nat}Sn(d,x)^{124}Sb$ reaction

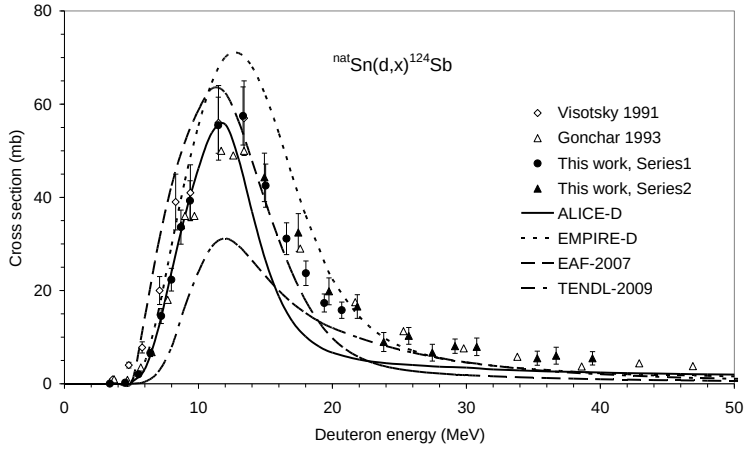

Figure 7: Excitation function of $^{197}Au(d,p)^{198g}Au$ reaction

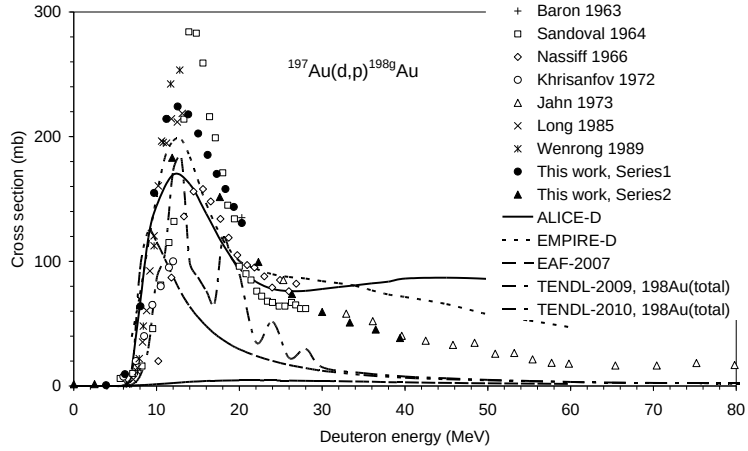

Figure 8: Excitation function of $^{100}Mo(d,x)^{ind99}Mo$ reaction

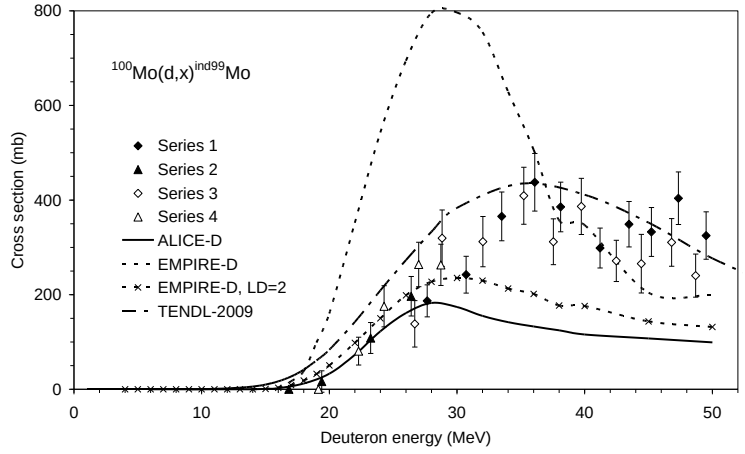

Summary and conclusions

We measured lots of data for applications and for comparison with scared earlier studies and with the results of theoretical models and the activation data libraries. The new experimental data improve the status of the available basic information for dedicated activation data files prepared in various projects at research and nuclear data centres

- to monitor deuteron beam parameters,
- for production of diagnostic and therapeutic radioisotopes,
- for thin layer activation technique,
- for accelerator and target technology.

Arising new tasks and applications as well as improvement of model codes need new measurements.

References

[1] Tarkanyi, F., *et al.*, "Determination of effective bombarding energies and fluxes using improved stacked-foil technique", *Acta Radiologica, Supplementum* 376, 72, (1991).

[2] *NuDat 2.5 database*, Data source: National Nuclear Data Center, Brookhaven National Laboratory, based on ENSDF and the Nuclear Wallet Cards, www.nndc.bnl.gov/nudat2.

[3] Andersen, H.H., J.F. Ziegler, *Hydrogen – Stopping powers and ranges in all elements*, Volume 3 of the Stopping and ranges of ions in matter, Pergamon Press, ISBN 0-08-021605-6, (1977).

[4] Ziegler, J.F., *SRIM-2010*, available from www.srim.org.

[5] Tarkanyi, F., *et al., Beam monitor reactions*, IAEA-TECDOC-1211, Chapter 4, p. 49, IAEA, Vienna (2001).

[6] *Guide to the expression of uncertainty in measurement*, International Organization for Standardization, Geneva, ISBN 92-67-10188-9, (1995).

[7] Dityuk, A.I., *et al., New advanced version of computer code ALICE-IPPE*, Report INDC(CCP)-410, IAEA, Vienna, (1998).

[8] Herman, M., *et al.,* "EMPIRE: Nuclear reaction model code system for data evaluation", *Nuclear Data Sheets* 108, 2655-2715, (2007).

[9] Young, P.G., *et al., Comprehensive Nuclear Model Calculations: Introduction to the Theory and Use of the GNASH Code*, LA-12343-MS, Los Alamos National Laboratory (1992).

[10] Koning, A.J., *et al.,* "TALYS-1.0", *Proceedings of the International Conference on Nuclear Data for Science and Technology (ND2007)*, Nice, France, p. 211-214, (2007).

[11] Iwase, H., *et al.,* "Development of General-Purpose Particle and Heavy Ion Transport Monte Carlo Code", *Journal of Nuclear Science and Technology*, 39, 1142–1151 (2002).

[12] Koning, A.J., D. Rochman, *TENDL-2009: Consistent TALYS-based Evaluated Nuclear Data Library including covariance data*, JEFF Project, JEF/DOC-1310, NEA Data Bank (2009).

[13] Forrest, R.A., J. Kopecky, "EASY-2007: a new generation of activation modelling including neutron-, proton- and deuteron-induced reactions", *Proceedings of the International Conference on Nuclear Data for Science and Technology (ND2007)*, Nice, France, p. 733-736 (2007).

[14] F. Tarkanyi, *et al.*, "Investigation of the production of the therapeutic radioisotope ^{114m}In through proton and deuteron induced nuclear reactions on cadmium", *Radiochimica Acta* 93, 561-569 (2005).

[15] Tarkanyi, F., *et al.*, "Activation cross-sections of the ^{169}Tm(d,2n) reaction for production of the therapeutic radionuclide ^{169}Yb", *Applied Radiation and Isotopes* 65, 663-668 (2007).

[16] Tarkanyi, F., *et al.*, "Study of the ^{192}Os(d,2n) reaction for production of the therapeutic radionuclide ^{192}Ir in no-carrier added form", *Applied Radiation and Isotopes* 65, 1215-1220 (2007).

[17] Satchler, G.R., *Direct Nuclear Reactions*, Clarendon Press, Oxford, (1983).

[18] Kalbach Walker, C., *Users Manual for PRECO-2000: Exciton Model Pre-Equilibrium Code with Direct Reactions*, Duke University, Durham, NC, (2001).

Extension of the calibration of an NE-213 liquid scintillator based pulse height response spectrometer up to 18 MeV neutron energy and leakage spectrum measurements on bismuth at 8 MeV and 18 MeV neutron energies

A. Fenyvesi,[1] **L. Oláh,**[2] **I. Valastyán,**[1] **J. Csikai,**[1,2] **A. Plompen,**[3] **R. Jaime,**[3] **G. Lövestam,**[3] **V. Semkova**[3]
[1]Institute of Nuclear Research (ATOMKI) of the Hungarian Academy of Sciences, Debrecen, Hungary
[2]Institute of Experimental Physics, University of Debrecen (UD-IEP), Debrecen, Hungary
[3]European Commission, Joint Research Centre, Institute for Reference Materials and Measurements (IRMM), Geel, Belgium

Abstract

Monoenergetic neutrons were produced at the Van de Graaff accelerator of the EC-JRC-Institute for Reference Materials and Measurements (IRMM, Geel, Belgium). An air-jet cooled D_2-gas target (1.2 bar, ΔE_d = 448 keV) was bombarded with E_d =4976 keV deuterons to produce neutrons up to E_n = 8 MeV energy via the D(d,n)^{3}He reaction. Higher energy neutrons up to E_n = 18 MeV were produced via the T(d,n)^{4}He reaction by bombarding a TiT target with E_d =1968 keV deuterons.

Pulse height spectra were measured at different neutron energies from E_n = 8 MeV up to E_n = 18 MeV with the NE-213 liquid scintillator based Pulse Height Response Spectrometer (PHRS) of UD-IEP. The energy calibration of the PHRS system has been extended up to E_n = 18 MeV. Pulse height spectra induced by gamma photons have been simulated by the GRESP7 code. Neutron induced pulse height spectra have been simulated by the NRESP7 and MCNP-POLIMI codes. Comparison of the results of measurements and simulations enables the improvement of the parameter set of the function used by us to describe the light output dependence of the resolution of the PHRS system at light outputs of L > 2 light units. Also, it has been shown that the derivation method for unfolding neutron spectra from measured pulse height spectra performs well when relative measurements are done up to E_n = 18 MeV neutron energy. For matrix unfolding purposes, the NRESP7 code has to be preferred to calculate the pulse height response matrix of the PHRS system.

Leakage spectra of neutrons behind bismuth slabs of different thicknesses have been measured with the PHRS system by using monoenergetic neutrons. The maximum slab thickness was d = 14 cm. Simulations of the measurements have been carried out with the MCNP-4c code. The necessary nuclear cross-sections were taken from the from the ENDF/B-VII and JEFF-3.1 data libraries. For both libraries, the agreement of measured and simulated neutron spectra is good for the 5 MeV ≤ E_n ≤ 18 MeV neutron energy region. However, for both libraries, the observed differences between measured and simulated neutron spectra are beyond statistical uncertainty for the E_n < 5 MeV region. Further experimental check of cross-section data of the two libraries for bismuth is recommended for the E_n < 5 MeV region.

Introduction

The Pb-Bi eutectic alloy (44.5% Pb and 55.5% Bi) has been used as coolant of the blanket in some types of fission fast reactors. The alloy has been used as target material of intense spallation neutron sources. It is a candidate for coolant of the fuel blanket of some accelerator driven systems to be used for nuclear waste transmutation. All these applications need detailed knowledge of the neutron transport and the necessary transport calculations need validated and consistent cross-section data libraries.

A 3-steps method developed by us [1] was used for integral testing of cross-section data sets. The method employs the Pulse Height Response Spectrometry (PHRS) technique, and the steps are a) performing measurements of spectra modified by slabs of different thicknesses exposed by different neutron sources, b) Monte Carlo simulations of the experiments with the MCNP-4C code [2] using differential cross-section data taken from measurements and/or libraries of evaluated data, c) comparison of the obtained experimental data with results of the simulations.

In this work we report results of our experiments and Monte Carlo simulations aiming at the extension of the calibration of our PHRS system up to E_n = 18 MeV neutron energy. We present results of leakage spectrum measurements obtained for bismuth using quasi-monoenergetic neutrons in the 8 MeV ≤ E_n ≤ 18 MeV neutron energy range. Also, we present results of the simulations of the experiments obtained using the MCNP-4c code taking cross-section data sets from the ENDF/B-VII and JEFF-3.1 evaluated data libraries.

Experimental

Production of quasi-monoenergetic neutrons

The experiments were performed at the 7 MV Van de Graaff (VdG) accelerator facility of the Neutron Physics Unit of IRMM. Deuteron beams were used to produce quasi-monoenergetic d+D and d+T neutrons. The uncertainty of the energy of the deuteron beam was ± 5keV. The accelerator settings for the experiments were calculated by the EnergySet (ver. 3) program [3]. The code can calculate energy spectra and fluences of the neutrons emitted by the sources, too.

d+D neutrons were produced via the $D(d,n)^3He$ nuclear reaction using an air jet cooled gaseous deuterium target with a 5 μm molybdenum entrance window and a tantalum plate as stop of the deuteron beam. The target was bombarded by E_d = 4976 keV deuterons to generate neutrons. The beam current was I_d = 1 μA. The pressure of the D_2-gas in the h = 40 mm target cell was kept at p = 1.2 bar. The energy loss of the deuteron beam was ΔE = 312 keV in the entrance foil and ΔE = 448 keV in the D_2-gas. At $\vartheta = 0^\circ$ angle measured from the direction of the bombarding beam, the centroid of the energy distribution of the neutrons was <En> = 8 MeV in the middle of the target and the width of the monoenergetic peak was FWHM = 436 keV.

d+T neutrons were produced via the $T(d,n)^4He$ nuclear reaction. An air jet cooled and wobbled TiT target (Target code: IRMM-20) was bombarded by E_d = 1.968 MeV deuterons to generate neutrons. The beam current was I_d = 7 μA. The TiT target layer was formed on a 0.5 mm thick silver backing. The amount of the deposited titanium was 1.936 $mgcm^{-2}$ and the ratio of the number of T atoms to the number of Ti atoms was N_T/N_{Ti} = 1.7. The energy loss of the deuteron beam was ΔE = 311 keV in the TiT layer. At $\vartheta = 0^\circ$ angle measured from the direction of the bombarding beam, the centroid of the energy distribution of the neutrons was $<E_n>$ = 17.999 MeV in the middle of the TiT layer and the width of the monoenergetic peak was FWHM = 440 keV.

Monitoring and logging of the irradiation parameters was done by the control system of the accelerator and beam transport system. In the case of the D_2-gas target, readings of the temperature sensor and the pressure sensor of the gas handling system were also recorded during irradiation. The neutron flux was monitored by two long counters with BF_3 proportional counter tubes.

The neutron spectrometer

The Pulse Height Response Spectrometry (PHRS) method was employed. The spectrometer was developed at IEP-DU [4]. The neutron detection was done by a NE-213 liquid scintillator encapsulated in an aluminium case of 0.5 mm wall thickness. The diameter and the length of the scintillator were 49 mm and 50.5 mm, respectively [5]. The scintillator was attached to a Hamamatsu R329 photomultiplier tube. The electronics of the spectrometer consisted of standard NIM modules and PC cards. The data acquisition was done by a multichannel analyzer (MCA) PC card in a personal computer (PC1 in Figure 1). At IRMM, measured data were recorded in event list mode, too, with a Modular MultiParameter Multiplexer module (MMPM) developed at IRMM and a data acquisition (DAQ) PC card. Counts of the two neutron monitors used were recorded by 32 bit scalers and a DAQ PC card. The block diagram of the PHRS spectrometer is shown in Figure 1.

Figure 1: Block diagram of the PHRS system used in the experiments

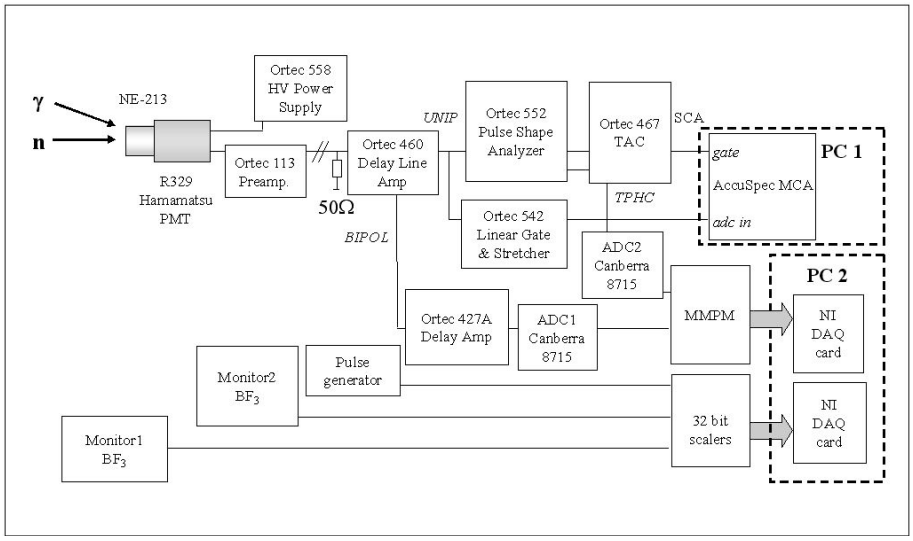

Pulse height spectra of protons recoiled by neutrons were derived via pulse shape discrimination and from the measured event lists. In the second case two dimensional contour plots were generated from the event lists that show the occurrence of the events in matrices of the measured pulse rise time to the measured pulse height. Then the intervals were set for separating the gamma and neutron induced events. In the next step the events induced by recoiled protons were selected and their corresponding pulse height spectra were derived as a function of the light output measured in light units (LU). Following the procedure described in Reference 4 the light output from recoiled protons was converted to neutron energy and a derivation method was used for obtaining the neutron spectrum from the measured pulse height spectrum.

Energy calibration

The linearity of the channel-to-energy conversion was checked via measurement and evaluation of gamma spectra of calibration sources emitting only one decay gamma-ray (^{22}Na, ^{54}Mn, ^{88}Y and ^{137}Cs). 4th order polynomials were fit to the Compton-edges in the spectra and channel positions of the maximum (CH_{max}) and half-maximum ($CH_{1/2}$) were identified for each Compton-edge. Using CH_{max} and $CH_{1/2}$ the channel position of the Compton-edge ($CH_{Compton}$) was interpolated following the procedure described in Reference 6 by Dietze and Klein [6]. Finally a linear fit to the obtained ($CH_{Compton}$; $E_{Compton}$) pairs was done.

The energy scale was converted to light output scale using the following linear relationship

$$L(E) = 1MeV^{-1} * (E - 0.005MeV) \quad (1)$$

where L is the light output that is induced in the scintillator by an electron of E energy. This scaling is valid for E > 50 keV electron energy in the case of the NE-213 liquid scintillator. This scaling is used by the GRESP and NRESP Monte Carlo codes [7, 8]. A transformation of this scaling was done in the cases of measurements with neutrons because the unfolding code of our PHRS system uses the scaling defined by Verbinski et al. [9]. Before and after each neutron irradiation gamma spectrum of a ^{22}Na calibration source was measured for checking the gain stability of the electronics.

Method of estimation of the energy resolution of the spectrometer using gamma photons

According to Reference 6 the $\Delta L_{FWHM}/L$ relative energy resolution of the spectrometer was estimated by the

$$\frac{\Delta L_{FWHM}}{L} \cong 1.5 * \frac{L_{1/2} - L_{max}}{L_{1/2}} \tag{2}$$

equation for each Compton-edge in the measured gamma spectra. The interpolation procedure described in Reference 6, too, was also performed and lead to more precise estimation of $\Delta L_{FWHM}/L$.

The light output dependence of the resolution was described by the

$$\frac{\Delta L_{FWHM}}{L} = \sqrt{A^2 + \frac{B^2}{L} + \frac{C^2}{L^2}} \tag{3}$$

function where A, B and C are constants. These constants were determined from fitting the (L; $\Delta L_{FWHM}/L$) pairs obtained from Eq. 2 and the interpolation.

The final values of the A, B and C constants were obtained from fitting each measured gamma spectrum. First, for each calibration source, the GRESP7 code was run for simulating the ideal pulse height distribution of the electrons induced in the scintillator by the gamma photons. Broadening of the ideal gamma lines was described by Gaussian distribution. The fitting function was the convolution of the ideal spectrum and the Gaussian function as

$$N(CH_i) = N_{norm} * \sum_{j=1}^{CH_{max}} \left\{ N_{GRESP7}(CH_j) * \frac{1}{\sqrt{2\pi}\sigma_j} e^{-\frac{k*(CH_j - CH_i)}{2\sigma_j^2}} \right\} \tag{4}$$

where $N(CH_i)$ is the number of counts in the i-th channel CH_i, N_{norm} is a normalisation constant, CH_{max} is the number of MCA channels in the measured spectrum, $N_{GRESP7}(CH_j)$ is the simulated value for the ideal pulse height distribution in the j-th channel and

$$\sigma_j = L_j \cdot \frac{\sqrt{A^2 + B^2/L_j + C^2/L_j^2}}{2\sqrt{2\ln 2}} \tag{5}$$

and

$$L_j = k*(CH_j - CH_{offset}) \tag{6}$$

and k denotes the channel-to-L conversion factor.

Leakage spectrum measurements

The arrangement of the leakage spectrum measurements is shown in Figure 2. The geometrical centres of both the NE-213 scintillator and the bismuth slabs were on the axis of the bombarding beam (ϑ = 0° direction). The front surface of the housing of the NE-213 scintillator and the 30 cm × 30 cm surfaces of the bismuth slabs were perpendicular to the ϑ = 0° direction. The distance between the air jet cooled back surface of the beam stop of the neutron emitting target and the front surface of the housing of the NE-213 scintillator was 200 ± 0.3 cm. The distance between the back side of the first bismuth slab and the front surface of the housing of the NE-213 scintillator was 5.8 cm. The maximum thickness of the bismuth block was d = 14 cm when all the 7 pieces of slabs were put between the detector and the target.

Figure 2: Arrangement of the leakage spectrum measurements

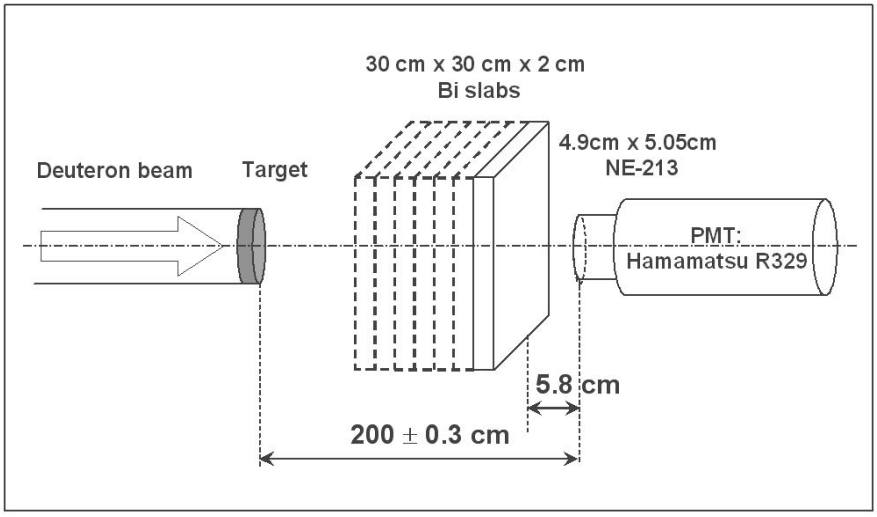

Background measurements

Background measurements were performed to estimate the effect of neutrons from room scattering and sky shine both for the d+D and d+T target. Neutrons emitted at forward angles were shadowed. In the first type of the background measurement a cone made of brass and a polyethylene disc with a nylon plug were put in between the target and the 14 cm thick bismuth block. In the subsequent measurement the 14 cm thick bismuth block was removed from the arrangement. For the D_2-gas target gas-in and gas-out measurements were done, too, to estimate contribution of neutrons from the components of the target holder cell.

Results

Measurements and simulations for the extension of the calibration of the spectrometer

Figure 3 shows, as an example, a colour map of the pulse rise time – pulse height matrix measured for d+T neutrons at E_n = 18 MeV. The intervals used for identification of neutron events are indicated in the figures. Similar matrices were measured for d+D neutrons, too. Figure 4 shows the measured pulse height spectra induced by d+T neutrons with energy in the 13.4 MeV ≤ E_n ≤ 18 MeV region

Figure 3: Identification of the region of neutron events in the pulse rise time – pulse height matrix

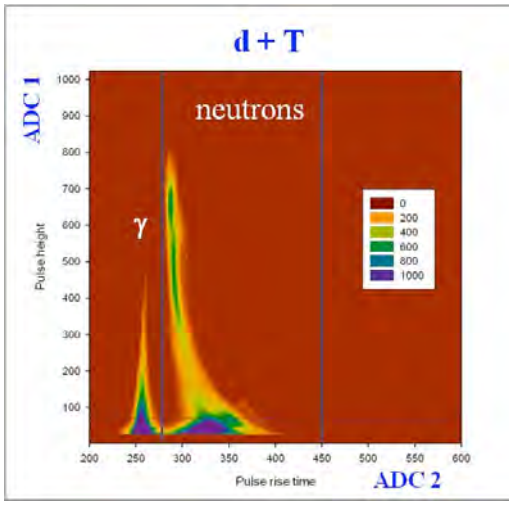

and the light output of the NE-213 scintillator as a function of the neutron energy. The new data points measured by us for extending the neutron energy calibration of our PHRS system are in good agreement with the calibration curve published earlier by Verbinski and his co-workers for the NE-213 liquid scintillator [9].

Figure 4: Measured pulse height spectra induced by d+T neutrons with energy in the 13.4 MeV ≤ E_n ≤ 18 MeV region (left) and the light output of the NE-213 scintillator as a function of the neutron energy (right)

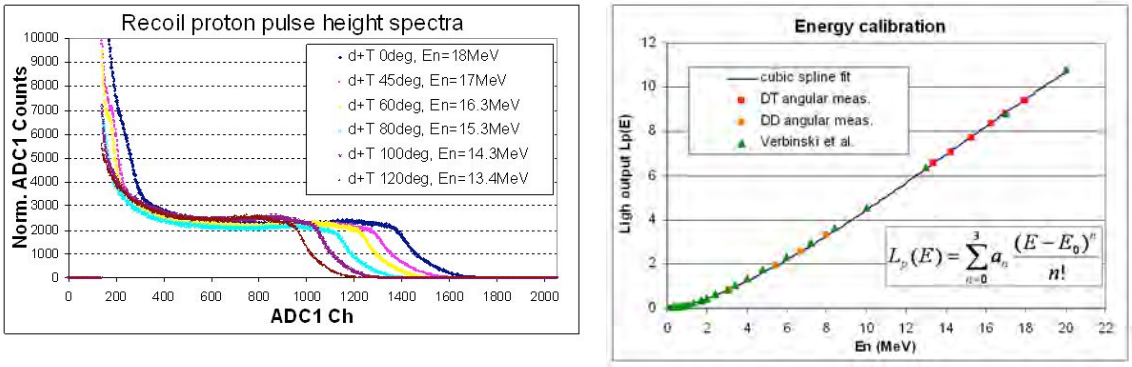

The left graph in Figure 5 shows the light output dependence of the $\Delta L_{FWHM}/L$ resolution of the NE-213 scintillator as a function of L^{-1}. The data points were obtained from evaluation of the measured gamma spectra of ^{22}Na, ^{54}Mn, ^{88}Y and ^{137}Cs calibration sources performing both the estimation and the interpolation procedure described in Reference 6. The curve was fitted to the data points that were obtained via interpolation. Constants of the fitted curve were used for obtaining the A, B and C constants (see Equation 5 above). The left graph of Figure 5 shows the pulse height spectrum measured for an ^{88}Y source and the fit obtained from the convolution of the result of the relevant GRESP7 simulation and a Gaussian function with light output depending σ. The σ(L) function was obtained using the A, B and C parameters and Equation 5. The agreement of the measured and simulated spectrum is good that validates the set of A, B and C for L ≤ 1.7 LU light outputs.

Figure 5: Light output dependence of the $\Delta L_{FWHM}/L$ resolution of the NE-213 scintillator obtained with calibration gamma sources (left). The pulse height spectrum measured for an ^{88}Y source and the fit obtained from GRESP7 simulation (right)

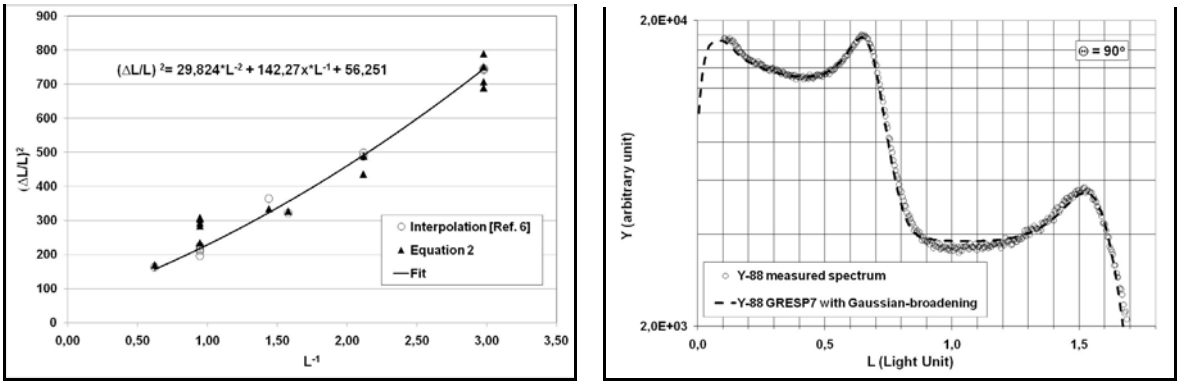

Figure 6 shows measured pulse height spectra that were induced by E_n = 8 MeV neutrons and by E_n = 18 MeV neutrons. Also, the results of NRESP7 simulations are shown in Figure 6. The disagreement for high L values indicates the limitations of the extrapolation of the $\Delta L_{FWHM}/L - L$ relationship obtained from gamma calibration measurements for L < 2 light outputs. In order to get a more realistic $\Delta L_{FWHM}/L - L$ relationship, that is valid in a much broader light output range, it is necessary to include in the procedure the neutron spectra induced by monoenergetic neutrons. The

Figure 6: Simulated and measured pulse height spectra induced by E_n = 8 MeV neutrons (left) and by E_n = 18 MeV neutrons (right)

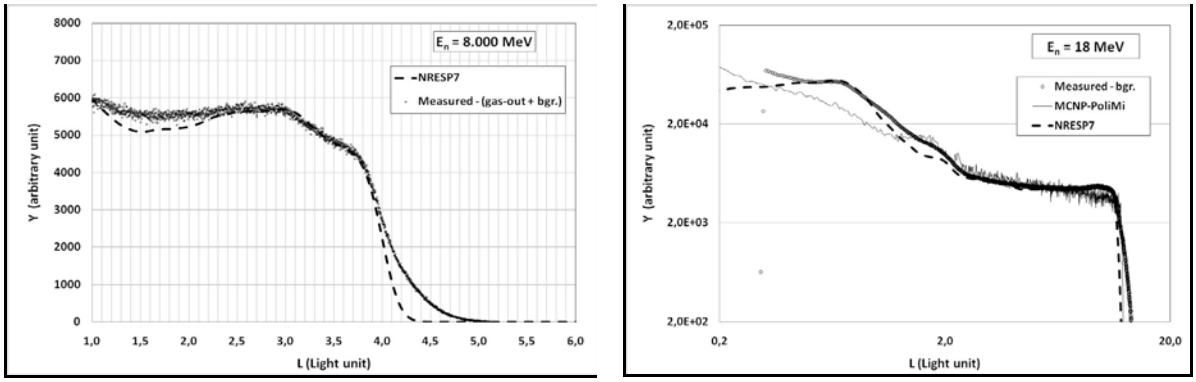

$\Delta L_{FWHM}/L$ values evaluated for the monoenergetic peak of the measured neutron spectra have to be added as new data points for the measured $\Delta L_{FWHM}/L - L$ relationship. Then the new set of the A, B and C parameters can be obtained from consecutive NRESP7 simulations and adjustment of values of A, B and C until a good agreement is reached between the measured and simulated pulse height spectra for each neutron energy.

In Figure 6 the right diagram also shows the pulse height spectrum for the d+T neutrons with E_n = 18 MeV energy comparing the result of a Monte Carlo simulation performed with the MCNP-PoliMi code with the data and the NRESP7 calculation. The agreement is acceptable for L > 1 light outputs even in linear scale. It has to be mentioned, however, that much worse result was obtained for d+D neutrons at E_n = 8 MeV energy.

The results of the simulations indicate that the NRESP7 code is a better choice for calculating a response matrix for our NE-213 liquid scintillator based PHRS system.

Leakage spectrum measurements

For d+D neutrons of E_n = 8 MeV neutron energy and for d+T neutrons of E_n = 18 MeV neutron energy, Figure 7 shows the neutron spectra measured by the spectrometer at a fixed position behind the bismuth blocks of different thicknesses. The spectra measured without bismuth block (d = 0 cm thickness) were used for estimating the $\Delta L_{FWHM}/L$ resolution of the spectrometer at E_n = 8 MeV and at E_n = 18 MeV as described above.

The peak below the main peak comes from protons recoiled by neutrons that interact with carbon nuclei in their first collision in the scintillator material. The main peak is induced by neutrons that recoil protons in their first collision in the scintillator material. The broadening of the peaks and the high energy tail of the monoenergetic peak are caused mainly by the finite resolution

Figure 7: Neutron spectra measured behind bismuth blocks of different thicknesses for d+D neutrons at E_n = 8 MeV (left) and for d+T neutrons at E_n = 18 MeV (right)

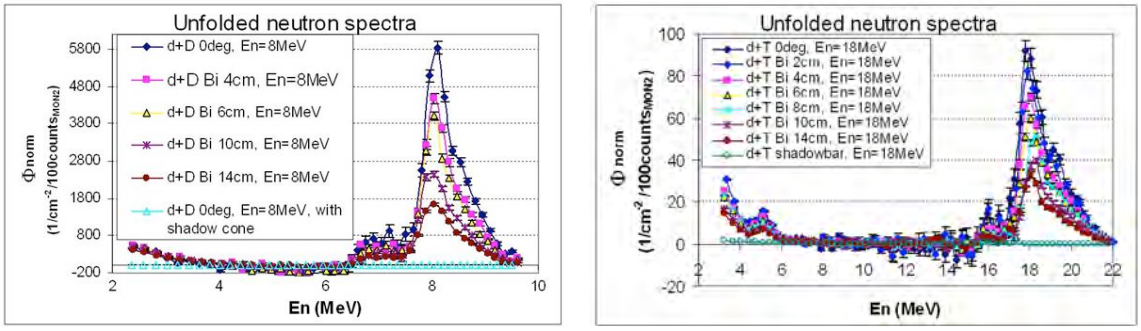

of the spectrometer and the numerical method used for calculation of the neutron spectrum from the measured pulse height spectrum induced by recoiled protons.

Results of the Monte Carlo simulations of the leakage spectrum measurements

Figure 8 shows results of MCNP-4c simulations for d+D neutrons at E_n = 8 MeV (left) and for d+T neutrons at E_n = 18 MeV (right). The neutron flux was averaged for the volume of the NE-213 scintillator. The thickness of the bismuth block was d = 14 cm. The results obtained taking cross-section data from the JEFF-3.1 evaluated library are compared to results obtained with ENDF-B/VII data. For the d+T neutrons the agreement is within the statistical uncertainty of the simulations in the whole energy region. In the case of d+D neutrons the disagreements observed at E_n < 5 MeV neutron energy are above the statistical uncertainty of the simulations.

In Figure 9 attenuation of the measured and simulated neutron fluxes integrated for the monoenergetic peaks are shown as a function of the thickness of the bismuth block. The neutron flux was averaged for the volume of the NE-213 scintillator. The simulations were performed using JEFF-3.1 data. The type of the exponential curve fitted to the attenuations was $\Phi(d) = A^{*}e^{-b^{*}d}$ for both the experimental and calculated data. The agreement of the experimental and calculated results is very good for the 18 MeV d+T neutrons for each slab thicknesses except d = 10 cm. The obtained ratio of the attenuation factors of the exponential fits was $b_{Calc.}/b_{Exp.}$ =1.005. Larger difference can be

Figure 8: MCNP-4c simulations for d+D neutrons at E_n = 8 MeV (left) and for d+T neutrons at E_n = 18 MeV (right). The neutron flux is averaged for the volume of the NE-213 scintillator. The thickness of the bismuth block is d = 14 cm.

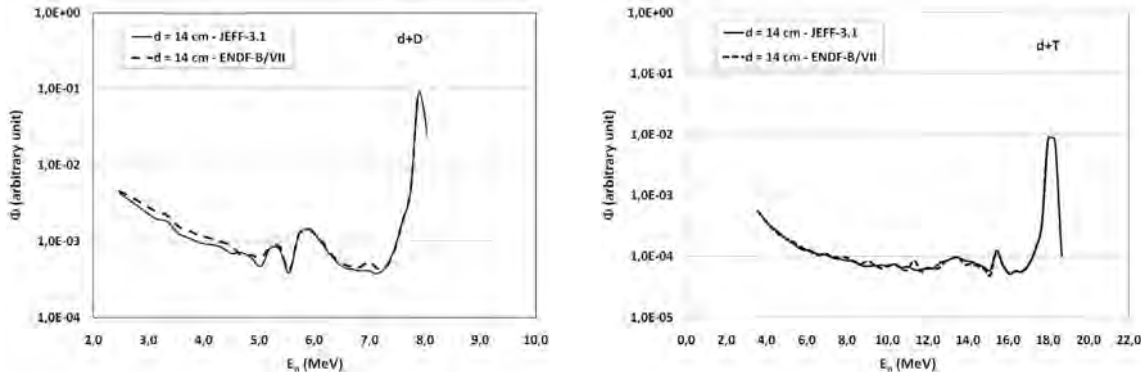

Figure 9: Attenuation of the neutron flux integrated for the monoenergetic peak of d+D neutrons at E_n = 8 MeV (left) and d+T neutrons at E_n = 18 MeV (right) as a function of the thickness of the bismuth block The neutron flux is averaged for the volume of the NE-213 scintillator.

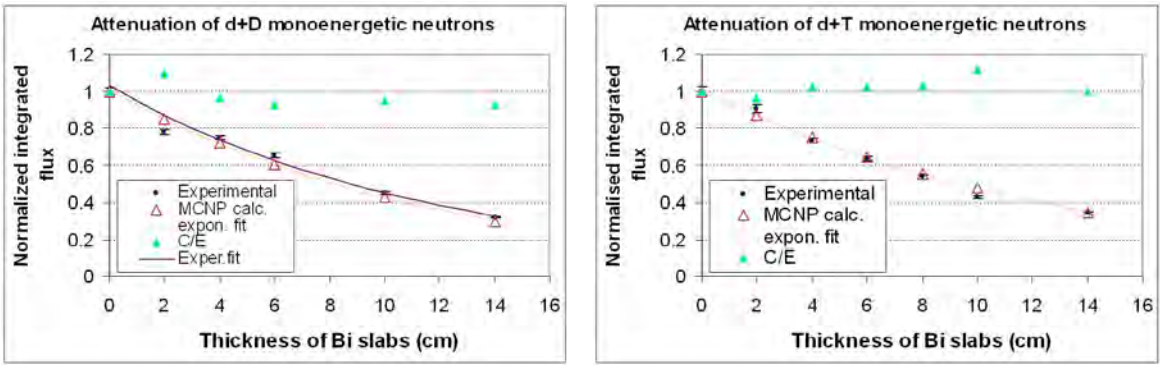

observed for each slab thicknesses in the case of the 8 MeV d+D neutrons. The difference is reflected

in the ratio of the *b* constants of the exponentials, too, that were fitted to the experimental and calculated data. The result for the ratio was $b_{Calc.}/b_{Exp.} = 0.94$.

Conclusions

The energy calibration of the PHRS system has been extended up to $E_n = 18$ MeV. Pulse height spectra induced by gamma photons have been simulated by the GRESP7 code. Neutron induced pulse height spectra have been simulated by the NRESP7 and MCNP-POLIMI codes. Comparison of the results of measurements and simulations has showed that the function used by us for describing the light output dependence of the resolution of our PHRS system can be used for interpolation in the $L < 2$ LU light output region. Extension of the function to the $L > 2$ LU region needs re-evaluation of the parameter set of the function. Also, it has been shown that the method used by us for calculating the neutron spectra from measured pulse height spectra performs well at $E_n \leq 18$ MeV neutron energies and the unfolded spectra can be used for relative measurements. For matrix unfolding purposes, the NRESP7 code has to be preferred to calculate the pulse height response matrix of the PHRS system.

The pulse height spectra obtained in our leakage spectrum measurements can be used for checking the validity of cross-section data sets of evaluated libraries via comparison of results of measurements and the relevant Monte Carlo simulations.

For both libraries, the agreement of measured and simulated neutron spectra is good for $5 \text{ MeV} \leq E_n \leq 18$ MeV neutron energies. However, for both libraries, the observed differences between measured and simulated neutron spectra are beyond statistical uncertainty for the $E_n < 5$ MeV region.

Further experimental check of cross-section data of the two libraries for bismuth is recommended for the $E_n < 5$ MeV region.

Acknowledgement

This work was supported by the Transnational Access programme at JRC-IRMM within the frame of the Neutron Data Measurements (NUDAME) FP6 project funded under the EURATOM Management of Radioactive waste programme.

References

[1] Jordanova, J. *et al.,* "Validation of neutron data libraries by comparison of measured and calculated neutron leakage spectra", *Nucl. Instr. and Meth. Phys. Res.* A 421, 522-530 (1999).

[2] Briesmeister, J.F., LANL Report, LA–13709–M, Los Alamos National Laboratory (LANL), New Mexico, USA, (2000).

[3] Lövestam, G., *EnergySet – a programme to calculate accelerator settings and neutron yield data for the IRMM VdG laboratory*, Institute for Reference Materials and Measurements Internal Report No. GER/NP/2/2002/06/20 (2002).

[4] Oláh, L., *Scintillation neutron spectrometry and its applications*, PhD Thesis, Faculty of Sciences, Lajos Kossuth University, Debrecen, Hungary (2000).

[5] Sztaricskai, T., Private communication.

[6] Dietze, G., H. Klein, "Gamma-calibration of NE 213 Scintillation Counters", *Nucl. Instr. Meth.* 193, 549-556 (1982).

[7] Tichy, M., H. Klein, J. Pulpan, *Calibration of an NE213 Scintillator*, PTB-7.2-1992-1, Physikalisch-Technische Bundesanstalt, Braunschweig, Germany (1992).

[8] Dietze, G., H. Klein, *NRESP4 and NEFF4 Monte Carlo codes for the calculation of neutron response functions and detection efficiencies for NE-213 scintillation detectors*, PTB-ND-22, Physikalisch-Technische Bundesanstalt, Braunschweig, Germany (1982).

[9] Verbinski, V.V., *et al.*, "Calibration of an organic scintillator for neutron spectrometry", *Nucl. Instr. and Meth.* 65, 8 (1968).

Tritium production in neutron induced reactions

A. Krása,[1] **E. Andreotti,**[1] **M. Angelone,**[2] **M. Hult,**[1] **G. Marissens,**[1] **M. Pillon,**[2] **A. Plompen**[1]
[1]European Commission, Joint Research Centre,
Institute for Reference Materials and Measurements, Geel, Belgium
[2]Associazione EURATOM-ENEA sulla Fusione, Centro Ricerche Frascati, Rome, Italy

Abstract

We present an overview of the present knowledge of (n,t) reaction excitation functions in the 14-21 MeV energy range for Cd, Cr, Fe, Mg, Mo, Ni, Pb, Pd, Ru, Sn, Ti, Zr. Experimental data are compared with evaluated data libraries, cross-section systematics, and TALYS calculations. The new values for the $^{50}Cr(n,t)^{48}V$ *cross-section measured using* γ*-spectrometry at 15, 16, 17.3 MeV are presented.*

Introduction

Tritium is a β^--radioactive isotope with $T_{1/2}$ = (12.33 ± 0.02) y [1]. It is produced in almost all structural materials exposed to high-energy neutron fields provided that the neutron energies are above the threshold of approximately 10 MeV. Investigation of this energy domain was of minor importance for classical light-water nuclear reactors, but it will be important for radiation safety in future fusion reactors and accelerator driven systems. In these facilities intensive neutron fluxes will be produced, making even neutron-induced tritium production, which has a low cross-section, important.

The mean energy of electrons emitted during tritium β-decay is 5.69 keV (with an endpoint of 18.6 keV). Such low-energy electrons are practically impossible to detect, because they are usually stopped inside the sample itself (self-absorption). Those rare electrons that penetrate outside the sample are absorbed in the packing of a detector. The only possibility to detect low-energy electrons is by a liquid scintillation technique – to admix a sample in a liquid scintillator. In addition, this method is non-selective requiring not only very high purity elemental samples, but even very highly isotopically enriched samples if the goal is a measurement for well defined reaction channels. In addition, preparation of solid samples for liquid scintillation is difficult and we have therefore decided to measure tritium production indirectly – by detecting the residual nuclei of the (n,t)-reactions. These residual nuclei can be produced from a specific nucleus via three channels:

$$^{A}_{Z}X + n \rightarrow {}^{A-2}_{Z-1}Y + t,$$

$$^{A}_{Z}X + n \rightarrow {}^{A-2}_{Z-1}Y + n' + d,$$

$$^{A}_{Z}X + n \rightarrow {}^{A-2}_{Z-1}Y + p + 2n.$$

The threshold energy of the tritium production channel is several MeV lower than those of the other two channels, see Table 1. Moreover, when charged particles are emitted, they have to overcome the Coulomb barrier whereby a significant cross-section is only found several MeV above the threshold, see Figure 1. Therefore, in a certain neutron energy domain (usually up to 20-22 MeV), we can be sure that a residual nucleus was produced along with a tritium nucleus.

Present knowledge in (n,t) cross-sections

The present knowledge of excitation function of (n,t) reaction is insufficient in most cases.

Experimental data

Early experimental data around 14.6 MeV are mostly not reliable enough, as they do not agree between each other and discrepancies can reach a factor of 2 or 3 (*e.g.*, ^{50}Cr, ^{58}Ni, ^{54}Fe, ^{46}Ti), see Figures 2-5. For a few isotopes, there is only one experimental point (*e.g.*, ^{90}Zr, ^{102}Pd, ^{106}Cd, ^{112}Sn), see Figures 7-10. The uncertainties are large (25-50%) or completely missing.

Several measurements were performed at higher energies (*e.g.*, ^{50}Cr, ^{58}Ni, ^{54}Fe, ^{92}Mo), see Figures 2-4, 6. A few data are reported at 22.5 MeV [2], but they cannot be considered as real cross-sections, because they come from irradiations with a very broad neutron spectrum (FWHM = 15.8 MeV). Such effective cross-sections should be considered as integral data.

Evaluations

Some evaluated data files contain data for (n,t) reactions from threshold up to 20 MeV. Large discrepancies can be observed among different libraries. A particularly strange behaviour is shown by the BROND-2.2 library for the ^{90}Zr and ^{204}Pb nuclides, see Figures 8 and 12. For many nuclides, there are no experimental data and the evaluations are based only on nuclear model calculations (*e.g.*, ^{96}Ru, see Figure 12). For some isotopes, there are neither experimental nor evaluated data available (*e.g.* ^{24}Mg, see Figure 13).

Therefore, a deterministic code TALYS [3] (version 1.0 with a default setting of nuclear models) was used to calculate excitation functions of (n,t) reactions, see Figures 2-13 (and other channels leading to the same residual nuclei, see Figure 1) from threshold up to 24 MeV. In relevant cases, calculation of both ground and isomeric states were performed. At lower energies, TALYS systematically predicts significantly lower (n,t) cross-sections than measured.

Additionally, we made a comparison with (n,t) reaction cross-section systematics of Konobeyev [4], which applies to isotopes with A ≥ 40 and neutron energies at 14.5 and 20 MeV, see Figures 2-13. Cross-section systematics is usually an analytical formula derived from the analysis of experiments. Konobeyev developed a new approach based on pre-equilibrium exciton and evaporative models. It fits in the range of experimental data around 14.5 MeV, but it strongly overestimates experimental data around 20 MeV, which were obtained after the systematics was created.

Table 1: The threshold energies are given for the three possible channels leading to the same residual nucleus. The target isotopes are ordered by mass number. The energies were calculated using Qtool [5] with the masses given by Audi and Wapstra [6]. Half-lives and main γ-lines (rounded values) of the residual nuclei are taken from Nuclear Data Sheets.

Target	Reaction	Residue	Threshold [MeV]	Residue half-life	E_γ [keV] (I_γ)
12-Mg-24	(n,t)	11-Na-22	16.3	2.6 y	1274.5 (100%)
	(n,n'd)		22.8		
	(n,p2n)		25.1		
22-Ti-46	(n,t)	21-Sc-44	13.5	4 h (g.s.) 59 h (isomer)	1157 (100%) – g.s. 270.9 (87%) – isomer
	(n,n'd)		19.9		
	(n,p2n)		22.2		
24-Cr-50	(n,t)	23-V-48	12.9	16 d	983.5 (100%) 1312 (98%)
	(n,n'd)		19.3		
	(n,p2n)		21.6		
26-Fe-54	(n,t)	25-Mn-52	12.7	5.6 d (g.s.) 21 min (isomer)	1434 (100%) – g.s. 1434 (98%) – isomer 935.5 (95%) – g.s.
	(n,n'd)		19.0		
	(n,p2n)		21.3		
28-Ni-58	(n,t)	27-Co-56	11.3	77 d	846.8 (100%) 1238 (67%)
	(n,n'd)		17.6		
	(n,p2n)		19.9		
40-Zr-90	(n,t)	39-Y-88	11.5	107 d	1836 (99%) 898.0 (94%)
	(n,n'd)		17.8		
	(n,p2n)		20.1		
42-Mo-92	(n,t)	41-Nb-90	11.1	15 h	1129 (93%) 2319 (82%)
	(n,t)		13.5		
	(n,n'd)		19.9		
44-Ru-96	(n,t)	43-Tc-94	8.9	4.9 h (g.s.) 52 min (isomer)	871.1 (100%) – g.s. 871.1 (94%) – isomer 702.6 (100%) – g.s.
	(n,n'd)		15.2		
	(n,p2n)		17.5		
46-Pd-102	(n,t)	45-Rh-100	9.3	21 h	539.5 (81%) 2376 (33%) 822.7 (21%)
	(n,n'd)		15.6		
	(n,p2n)		17.9		
48-Cd-106	(n,t)	47-Ag104	9.0	69 min (g.s.) 34 min (isomer)	555.8 (93%) – g.s. 555.8 (91%) – isomer 767.7 (66%) – g.s.
	(n,n'd)		15.3		
	(n,p2n)		17.6		
50-Sn-112	(n,t)	49-In-110	9.2	4.9 h (g.s.) 69 min (isomer)	657.8 (98%) – g.s. 657.8 (99%) – isomer 884.7 (93%) – g.s.
	(n,n'd)		15.5		
	(n,p2n)		17.7		
82-Pb-204	(n,t)	81-Tl-202	6.0	12.2 d	439.6 (91%)
	(n,n'd)		12.3		
	(n,p2n)		14.6		

Figure 1: Excitation functions of the sum of the (n,t), (n,n'd), and (n,p2n) reactions calculated using TALYS. A concave part of a curve corresponds solely to (n,t) reaction. Above a characteristic inflection point, which depends on a target nucleus, other reaction channels become important.

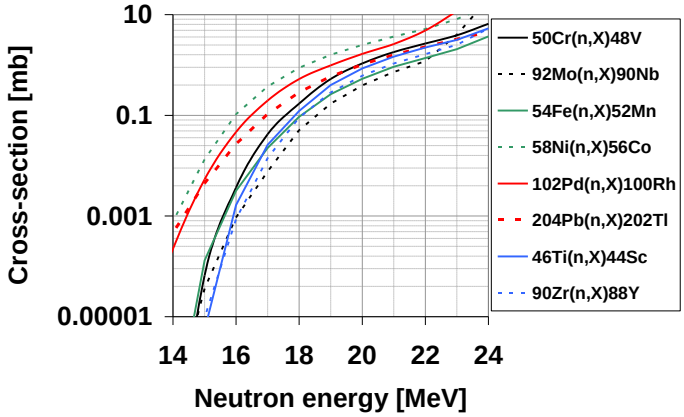

Figure 2: Cross-sections of $^{50}Cr(n,t)^{48}V$ reaction measured to date [7-10] are compared with evaluated data libraries, cross-section systematics, and TALYS calculations

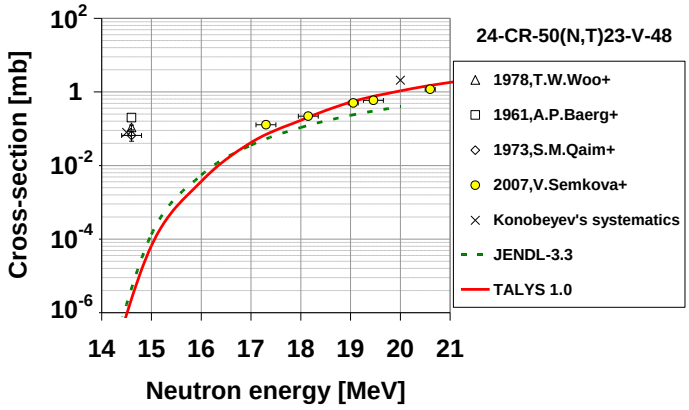

Figure 3: Cross-sections of $^{58}Ni(n,t)^{56}Co$ reaction measured to date [7,10-13] are compared with evaluated data libraries, cross-section systematics, and TALYS calculations

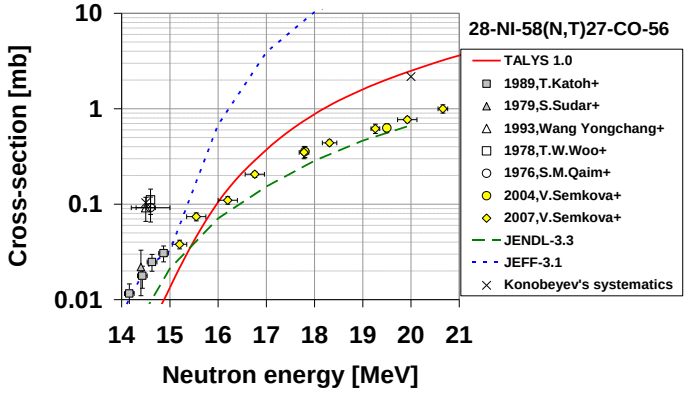

Figure 4: Cross-sections of the $^{54}Fe(n,t)^{52}Mn$ reaction measured to date [8,9,12,16-19] are compared with evaluated data libraries, cross-section systematics, and TALYS calculations. Experimental cross-sections for isomeric (M), ground state (G), and their sum (G+M) are distinguished by different colours.

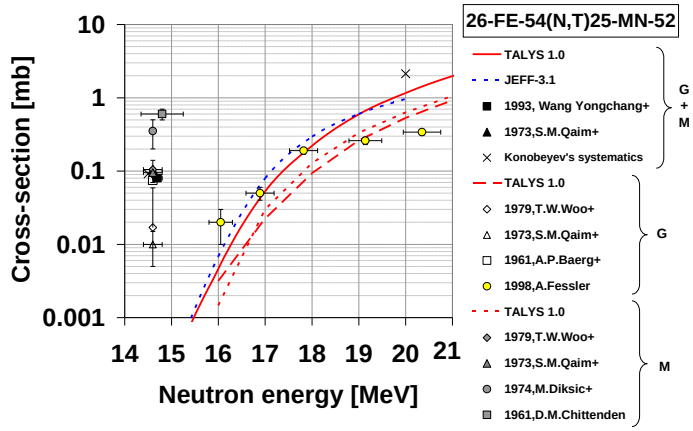

Figure 5: Cross-sections of the $^{46}Ti(n,t)^{44}Sc$ reaction measured to date [7-15] are compared with evaluated data libraries, cross-section systematics, and TALYS calculations. Experimental cross-sections for isomeric (M), ground state (G), and their sum (G+M) are distinguished by different colours.

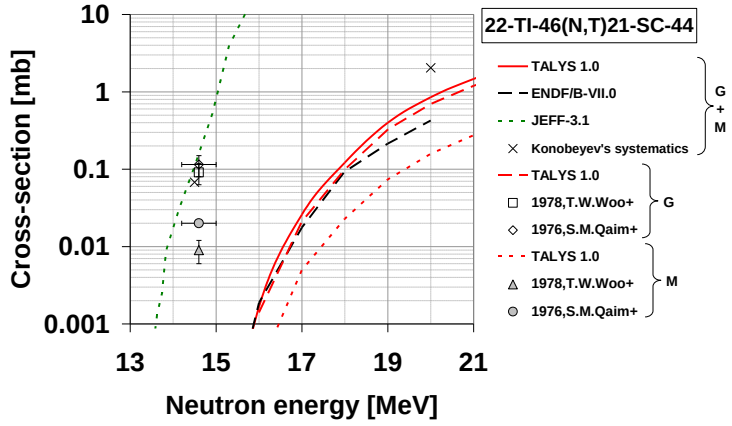

Figure 6: Cross-sections of the $^{92}Mo(n,t)^{90}Nb$ reaction measured to date [7,9,20] are compared with evaluated data libraries, cross-section systematics, and TALYS calculations

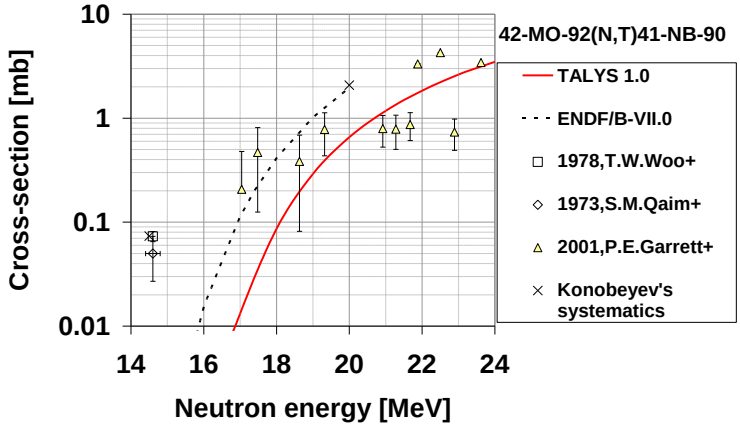

Figure 7: Cross-sections of the $^{90}Zr(n,t)^{88}Y$ reaction measured to date [15] are compared with evaluated data libraries, cross-section systematics, and TALYS calculations

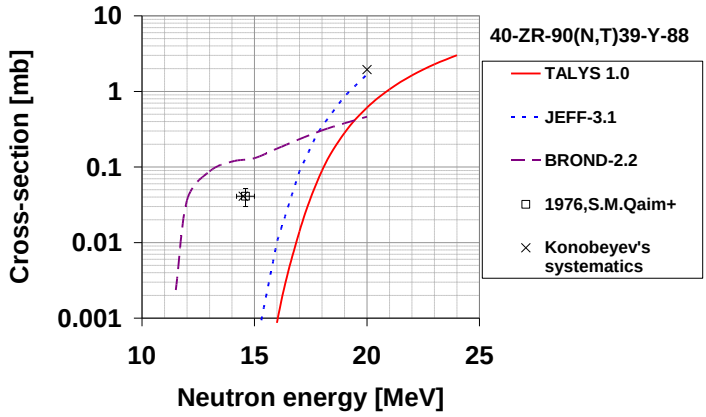

Figure 8: Cross-sections of the $^{102}Pd(n,t)^{100}Rh$ reaction measured to date [7] are compared with evaluated data libraries, cross-section systematics, and TALYS calculations

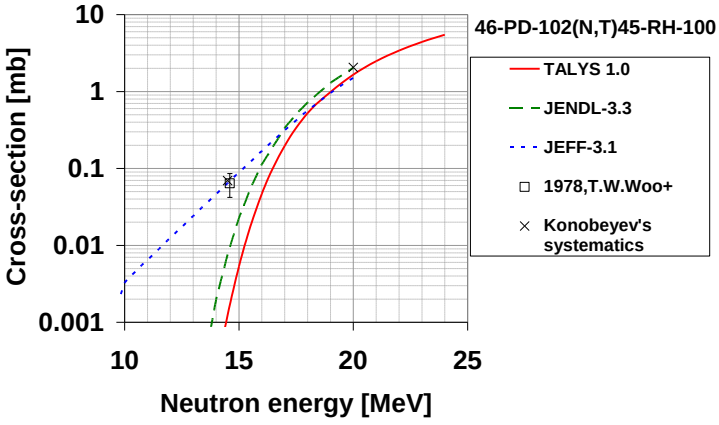

Figure 9: Cross-sections of the $^{106}Cd(n,t)^{104}Ag$ reaction measured to date [16] are compared with evaluated data libraries, cross-section systematics, and TALYS calculations. Experimental cross-sections for isomeric (M), ground state (G), and their sum (G+M) are marked by different colours. TALYS calculations of M and G are shown up to 20 MeV, because (n,n'd) reaction becomes important for higher energies.

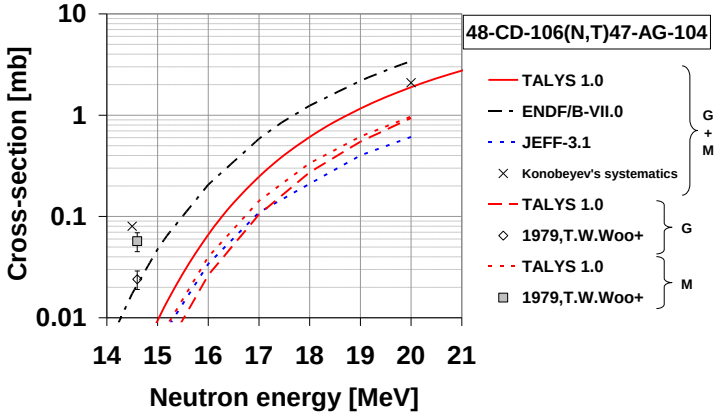

Figure 10: Cross-sections of the $^{112}Sn(n,t)^{110}In$ reaction measured to date [16] are compared with evaluated data libraries, cross-section systematics, and TALYS calculations. Experimental cross-sections for isomeric (M), ground state (G), their sum (G+M) are distinguished by different colours.

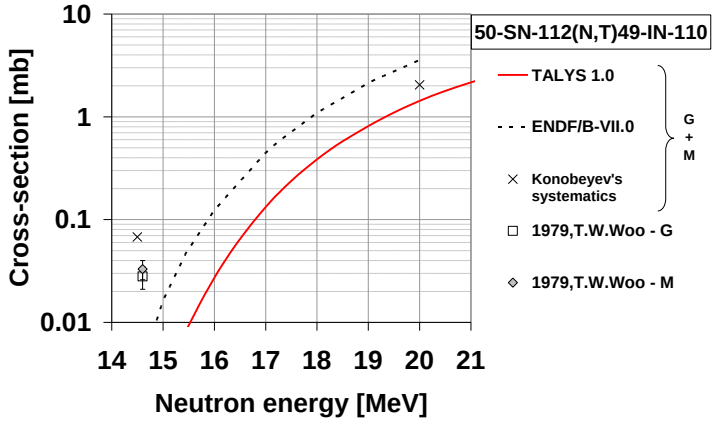

Figure 11: Cross-sections of the $^{204}Pb(n,t)^{202}Tl$ reaction measured to date [15,16] are compared with evaluated data libraries, cross-section systematics, and TALYS calculations

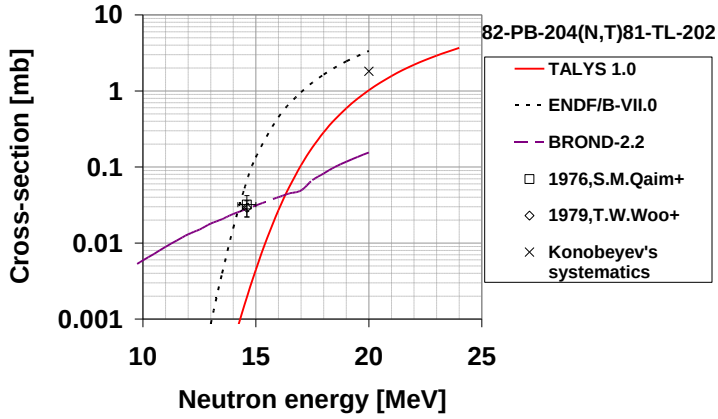

Figure 12: Cross-section systematics of the $^{96}Ru(n,t)^{94}Tc$ reaction are compared with evaluated data libraries and TALYS calculations

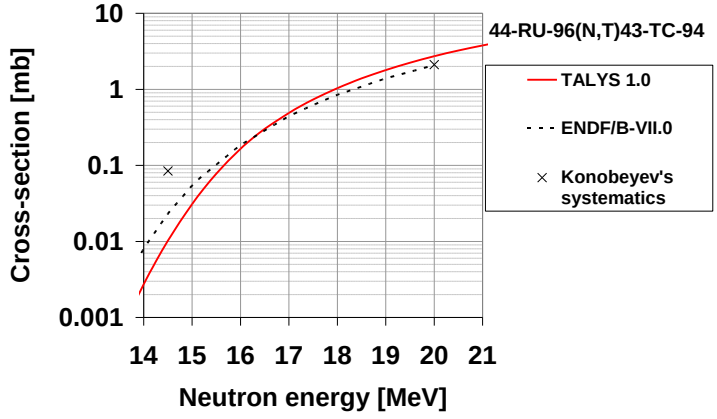

Figure 13: The excitation function of $^{24}Mg(n,t)^{22}Na$ reaction calculated with TALYS

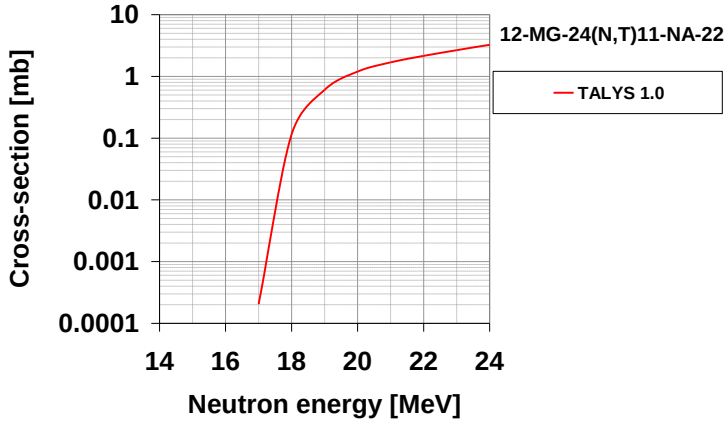

Materials and methods

Selection of samples

When using samples of natural isotopic abundance, the (n,t) reaction can be measured free from interferences for the stable isotope that has the lowest number of neutrons among the stable isotopes of one element (*i.e.* an isotope on the neutron deficient side of the valley of stability, see Figure 14) by the proposed method. If the (n,t) reaction on this isotope leads to a β^--radioactive isotope with appropriate half-life and γ-lines, then, γ-spectrometry can be used to determine the activity of a residual nucleus and the (n,t) cross-section may be deduced.

Contributions from other isotopes of the same element can be excluded in the considered energy region (14-22 MeV), but it is necessary to pay attention to elemental purity of samples, because of possible interferences with other reactions on other nuclides. The most important candidate interference is with the (n,2n) channel from an isotope that has one proton less (the isotope that is under the investigated isotope in the chart of nuclides). For example, in the case of the $^{46}Ti(n,t)$ reaction there is a possible interference with the $^{45}Sc(n,2n)$ reaction, see Figure 14.

Figure 14: Depiction of the (n,t) reaction on the chart of nuclides. Four examples of isotopes selected as feasible for our experiments (^{58}Ni, ^{54}Fe, ^{50}Cr, ^{46}Ti) and the possible interference with the (n,2n) channel are shown. Adapted from [21].

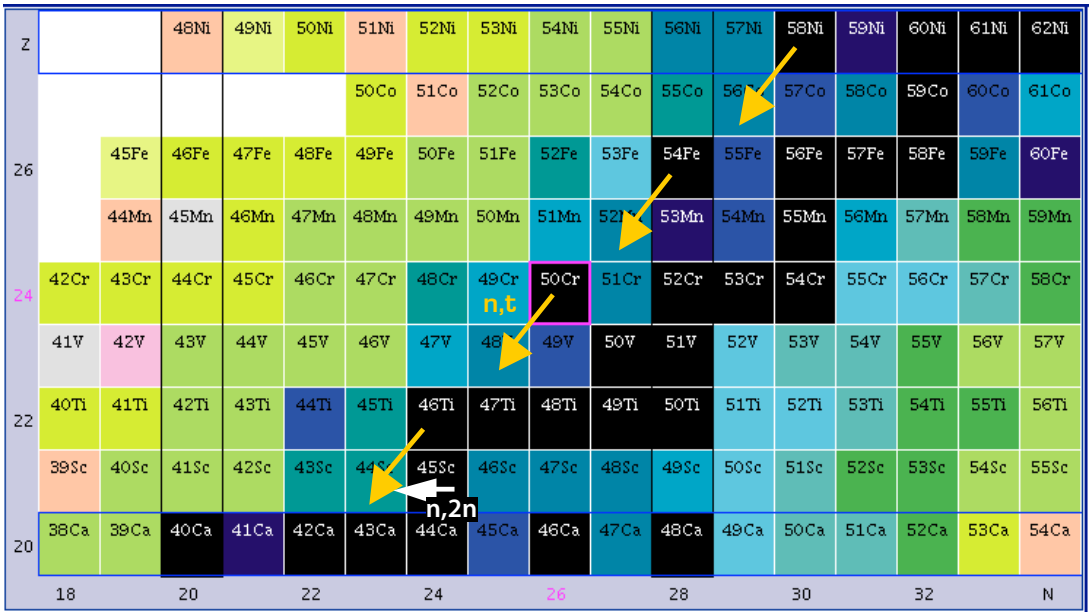

The (n,t) cross-sections around 15 MeV are roughly 50 μb, while the (n,2n) cross-sections are about 500 mb. To suppress the (n,2n) channel down to 1% of the (n,t) cross-section, the maximum permitted level of impurity is ~ 10^{-6}. For example, the ratio of the amount of ^{45}Sc nuclei to the amount of ^{46}Ti nuclei in a sample should not be bigger than 10^{-6}.

Neutron source

We use the Van de Graaff accelerator at IRMM in Geel, Belgium, for the production of quasi-mono-energetic neutrons via the T(d,n)^{4}He reaction. Deuteron beams with kinetic energies of 1–4 MeV and currents of about 10 μA directed to a solid T/Ti target (with the thickness of 2 mg/cm^2 on a Au backing) produce quasi-monoenergetic neutrons with energies between 16.1 and 20.7 MeV in the forward direction and down to 13 MeV at backward angles. Typical neutrons fluxes are up to 10^8 n sr^{-1}s^{-1}.

Neutron energies are calculated using the EnergySet code [22] based on the reaction tables of Ref. [23] and the stopping powers of Ref. [24]. Neutron spectra measurements at the IRMM VdG were performed recently using the time-of-flight technique [25]. A detailed measurement of neutron spectra will be carried out soon using a single crystal diamond detector [26].

Absolute neutron fluences are measured using thin foils from materials with well known excitation functions in the considered energy region and with similar threshold energies as those of the (n,t) reactions, see Figure 15. The time dependence of the neutron flux is measured by a long counter detector in relative terms [27].

Figure 15: Examples of excitation functions of neutron fluence monitors: ^{93}Nb(n,2n)^{92m}Nb [29], ^{90}Zr(n,2n)^{89}Zr [30], ^{59}Co(n,2n)^{58}Co [30]

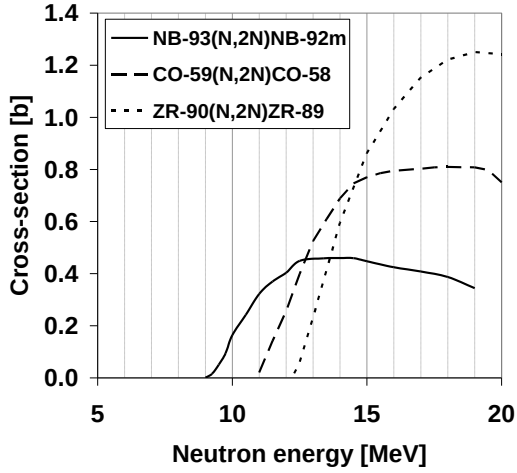

γ*-spectrometry*

Activated samples and monitor foils are measured in the IRMM VdG laboratory with a HPGe spectrometer (100% rel. efficiency) surrounded by a 10 cm Pb shielding (of which the inner 3 cm are low in ^{210}Pb) with an inside 1 mm Cu layer.

In the case of a low activity measurement, samples are measured in IRMM's Ultra Low-level Gamma-ray Spectrometry (ULGS) facility located in the underground laboratory HADES, on the premises of SCK·CEN, situated at a depth of 225 m. Seven HPGe spectrometers are presently in operation there; all detectors are constructed using specially selected radiopure materials optimized for use underground. The detector shieldings are composed of 15-20 cm of Pb lined with 5-15 cm of electrolytic Cu. The best present value of background is 220 counts/day/kg of Ge (in the energy region 40-2700 keV) [28].

The chromium experiment

The $^{50}Cr(n,t)^{48}V$ reaction is the first one we measured and is described in detail in this section. The experimental data at 14.6 MeV measured by liquid scintillation technique differ by a factor of 3; huge discrepancies (five orders of magnitude) are observed between the experimental data and theory, see Figure 2. This energy region is especially intricate as it is a steeply increasing part of the excitation curve.

Experimental data at higher energies were measured recently using γ-spectrometry [10]. Good agreement can be seen for experimental data and TALYS calculations in the region between 18 and 21 MeV. The experimental point at 17.3 MeV is twice as much as the TALYS calculation. This could indicate that TALYS underestimates cross-sections for $E_n < 18$ MeV. The JENDL-3.3 library underestimates experimental data in the whole energy range.

We decided to repeat the 17.3 MeV experiment in order to check if we get the same result as V. Semkova *et al*. [10] and to measure $^{50}Cr(n,t)^{48}V$ at two lower neutron energies to prove whether early experimental data or TALYS calculations correspond to reality.

Irradiation

The expected low cross-sections (~10-100 μb) required massive samples and long irradiation time. Three ^{nat}Cr samples (4.345% abundance of ^{50}Cr) in form of discs with 5 mm in thickness and 30 mm in diameter ($m \approx 25$ g) were irradiated at the same time. The 3.5 MeV deuteron beam was directed to a tritium target and the produced neutron field was used to irradiate the three Cr samples. They were placed at the angles of 95°, 81°, 63° with respect to the incident deuteron beam, which resulted in the irradiations with neutrons with the energies of (15.0±0.6), (16.0±0.4), (17.3±0.4) MeV, respectively.

Thin foils of Zr (0.15 mm thick) and Nb (0.05 mm thick) were used as beam monitors, see Figure 15. They were placed in front of and behind each Cr sample.

Measurement

After 12 days of irradiation, the activities of monitor foils were measured with a HPGe detector at IRMM. The Cr samples were transported to the HADES laboratory, where each sample was measured on two different HPGe detectors (a 60% rel. eff. coaxial detector and a 50% rel. eff. planar detector - BEGe-type); a single measurement lasted about 7 days. The Cr samples were placed in special Teflon containers with centring rings, in order to assure that the samples are placed in the centre of each container. The distances between a Cr sample and a detector endcap were 1.8 and 2.0 mm (for the two different detectors used).

The ^{48}V activities in the samples immediately after the irradiation were ~ 100 mBq. The total sample activities were dominated by ^{51}Cr (~ 10 kBq) coming from the $^{52}Cr(n,2n)^{51}Cr$ reaction, but the detection limits of ^{48}V were not seriously affected due to the lower energy of the ^{51}Cr γ-ray (320 keV).

Data analysis

Data analysis was performed using the two following γ-lines of ^{48}V ($T_{1/2} = 15.9735$ d): $E_\gamma = 983.525$ keV with $I_\gamma = 99.98\%$ and $E_\gamma = 1312.106$ keV with $I_\gamma = 98.2\%$ [31]. Standard spectroscopy corrections were applied to calculate the number of produced ^{48}V nuclei in each Cr sample; the neutron fluences obtained from monitor foils were used to calculate the $^{50}Cr(n,t)^{48}V$ cross-sections.

The EGS4 (Electron–Gamma–Shower) Monte Carlo code [32] was used to simulate the full energy peak efficiencies of the HPGe detectors. The simulations were based on the following data:

- the measured dimensions and estimated composition of samples (homogeneous activity distribution in samples assumed),
- the manufacturer's information on dimensions of HPGe detectors,

- the dimensions of Ge deadlayer and crystal position when cooled derived from detector radiographs followed by experimental calibration measurements performed with standardized point-like sources.

EGS4 was also used for the determination of cascade coincidences, which resulted in the correction factor of up to 40%. Isotropic and uncorrelated γ-ray emissions were assumed.

The reported uncertainties are the combined standard uncertainties (coverage factor k=1). The following components contribute to the total uncertainties:

- the uncertainty of the efficiency determination (which is about 5%, as obtained through validations in proficiency testing exercises [33]),
- the systematic uncertainty caused by inhomogeneous activity distribution inside Cr samples (about 2% as estimated from EGS4 simulations),
- the statistical uncertainty of the Gaussian fit of γ-peaks (2-7%).

Other sources of uncertainties like measurement time, half-life, γ-emission probability are negligible (less than 0.1%).

Results and discussion

The measured cross-sections are plotted in Figure 16. The cross-section at 17.3 MeV is slightly higher than the one measured by V. Semkova [10], but still in a reasonable agreement. The trend down to lower energies is clear - the cross-sections at 15 and 16 MeV are significantly below the earlier experimental data at 14.6 MeV. At the same time, they are one order of magnitude higher than TALYS and JENDL-3.3 at 16 MeV and two orders of magnitude higher at 15 MeV.

Figure 16: Experimental cross-sections of ^{50}Cr(n,t)^{48}V reaction (data presented in this paper are highlighted in red) compared with JENDL-3.3, cross-section systematics, and TALYS calculations

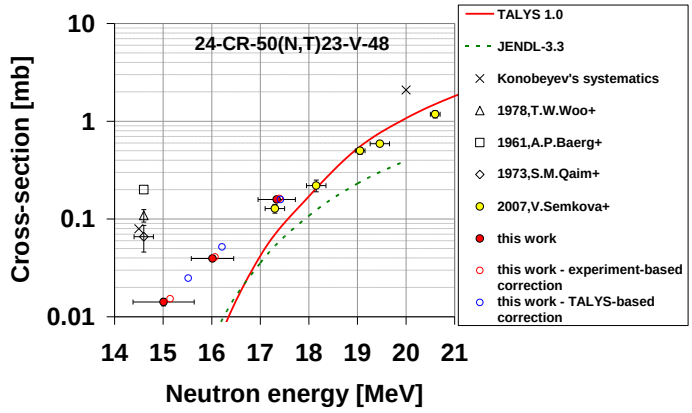

Large uncertainties in neutron energies are due to the big size of the samples covering large angles and resulting in broad neutron spectra in each sample. Because the high energy part of the neutron field passing a Cr sample contributes more to the reaction rate than the low energy part, the effective cross-section at the mean energy is not close to the actual cross-section at the mean neutron energy taken in the usual sense $\langle E\rangle_1 = \frac{\int E\phi dE}{\int \phi dE}$. Instead we investigated whether a closer match would be obtained with a mean energy given by $\langle E\rangle_2 = \frac{\int E\sigma\phi dE}{\int \sigma\phi dE}$. To determine this energy an energy dependence of the cross-section must be assumed. The excitation function $\sigma(E)$ was fitted with the power law $\sigma(E) \sim E^{\alpha}$ for the two cases – the experimental trend and the TALYS prediction (the JENDL prediction gives almost the same α-coefficients in the 15-17.3 MeV region). The required

neuron spectra were obtained from EnergySet. In addition, the cross-sections values were corrected according to the calculated difference between $\langle\sigma\rangle = \frac{\int\sigma\phi dE}{\int\phi dE}$ and $\sigma(\langle E\rangle_2)$ for the power law.

The corrected cross-sections at the corrected mean energies are plotted in Figure 16. It is obvious that they are strongly model dependent. The next apparent finding is that even the TALYS-based correction does not help to reach agreement between the measured values and the TALYS calculations. In fact, the excitation curve from either set of corrected values remains unaltered. The experimental results show that TALYS strongly underestimates the excitation curve in the 15-17 MeV energy region and it seems that the excitation curve has a more moderate slope in this energy region, while the steep part is at lower energies.

Conclusion and outlook

We measured the cross-sections of $^{50}Cr(n,t)^{48}V$ at 15-17.3 MeV. The trend of the results confirm that while early experimental data at 14.6 MeV are strongly overestimated, the calculations performed with the default version of TALYS strongly underestimate the excitation curve in the measured energy region.

We intend to perform fine tuning of TALYS nuclear models parameters for the description of triton emission. The reason for systematic overestimations of data at 14.6 MeV is also an issue to investigate.

We plan to measure $^{50}Cr(n,t)^{48}V$ at 14 MeV and (n,t) cross-sections for other isotopes between 15 and 21 MeV. To suppress the large uncertainties in neutron energy, we consider to repeat some of the measurements using larger target-sample distances, which should be possible as the counting statistics were sufficient.

Acknowledgements

We are grateful to the VdG operators Carlos Chaves de Jesus, Thierry Gamboni, and Wouter Geerts (in alphabetical order) for the dedicated work to reach conditions necessary for a successful irradiation.

References

[1] Lucas, L.L., M.P. Unterweger, *Journal of Research of the National Institute of Standards and Technology* 105, 541-9 (2000).

[2] Qaim, S.M., R. Wölfle, *Nuclear Physics* A 295, 150-162 (1978).

[3] Koning, A.J., S. Hilaire, M.C. Duijvestijn, *AIP Conf. Proc.* 769, 1154-9 (2005).

[4] Konobeev, A.Yu., Yu. A. Korovin, *Atomic Energy* 85, 556-563 (1998).

[5] *Qtool: Calculation of reaction Q-values and thresholds*, T-2 Nuclear Information Service, LANL, USA, *http://t2.lanl.gov/data/qtool.html*.

[6] Audi, G., A. H. Wapstra, C. Thibault, *Nucl. Phys.* A 729, 337-676 (2003).

[7] Woo, T.W., G.N. Salaita, *Transactions of the American Nuclear Society* 28, 91 (1978).

[8] Baerg, A.P., G.C. Bowes, *Canadian Journal of Chemistry* 39, 684 (1961).

[9] Qaim, S.M., G.L. Stoecklin, *Journal of Inorganic and Nuclear Chemistry* 35, 19 (1973).

[10] Semkova, V., *et al.*, *Proc. of ND2007*, Nice, France, pp 559-562 (2008).

[11] Semkova, V., A.J.M. Plompen, D.L. Smith, *Proc. of ND2004*, Santa Fe, Vol.1, p.1019 (2005).

[12] Wang Yongchang, *et al.*, *High Energy Phys. and Nucl. Phys.* (Chinese ed.), 17, 289 (1993).

[13] Katoh, T., K. Kawade, H. Yamamoto, JAERI-M Reports 89-083 and 89-026, p. 293 (1989).

[14] Sudar, S., J. Csikai, *Nuclear Physics* A 319, 157 (1979).

[15] Qaim, S.M., G. Stoecklin, *Nuclear Physics* A 257, 233 (1976).

[16] Woo, T.W., G.N. Salaita, *Proc. Conf. Nucl. Cross-Sections F. Techn.*, Knoxville, USA, p. 853 (1979).

[17] Fessler, A., Kernforschungsanlage, Jülich, report series No.3502 (1998).

[18] Diksic, M., P. Strohal, I. Slaus, *Journal of Inorganic and Nuclear Chemistry* 36, 477 (1974).

[19] Chittenden Ii, D.M., D.G. Gardner, R.W. Fink, *Physical Review* 122, 860 (1961).

[20] Garrett, P.E., *et al.*, *Physical Review* C 62, 054608 (2000).

[21] Interactive Chart of Nuclides, www.nndc.bnl.gov/chart.

[22] Lövestam, G., JRC-IRMM internal report GER/NP/2/2002/06/20, Geel, Belgium (2002).

[23] Liskien, H., A. Paulsen, *Atomic Data and Nuclear Data Tables* 11, 569-619 (1973).

[24] Ziegler, J.F., J. P. Biersack, *SRIM-2000 v.40*.

[25] Nuclear Energy Agency (NEA), "Neutron activation cross-section measurements from threshold to 20 MeV for the validation of nuclear models and their parameters", *International Evaluation Co-operation*, Vol. 19, NEA/WPEC-19, OECD/NEA, Paris (2005).

[26] Pillon, M., *et al.*, "Experimental Response Functions of a Single-Crystal Diamond Detector for 5-20.5 MeV Neutrons", submitted to *Nucl. Instr. and Meth. A*.

[27] Leroy, J.L., J.L. Huet, J. Gentil, *Nucl. Instr. and Meth.* 88, 1-11 (1970).

[28] Andreotti, E., *et al.*, to be published in *Proc. 3rd Int. Conf. on Current Problems in Nuclear Physics and Atomic Energy - NPAE*, Kyiv (2010).

[29] Vonach, H., *Nuclear data standards for nuclear measurements*, Ed. H. Condé, Report NEANDC – 311"U", INDC(SEC)-101, OECD/NEA (1992).

[30] Chadwick, M.B., *et al.*, *Nuclear Data Sheets* 107, 2931-3060 (2006),
See also www.nndc.bnl.gov/exfor/endf00.htm.

[31] Burrows, T.W., *Nuclear Data Sheets* 107, 1747 (2006).

[32] Nelson, W.R., H. Hirayama, D.W.O. Rogers, SLAC Report 265 (1985).

[33] Andreotti, E., *et al.*, "The half-life of the beta decay ^{115}In (9/2+)→^{115}Sn (3/2+)", submitted to *Physical Review C*.

High-energy neutron beams at U120-M cyclotron in NPI Řež – Nb activation cross-section studies

M. Honusek,[1] P. Bém,[1] U. Fischer,[2] M. Götz,[1] J. Novák,[1] S.P. Simakov,[3] E. Šimečková[1]
[1]Nuclear Physics Institute, Řež, Czech Republic
[2]Karlsruhe Institute of Technology, Karlsruhe, Germany
[3]Nuclear Data Section, International Atomic Energy Agency, Vienna, Austria

Abstract

The Nb-Zr alloy (99% niobium and 1% zirconium) presents a constituent part of construction material for the high-flux test module of IFMIF (International Fusion Material Irradiation Facility). Therefore systematic studies of neutron activation of ^{93}Nb in both the white ($p+D_2O$) - and quasi-monoenergetic ($p+^{7}Li$) neutron fields at neutron energies relevant to IFMIF were carried out using the NPI cyclotron-based fast neutron facility. The nuclear spectroscopy methods with HPGe detector technique were used to obtain the activities of produced isotopes.

Seven proton beam energies between 19.8 and 37.4 MeV were used to produce quasi-monoenergetic neutrons. Reactions (n,2n), (n,3n), (n,4n), (n,^{3}He), (n,α) and (n,2nα) were investigated. Nb cross-section data for neutron energies higher than 22.5 MeV do not exist in the literature.

The reactions (n,2n), (n,3n) and (n,4n) only were observed in the experiments with white neutron spectrum. Integral benchmark – C/E values (E means experimental results and C means calculated ones) are discussed.

Measured activation data are compared with predictions of the EAF-2007 library.

Introduction

Two neutron generators are employed to study cross-section data using activation foils method. Both generators are based on proton beam (maximum energy of 40 MeV) of Rez U120-M isochronous cyclotron. Rez apparatus is described in details in ref. [1]. One neutron generator is based on p+D_2O reaction and produces white (IFMIF like) neutron spectrum. Second generator is based on p+^{7}Li reaction and produces quasi-monoenergetic neutron (QME) spectra. We are able to measure cross-section data at incident neutron energies higher than 20 MeV, where such data are scarce. The irradiated foils are studied using gamma-spectroscopic technique.

Isotopes obtained in the reactions (n,2n), (n,3n), (n,4n), (n,^{3}He), (n,α) and (n,α2n) on ^{93}Nb were studied using p+^{7}Li reaction (quasi-monoenergetic neutrons). The reactions (n,2n), (n,3n) and (n,4n) only were observed [2] in the experiments using p+D_2O reaction (white spectrum of neutrons). According these measurements the experimental cross-section values (QME) and C/E values (white spectrum) are obtained. (E means experimental results and C means calculated ones). In both cases the experimental results are compared with predictions of EAF-2007 library [2]. The cross-section data for Nb for neutron energies higher than 23 MeV do not exist.

Neutron spectra

White spectrum (p+ D_2O)

Heavy-water-stream target (~ kW beam-power) is used to produce white spectra at proton beam energy of 37 MeV. Mean neutron energy is 13.9 MeV, energy range is up to 33.0 MeV. Flux density is up to 3x10^{11} n/cm^2/s for 15 μA of proton beam. The neutron spectrum for proton beam energy 37 MeV, beam current of 15 μA and distance from D_2O target 3 mm is shown in the Figure 1.

Figure 1: White neutron spectrum (p+D_2O), see text

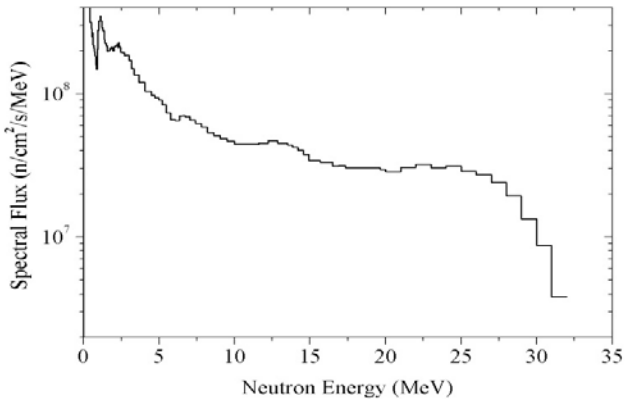

Spectra were determined by combination of dosimetry foils method (experiment) and the MCNPX simulation of experimental setup [3].

Quasi-monoenergetic spectrum (p+^{7}Li) (QME)

^{7}Li (C backing to stop protons) target is used to produce QME spectra. It reliably operated at beam-power of 600 W. Proton beam energy range is 18-38 MeV. Flux density is ~ 10^8 n/cm^2/s calculated (in peak) for 30 MeV and 1 μA proton beam at minimum t-s distance of 50 mm. The scheme of reaction chamber is shown in the Figure 2.

Quasi-monoenergetic spectrum (p+ ^{7}Li) consist of quasi-monoenergetic part corresponding to the reactions to g.s. and 0.429 MeV state in ^{7}Be, low-energy tail generated by reactions on ^{7}Li leading to further excited states in ^{7}Be, other reactions on ^{7}Li and reactions of protons on carbon stopper. See Figure 3.

Figure 2: Scheme of reaction chamber for QME neutron production (p+^{7}Li)

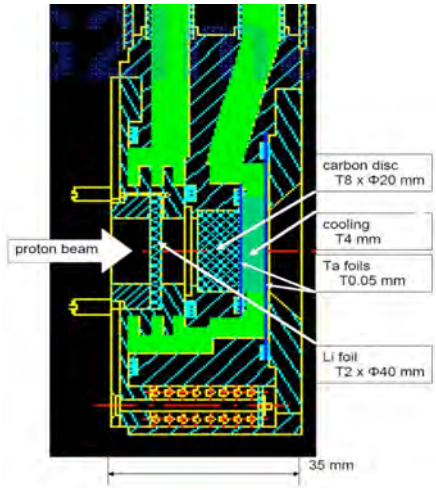

Figure 3: Typical spectrum of QME neutrons (p+^{7}Li reaction). Carbon stopper included.

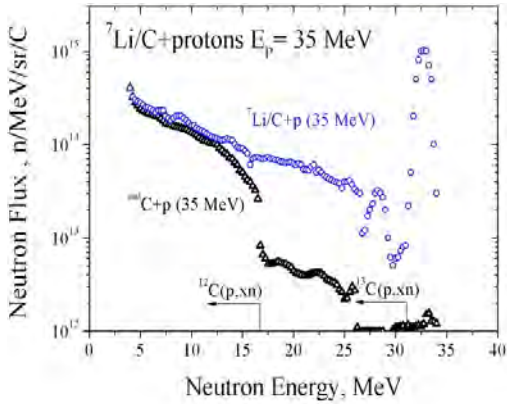

Two sets of neutron spectra are used in our analysis.

Spectra adopted from TOF data of Y.Uwamino et al. [4]. Simple r-square law is utilized and geometry factors are neglected.

Spectra calculated by the MCNPX simulation of present experimental setup, S.P.Simakov et al., [5]. Simulated data included experimental geometry conditions (Li foil, thick C beam stopper, alcohol coolant, flanges and experimental hall). MCNPX and LA-150h proton cross-sections library were used for this purpose.

Experimental conditions

Nb foils diam. 15 mm and weight approx. 0.75 g were irradiated.

Measurement using white spectrum, p+D_2O source. The distance of the foil to neutron source was 57 mm, typical proton beam current was 15 μA and typical irradiation time was 20 h.

Measurements using quasi-monoenergetic spectra, p+^{7}Li source. The distances of Li target to foils were of 48 and 88 mm. Typical proton beam was 3 μA and typical irradiation time was 20 h. Proton beam energies of 19.8, 25.1, 27.6, 30.1, 32.6, 35.0 and 37.4 MeV were used.

Proton beam intensity vs. time was recorded.

The activities of obtained isotopes were measured by methods of gamma spectroscopy. For this purpose two HPGe detectors of 23 and 50% efficiencies and resolution of 1.8 keV at 1.3 MeV were utilized. Spectra were measured at different cooling times. Activated isotopes were identified on the basis of $T_{1/2}$, γ-ray energies and intensities.

Observed isotopes (reaction) are shown in Table 1.

Table 1: Isotopes obtained in the reaction of neutrons on Nb target

Isotope	$T_{1/2}$	Reaction	Threshold (MeV)
Nb90	14.60 h	(n,4n)	29.078
Nb91m	60.86 d	(n,3n}	16.999
Nb92m	10.15 d	(n,2n)	9.063
Y91m	49.71 m	(n,He3)	8.362
Y90m	3.19 h	(n,α)	0
Y88	106.65 d	(n,α 2n)	13.554

Experimental results and their errors

Experimental results (RR) are obtained in the form: Activity / 1 μC of proton beam / 1 kg target. In the case of the reactions (n,2n) and (n,α) we have firstly to subtract low energy bump, En<20 MeV. The library EAF-2007 is used for these purposes.

RR ~ ∫ spectrum(E) x CS(E) x d(E) → CS(E), RR ~ ∑ spectrum(E) x CS(E) ΔE. We have more neutron spectra; therefore we have to solve set of equations to obtain cross-sections (CS).

The errors (assumed as an estimation of standard deviation) are presented in Table 2.

Table 2: Error estimations

Error of proton-beam current from Y.Uwamino [4] (TOF)	10%
Error of our proton-beam current	5%
Estimation of the uncertainty of spectra simulation MCNPX [5] QME peak	10%
Estimation of the uncertainty of D2O spectrum [3] Ep < 25 MeV	6%
Estimation of the uncertainty of D2O spectrum [3] Ep> 25 MeV	20 – 30%
Error of activity measurement	min 3%

The uncertainty of MCNPX (QME) simulated spectra in the low-energy tail is under investigation. The possible effect of proton beam energy uncertainty is discussed in the next parts.

The errors of the activity measurement only are shown in the next figures.

Cross-sections and C/E results obtained in the experiments

Experimental results are presented in the next part. The cross-section values obtained using QME spectra are analysed for both distances source – foil (48 and 88 mm) using UwTOF [4] and MCNPX [5] spectra. In the cases of reactions (n,xn) the results are compared with C/E ratios obtained in the white spectra measurements. EXFOR data are shown as well.

The results are compared with EAF-2007 database. These values included the decays throw isomeric states, if needed. All possible channels are included as well (*e.g.* (n,α) means (n,α+)).

The low energy tail in the reactions (n,2n) and (n,α) is subtracted using EAF-2007 library.

The energy bins of VITAMIN J+ structure for energies > 17.33 MeV seems to be too wide.

Reaction (n,2n)

QME. The effect of low energy tail is important, error of subtracted part is assumed as 5%. The higher energy bump (when we use TOF spectra) in the cross-section behaviour seems to be unphysical. The MCNPX correctly simulated geometry of the experiment. See Figure 4. The overall agreement of experimental and EAF-2007 cross-section data is seen.

Figure 4: Reaction (n,2n), QME spectrum

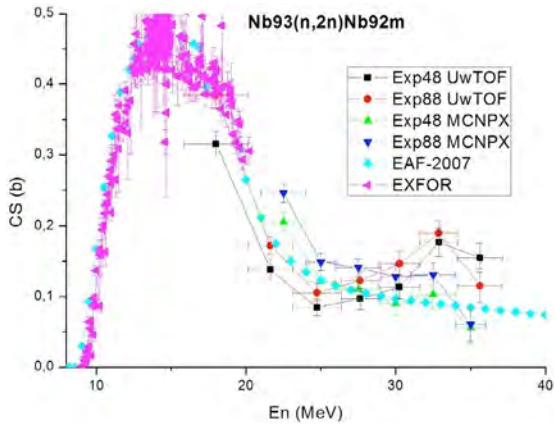

White spectrum. Obtained C/E value is 0.951, error is 3%. Error due to the 3% possible uncertainty of proton beam energy is 3%.

Reaction (n,3n)

QME. EAF-2007 overestimates measured CS data. We can estimate C/E ratio as ~ 1.4 – 1.5. See Figure 5.

Figure 5: Reaction (n,3n), QME spectrum

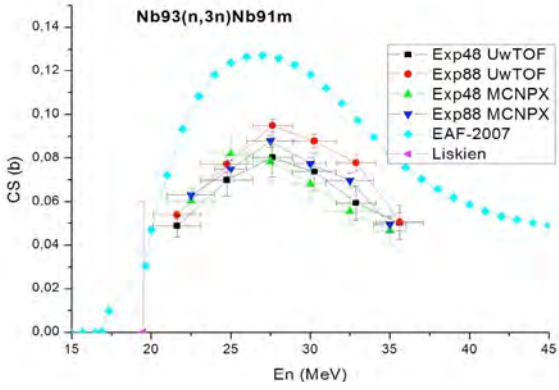

White spectrum. C/E = 0.803, error 9%. Error due to the 3% uncertainty of proton beam energy is 10%. For the agreement between QME and white spectrum we need two standard deviations including both the error of the white neutron spectrum and error due to the uncertainty of beam energy.

Reaction (n,4n)

QME. EAF-2007 overestimates CS data. We can estimate C/E ratio as ~ 2.5. See Figure 6.

Figure 6: Reaction (n,4n), QME spectrum

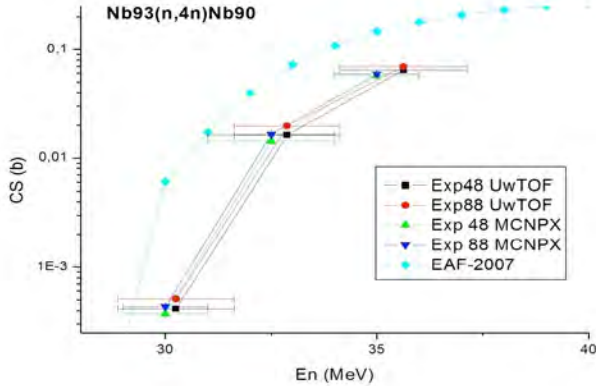

White spectrum. C/E =2.32, error 13%. The values estimated from QME spectra and white spectrum agree. But we have to take into account that only points of white spectrum with energies higher than 30 MeV are included and the error of neutron spectrum is 20 – 30%. Moreover, error interval due to the uncertainty of 3% of proton beam energy is 0.3 – 3. Even for the beam energy uncertainty of 1% the error interval is 0.75 – 1.7.

Reaction (n,α)

The effect of low energy tail of the spectrum is important, error of subtracted part is assumed as 10%. EAF does not correctly describe the reaction. See Figure 7.

Figure 7: Reaction (n,α), QME spectrum

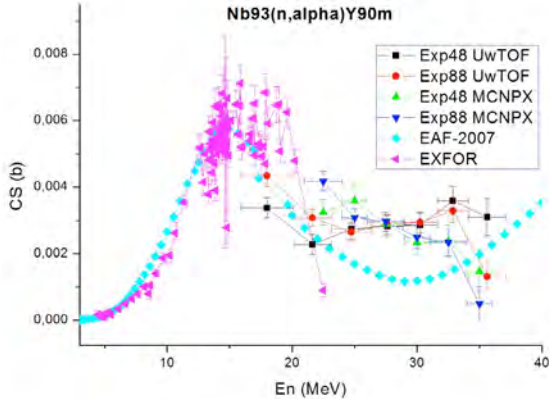

Figure 8: Reaction (n, ^{3}He), QME spectrum

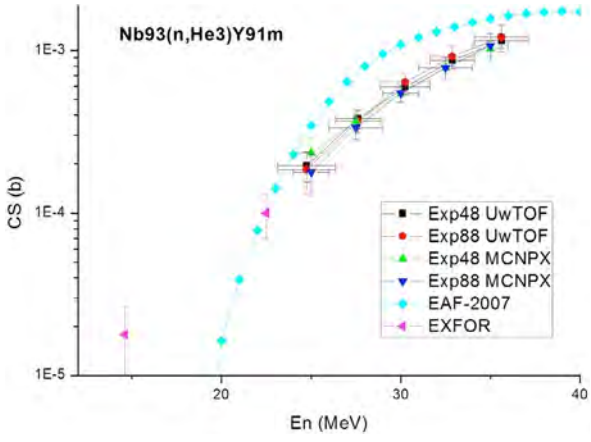

Reaction (n,^{3}He)

The library EAF-2007 overestimates experimental CS data. See Figure 8.

Reaction (n,α 2n)

The library EAF-2007 properly describes experimental CS data. See Figure 9.

Figure 9: Reaction (n, α 2n), QME spectrum

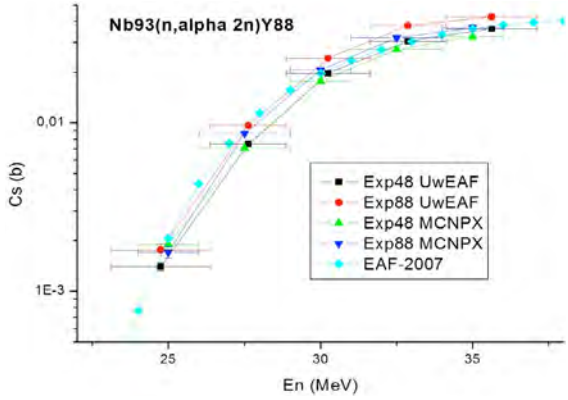

Some comments to the error analysis (QME neutrons)

Effect of subtraction of low-energy tail contribution to the experimental CS values

Subtracted parts effect is estimated using formula: M x ∫Neutr.sp.(En) x CS[EAF](En) dEn, En < our first exp. point. The coefficient M is a measure of deviation from EAF-2007 data.

Example Nb93(n,2n)Nb92m, MCNPX spectra, distance target foil 48 mm is shown on Figure 10. Errors of subtracted parts were assumed as 5%.

Example Nb93(n,α)Y90m, MCNPX spectra, distance target foil 48 mm is shown on Figure 11. Errors of subtracted parts were assumed as 10%.

Figure 10: Reaction (n, 2n), dependence on coeff. M

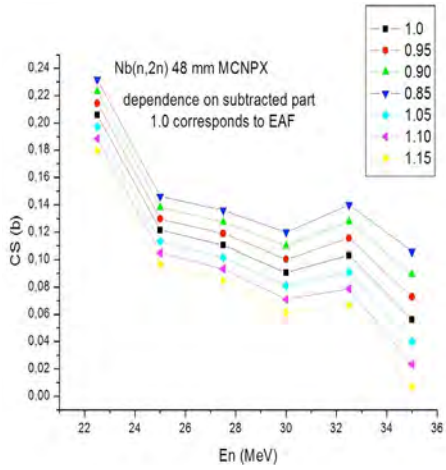

Figure 11: Reaction (n, α), dependence on coeff. M

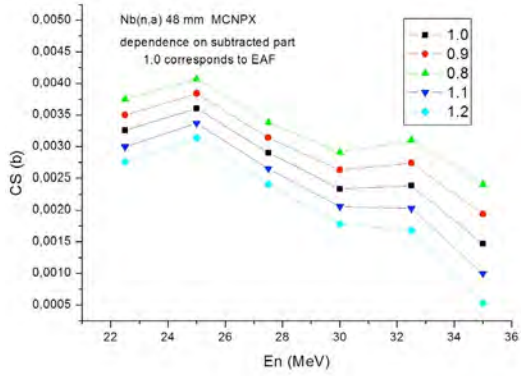

Error bars are not shown in the Figures 10 and 11 because of its complexity. Results for multiplication coefficient 1 and others are within errors or close to these values.

Effect of correlations coefficients obtained during the calculations of experimental data

It concerns all reaction. We assumed that the low energy tail in the reactions (n,2n) and (n,α) are already subtracted. We can formulate our problem RR=A*CS as the matrixes. Then the error matrix for CS is $(A'WA)^{-1}$, W_{ii} are weights of RR_i, otherwise zero.

Correlation coefficients are negative and usually small (~ -0.05). The effect of correlation coefficients is (in our cases) small.

Conclusions

Quasi-monoenergetic high energy neutrons based on p-^{7}Li source are used to study neutron reactions on ^{93}Nb target. Seven different proton beam energies were employed. We presented new cross-section data for neutron energies higher than 23 MeV. Results are compared with EAF-2007 library. Present data on (n,2n) and (n,α 2n) reactions well correspond to the EAF predictions, some under- and overestimations of EAF cross-sections are indicated for reactions, (n,α), (n,3n) and (n,^{3}He).

The data from measurements with QME neutrons are compared with results of integral benchmark experiments (by the C/E ratio) carried out with the white-spectrum neutrons from D2O source for the reactions (n,2n), (n,3n) and (n,4n). Both sets of data are in the agreement, but in the case (n,3n) reactions within two standard deviations only.

The sources of possible errors are analyzed.

The effect of energy-bin structure of VITAMIN J+ to simulation of the spectra and to cross-section data at higher energy region is indicated.

Acknowledgements

This work was supported partly by the Ministry of trade and industry CR (Project 1H-PK/07) and by Fusion for Energy under the grant contract No F4E-2008-GRT-014 (ES-AC). The views and opinions expressed herein reflect only the author's views. Fusion for Energy is not liable for any use that may be made of the information contained therein. The authors are indebted to the operating crew of the U-120M cyclotron for the ready assistance.

References

[1] Bém, P., *et al.*, "The NPI cyclotron-based fast neutron facility", *Proc. Int. Conf. on Nuclear Data for Science and Technology (ND 2007)*, Nice, France, p.555 (2007).

[2] Forrest, R.A., *et al.*, *Validation of EASY-2007 using integral measurements*, UKAEA FUS 547, UKAEA, United Kingdom (2008).

[3] Simakov, S.P., *et al.*, "Determination of neutron spectrum by the dosimetry foil method up to 37 MeV". *Proc. 13th International Symposium on Reactor Dosimetry*, Akersloot, The Netherlands, p. 532 (2009).

[4] Uwamino, Y., *et al.*, "High-energy p-Li neutron field for activation experiment", *Nucl. Instr. Meth.* A389, 463 (1997).

[5] Simakov, S.P., *et al.*, "Analysis of the dosimetry cross-section measurement up to 35 MeV with ^{7}Li(p,xn) quasi-monoenergetic neutron source", *Proc. Int. Conf. on Nuclear Data for Science and Technology (ND 2010)*, Jeju Island, Korea, forthcoming.

Deuteron activation measurements at energies up to 20 MeV Using NPI isochronous cyclotron

Eva Šimečková,[1] Pavel Bém,[1] Ulrich Fischer,[2] Miloslav Götz,[1] Milan Honusek,[1] Jaromír Mrázek,[1] Jan Novák,[1] Stanislav P. Simakov,[2] Milan Štefánik,[1] Lukáš Závorka[1]
[1]Nuclear Physics Institute As CR, Řež, Czech Republic
[2]Karlsruhe Institute for Technology, Karlsruhe, Germany

Abstract

The proton and deuteron induced reactions are of great interest for the assessment of the induced radioactivity of accelerator components, targets and beam stoppers as well as isotope production for medicine. In particular, the IFMIF (International Fusion Material Irradiation Facility) needs such data for estimation of the potential radiation hazards from the accelerating cavities and beam transport elements (Al, Fe, Cr, Cu, Nb) and metal and gaseous impurities of the Li loop (Be, C, O, N, Na, K, S, Ca, Fe, Cr, Ni). In order to investigate the first important nuclides relevant to the IFMIF, the irradiation experiments with the variable-energy cyclotron U-120M of the Nuclear Physics Institute Řež were carried out. The deuteron induced reaction cross-sections were investigated by irradiation of aluminium, copper, iron (natural isotope abundance) foils by deuteron beam of 20 MeV energy. The stacked-foil technique was utilized. The absolute values of cross-sections were calculated from the induced activities measurements by calibrated HPGe detectors. The comparison of present results with data of other authors and prediction of EAF-2007 library is discussed.

Introduction

The proton and deuteron induced reactions are of a great interest of induced radioactivity in the accelerator components, target and beam stoppers as well. In particular, the IFMIF facility needs such data for estimation of potential hazards from the accelerating cavities and beam transport elements. The cross-sections are needed in the energy range from the threshold up to 40 MeV both for deuterons and protons. The description of deuteron nucleus interaction presents an important test for both the quality of reaction mechanics models and evaluation of nuclear data request especially for fusion reactor technology.

FISPACT [1] is the inventory code included in the European Activation System (EASY), has been adopted by the ITER as the reference activation code. FISPACT has been developed for neutron-induced activation calculations for materials in fusion devices. From the version FISPACT-2007 it has been extended to proton- and deuteron-induced activation. FISPACT code uses external libraries (EAF-libraries) of reaction cross-sections. The deuteron cross-section data are recorded in VITAMIN-J+ (211 bins) standard group structure (up to 55 MeV).

The variable-energy NPI cyclotron provides protons and deuterons in the energy range 11-37 MeV and 11-20 MeV, respectively. A few years ago a program to verify the EAF-2007 charged particle cross-section data using NPI cyclotron was started. In the present paper, the experimental investigation of deuteron induced reaction cross-sections on aluminium, copper and iron (natural isotope abundance) is reported for deuteron energies up to 20 MeV.

Experimental procedure

Irradiation

The irradiation was carried out using an external deuteron beam of the NPI variable-energy cyclotron U-120M operating in the negative-ion mode of acceleration. From the stripping-foil extractor the beam was delivered to the reaction chamber through beam line consisting of one dipole - and two quadrupole magnets.

The incident deuteron energy was determined by the computational procedure based on measured trajectory (the frequency and actual extraction radius) of acceleration. This procedure was experimentally tested using the activation foil method and the surface-barrier-detector technique. The energy was determined with resulting accuracy of 1.0%, the FWHM spread of incident beam up to 1.8% was observed.

The activation cross-sections were measured by a stacked-foil technique. Collimated deuteron beam strikes the stack of foils in a Faraday-cup-like reaction chamber enabling to employ the cooling of stacked foils without the lost of accuracy in the beam current and charge monitoring (5%). Stacked foils were irradiated at 200–400 nA deuteron beam in a set of expositions for time up to 600 sec.

The high purity metallic foils (Goodfellow product) of Cu, Fe (25 μm declared thickness) and Al (50 μm declared thickness) were weighted (within 2% of accuracy) to avoid relatively large uncertainties in the foil thickness declared by producer. The mean energy, energy thickness and energy spread in each foil was set out by SRIM 2003 code [2]. The foils of examined elements (Cu, Fe) were inserted in the chamber by turn with the Al foils, which was utilized for additional monitoring of beam current and for appropriate reduction of deuteron energy as well.

Activity measurement

The gamma-rays from the irradiated foils were measured repeatedly by two calibrated HPGe detectors of 23 and 50% efficiency and of FWHM 1.8 keV at 1.3 MeV. Experimental reaction rates were calculated from the specific activities at the end of the irradiation corrected to the decay during irradiation using total charge and foil characteristic as well. The measurement with different cooling times lasted up to 100 days after irradiation.

Results

Aluminium and natural copper irradiation

As the first experiment, the high purity natural Al and Cu foils were bombarded by deuterons from U-120M NPI cyclotron with initial deuteron energy 20.4 MeV. Two irradiation runs were carried out with mean current 0.09 μA and 0.33 μA during 15 min and 5 min, respectively, to check internal consistency of the measurement.

In the Figure 1, the widely known values of the cross-sections for the (d,pα) reaction on ^{27}Al are shown. This reaction also served as a standard for normalization. From the picture where our data are compared to the data of others authors from EXFOR [3] and the recommended excitation function [3] is seen that present data are in overall agreement with other authors, slightly overestimating the recommended ones. The cross-sections of ^{27}Mg and ^{28}Al products with half life in range of minutes were measured as well [4,5].

Figure 1: The comparison of present data on the ^{27}Al(d,pα)^{24}Na excitation function with cross-section values from other authors from EXFOR database [3]. Only statistical errors and energy foil thicknesses are shown.

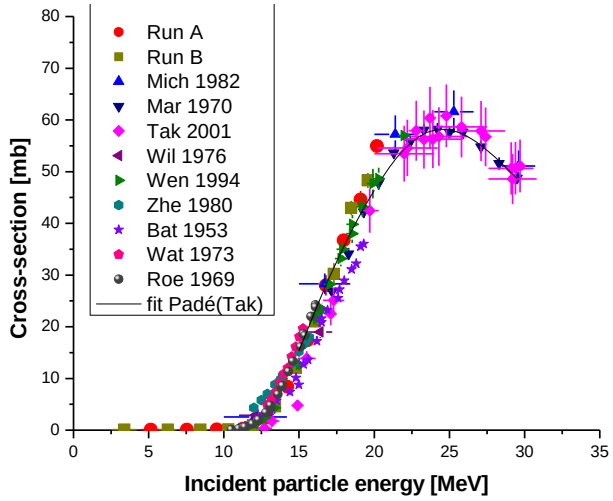

Figure 2: The comparison of present data on the ^{65}Cu(d,2n)^{65}Zn excitation function with cross-section values from other authors from EXFOR database [3] (data presented as natural copper reactions are converted to only deuteron induced reaction on ^{65}Cu) and EAF-2007 database. Only statistical errors and energy foil thicknesses are shown.

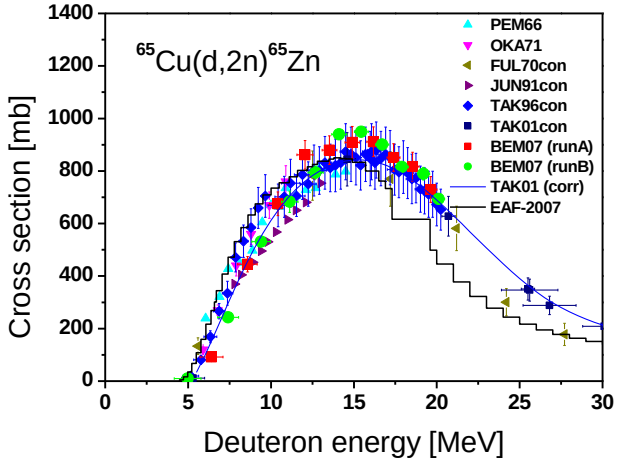

Natural copper consists of two stable isotopes – ^{63}Cu (69.2%) and ^{65}Cu (30.8%). As an example the ^{65}Cu(d,2n)^{65}Zn and ^{63}Cu(d,2n)^{63}Zn cross-sections are shown in Figures 2 and 3, respectively. The generation of ^{65}Zn by irradiation of the natural copper may proceed in two contributing reactions: radioactive capture ^{63}Cu(d,γ) (threshold 0 MeV) and ^{65}Cu(d,2n) (threshold 5.5 MeV) reaction, as well. The radioactive capture reaction is known to be very small. Hence, the ^{63}Cu(d,γ) reaction would not be expected to contribute significantly to the measured yield of ^{65}Zn. On the other hand it is only the ^{63}Cu(d,2n) reaction which can produces the ^{63}Zn in an energy range up to 25 MeV (when the ^{65}Cu(d,4n)^{63}Zn reaction starts). It is seen from the Figure 3 that the EAF-2007 data underestimate the experimental cross-sections in the energy region above 3 MeV.

Figure 3: The comparison of present data on the ^{63}Cu(d,2n)^{63}Zn excitation function with cross-section values from other authors from EXFOR database [3] (data presented as natural copper reactions are converted to only deuteron induced reaction on ^{63}Cu) and EAF-2007 database. Only statistical errors and energy foil thicknesses are shown.

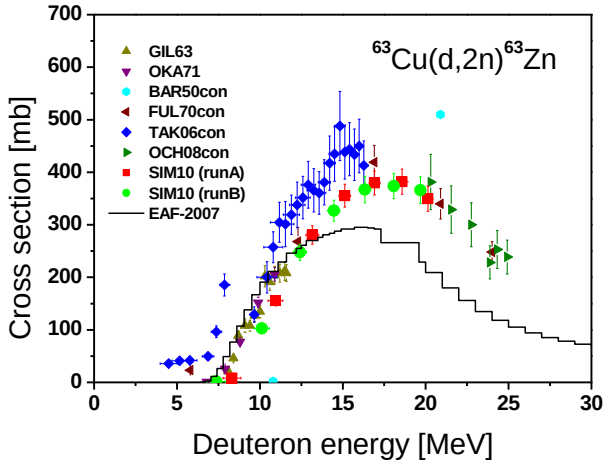

Natural iron irradiation

Natural iron consists of four stable isotopes – ^{54}Fe (5.8%), ^{56}Fe (91.8%), ^{57}Fe(2.1%) and ^{58}Fe (0.3%) – which leads to many channel opening. The irradiation was carried up in two runs to see inner consistency of results obtaining. The characteristic of single runs are in Table 1.

Table 1: The natural iron irradiation characteristics

Run	Initial energy [MeV]	Mean current [μA]	Irradiation time
A	20.01	0.20	30.33 min
B	20.04	0.24	27.44 min

The reaction ^{nat}Fe(d,*)^{56}Co belongs to the reactions recommended for the cross-section measurement normalization. The comparison of present results (Run A and run B are shown separately to see inner consistency of results derivation) with results of another authors from EXFOR database, recommended excitation function [3] and EAF-2007 cross-sections [1] (data are converted to a natural composition of iron) is shown in Figure 4.

In contrast to well explored reaction ^{nat}Fe(d,*)^{56}Co, the excitation function of the ^{nat}Fe(d,*)^{56}Mn is known very scarce. The reason is that the strong gamma-lines 846.8 keV (I_γ – 98.9%), 1810.77 keV (I_γ – 27.2%), 2113.12 keV (I_γ – 14.3%), decaying ^{56}Mn ($T_{1/2}$ = 2.5785 h) interfere with those lines from ^{56}Co ($T_{1/2}$ = 77.27 d) decay. To determine specific activity at the end of irradiation, the cooling time measurements were taken for a period up to 100 days. The experimental obtained dependence of activity on the time measurement was fitted to a sum of two exponential functions accordant with ^{56}Co and ^{56}Mn decays using MINUIT code [6] and the specific activities for the ^{56}Co and ^{56}Mn were obtained separately. The correctness of this approach is seen from Table 2, where the comparison

of specific activities at the end of irradiation calculated from different gamma-lines is shown. The $^{nat}Fe(d,*)^{56}Mn$ excitation function is shown in Figure 5 where it is seen the EAF-2007 cross-sections underestimate the experimental in the deuteron energy up to 12 MeV.

The present $^{nat}Fe(d,*)^{54}Mn$ cross-section data are in agreement with the previous experiments and slightly underestimate the EAF-2007 data in deuteron energy region up to 10 MeV, as it is seen from Figure 6.

Figure 4: The comparison of present data on the $^{nat}Fe(d,*)^{56}Co$ excitation function with cross-section values from other authors from EXFOR database [3], recommended values [3] and EAF-2007 database corrected for isotopic abundance. Only statistical errors and energy foil thicknesses are shown.

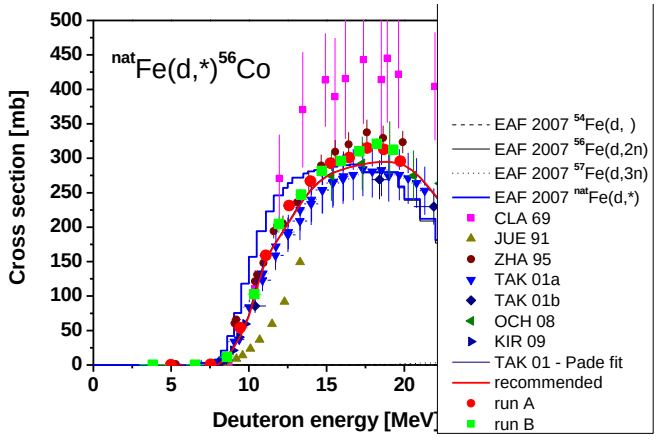

Table 2: The specific activity at the end of irradiation calculated from the interfered lines and from the rest of weak lines. E_d =19.3 (0.3) MeV.

Energy [keV]	^{56}Co Activity [Bq]	^{56}Mn Activity [Bq]
846.77	1.687E+4	5.667E+5
1810.77	1.768E+4	5.621E+5
2113.12	1.684E+4	5.513E+5
Others	1.680E+4	5.733E+5

Figure 5: The comparison of present data on the $^{nat}Fe(d,*)^{56}Mn$ excitation function with cross section values from other authors from EXFOR database [3] and EAF-2007 database corrected for isotopic abundance. Only statistical errors and energy foil thicknesses are shown.

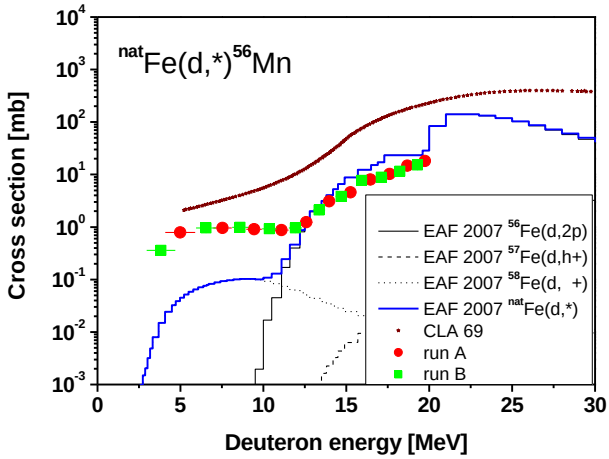

Figure 6: The comparison of present data on the $^{nat}Fe(d,*)^{54}Mn$ excitation function with cross section values from other authors from EXFOR database [3] and EAF-2007 database corrected for isotopic abundance. Only statistical errors and energy foil thicknesses are shown.

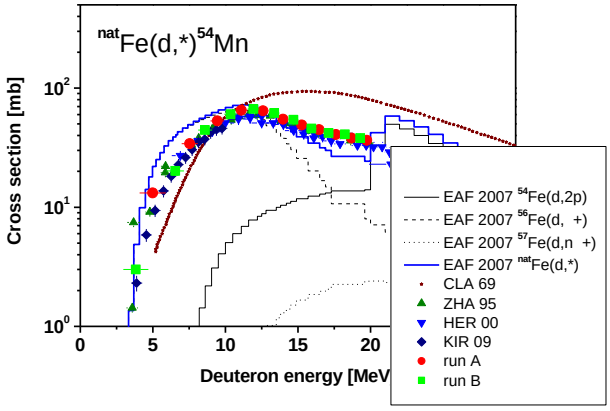

Figure 7: The comparison of present data on the $^{nat}Fe(d,*)^{52}Mn$ excitation function with cross section values from other authors from EXFOR database [3] and EAF-2007 database corrected for isotopic abundance. Only statistical errors and energy foil thicknesses are shown.

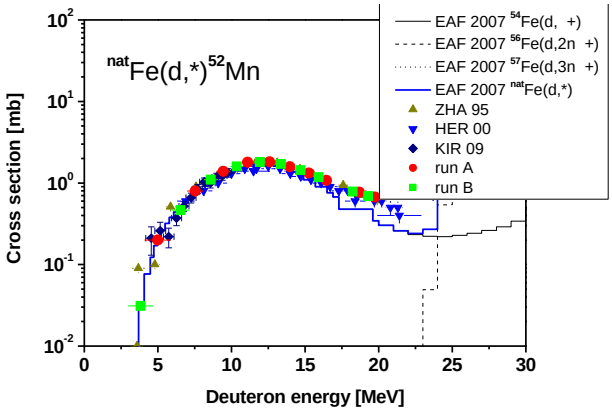

Figure 8: The comparison of present data on the $^{nat}Fe(d,*)^{52m}Mn$ excitation function with cross section values from other authors from EXFOR database [3] and EAF-2007 database corrected for isotopic abundance. Only statistical errors and energy foil thicknesses are shown.

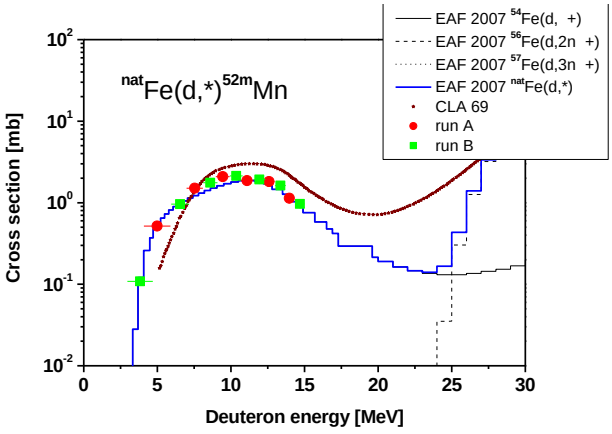

The ^{52}Mn ($T_{1/2}$ = 5.591 d) production cross-sections are actually $^{52(m+g)}$Mn ones, but only 1.7% (this effect is hidden in an experimental uncertainties) is fed from the isomeric state ($T_{1/2}$ = 21.1 m). This isomeric state decays mainly through 1434.07 keV (I = 98.3%) line which interferes with ^{52}Mn ground state decay. Using minimisation procedure [6] the ^{52m}Mn cross-section was determined. Excitation function for ^{nat}Fe(d,*)^{52}Mn and ^{nat}Fe(d,*)^{52m}Mn reactions are in agreement with the EAF 2007 data up to about 15 MeV as it is seen from Figures 7, 8.

While experimental Mn production cross-sections are in a sufficient agreement with the EAF-2007 prediction, the EAF-2007 library data overestimate the experimental data for the ^{55}Co (Figure 9) and ^{57}Co (Figure 10) production cross-sections (particular ^{54}Fe(d,n)^{55}Co and ^{56}Fe(d,n)^{57}Co – the main reaction channels).

Figure 9: The comparison of present data on the ^{nat}Fe(d,*)^{55}Co excitation function with cross section values from other authors from EXFOR database [3] and EAF-2007 database corrected for isotopic abundance. Only statistical errors and energy foil thicknesses are shown.

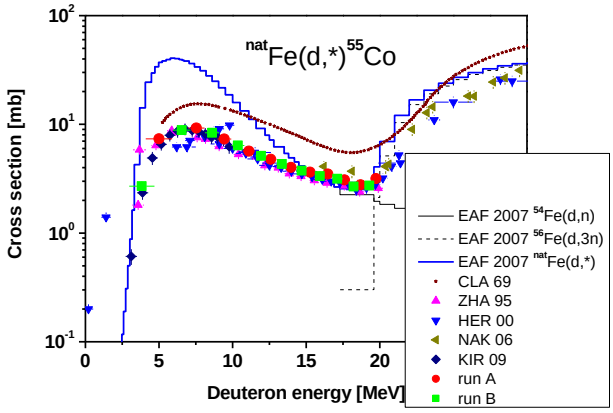

Figure 10: The comparison of present data on the ^{nat}Fe(d,*)^{57}Co excitation function with cross section values from other authors from EXFOR database [3] and EAF-2007 database corrected for isotopic abundance. Only statistical errors and energy foil thicknesses are shown.

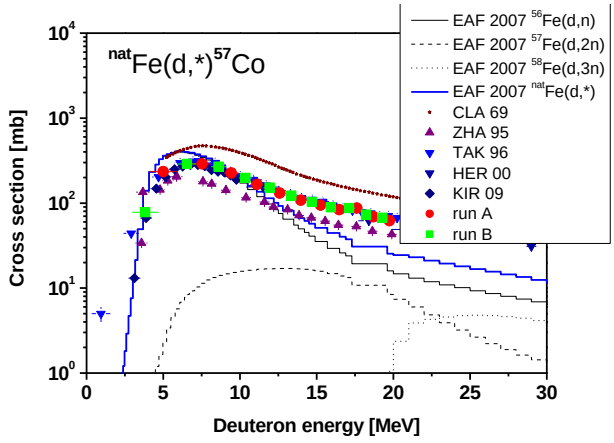

The ^{58}Co ($T_{1/2}$ = 70.86 d) has a long living metastable isomer ^{58m}Co ($T_{1/2}$ = 9.04 h) decaying through the 24.9 keV (I = 0.0389%) gamma-rays immeasurable by a HPGe detector. Moreover, the ^{58m}Co feeds the ^{58g}Co by 100%. It is used to obtain $^{58(m+g)}$Co production cross-section by measuring the product activity after long cooling time (90 days). Such results are shown in Figure 11. We did an attempt to specify ^{58}Co production cross-section for ^{58m}Co and ^{58g}Co in particular. To determine specific activities A^0_m and A^0_g at the end of irradiation equation (1) was minimized using MINUIT code [6].

$$A_g = \frac{\lambda_g}{\lambda_g - \lambda_m} A^0_m \left(e^{-\lambda_m t} - e^{-\lambda_g t}\right) + A^0_m e^{-\lambda_g t}, \quad (1)$$

Figure 11: The comparison of present data on the $^{nat}Fe(d,*)^{58}Co$ excitation function with cross-section values from other authors from EXFOR database [3]. Only statistical errors and energy foil thicknesses are shown.

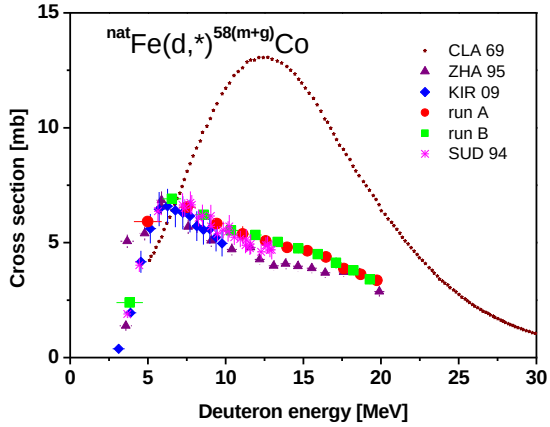

Figure 12: The comparison of present data on the $^{nat}Fe(d,*)^{57}Co$ excitation function with cross-section values from other authors from EXFOR database [3] and EAF-2007 database corrected for isotopic abundance. The results of SUD 96 [7] were performed by X-Ray spectrometric studies. Only statistical errors and energy foil thicknesses are shown.

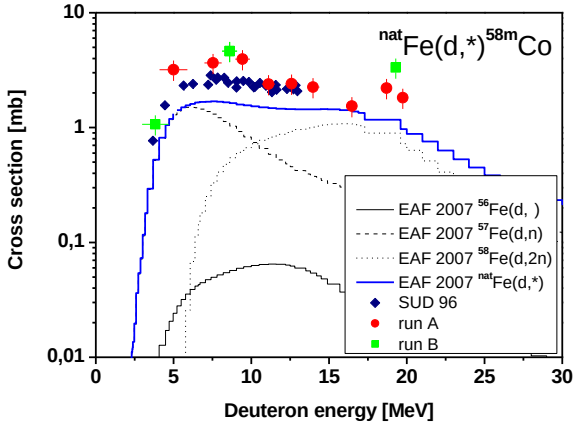

Figure 13: The comparison of present data on the $^{nat}Fe(d,*)^{57}Co$ excitation function with cross section values from other authors from EXFOR database [3] and EAF-2007 database corrected for isotopic abundance. Only statistical errors and energy foil thicknesses are shown.

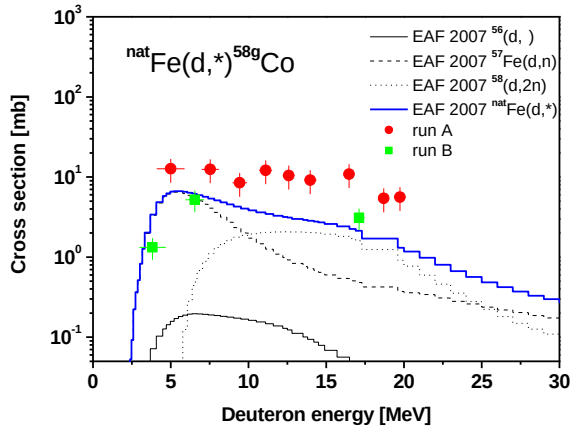

where Ag is the specific activity of the sample at cooling time t, λ_g and λ_m are the decay constant for ground and metastable isomer, respectively. Similar procedure was used for the determination of the correction of A^0_m and A^0_g for the decay during irradiation. In Figures 12 and 13 the evaluated (d,*) reaction cross-sections of meta-stable and ground-state of ^{58}Co are given. The ^{58m}Co production cross-section data [7] obtained by the X-ray spectroscopic studies using either Si(Li) or an intrinsic HPGe detector with Be window are shown in Figure 12.

The only reaction ^{58}Fe(d,p) produces ^{59}Fe isotope. The evaluated data underestimate the experimental ones as it is seen from Figure 14, where the EAF 2007 cross-section data are corrected for the natural abundance ^{58}Fe (0.3%).

The EAF 2007 cross-section data for the ^{nat}Fe(d,*)^{51}Cr reaction also slightly underestimate the experimental ones is it shown in Figure 15.

Figure 14: The comparison of present data on the ^{nat}Fe(d,*)^{59}Fe excitation function with cross section values from other authors from EXFOR database [3] and EAF-2007 database corrected for isotopic abundance. Only statistical errors and energy foil thicknesses are shown.

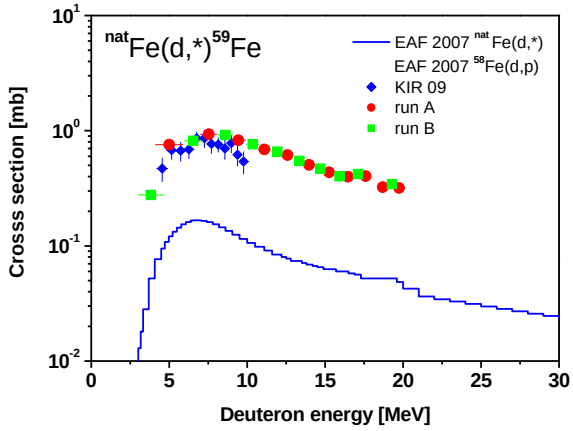

Figure 15: The comparison of present data on the ^{nat}Fe(d,*)^{51}Cr excitation function with cross section values from other authors from EXFOR database [3] and EAF-2007 database corrected for isotopic abundance. Only statistical errors and energy foil thicknesses are shown.

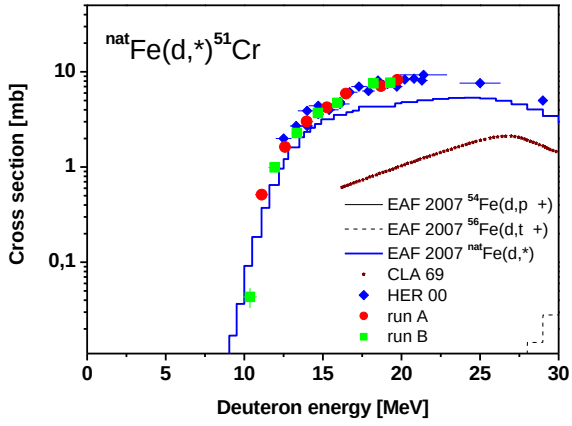

Conclusion

The deuteron induced activation cross-section measurements on Al, Cu and Fe natural samples were carried out using NPI variable energy cyclotron U120M and the gamma spectroscopy technique (HPGe) for the investigation of produced radioactive nuclides. The activation cross-sections were determined from induced specific activities related to the total charge of deuteron beam. In the determination of reaction rates, the time dependence of deuteron beam current was taken into account. Beside the mean statistical errors of about 3% in specific activities and energy foil thicknesses calculated using SRIM 2003 code shown in the figures, the systematic uncertainties are: the energy shift and energy spread of incident deuteron beam of about 1% and 1.8% respectively, the beam current measurements – 5% and the foil thicknesses – 2% (declared uncertainty was reduced by means of foil weighing). An improvement of monitoring characteristics (initial energy, beam charge measurement) is under progress.

Resulting cross-section data are in good agreement with the major part of previous reported experiments. Sufficient agreement is indicated in the comparison of present ^{54}Mn and ^{56}Co production cross-section data with those data from EAF-2007 library, especially the data of the ^{nat}Fe(d,*)^{52}Mn and ^{52m}Mn reactions. The EAF-2007 data for the ^{nat}Fe(d,*)^{56}Mn reaction underestimate the experiments in the energy region up to 10 MeV (where the only reaction ^{58}Fe(d,α+) contribute), and overestimate the experimental data for the production of ^{55}Co and ^{57}Co (where the main reaction channels are ^{54}Fe(d,n)^{55}Co and ^{56}Fe(d,n)^{57}Co, respectively). For the ^{59}Fe isotope (produced only through the ^{58}Fe(d,p) reaction), the EAF-2007 evaluation underestimate the experiment of about one order.

An attempt to determine cross-sections for ^{nat}Fe(d,*)^{58m}Co and ^{nat}Fe(d,*)^{58g}Fe separately was done as well. The ^{58m}Co cross-section values are in acceptable agreement with those data obtained by X-ray spectroscopic studies, the estimation of ^{58g}Co production cross-sections was made for the first time. However, the six cooling time measurements were not enough for a precise cross-section determination.

Present experimental investigation indicates necessity of further development of the EAF deuteron activation evaluation.

Acknowledgements

The work was supported partly by the NPI/KIT Karlsruhe contract and the grant of Czech Ministry of Trade and Industry No 2A-1TP1/101. The authors are indebted to the stuff of the NPI variable energy cyclotron U 120M for heavy-duty operation of the accelerator.

References

[1] Forrest, R.A., J. Kopecky, J.Ch. Sublet, *The European Activation File: EAF-2007 cross-section library*, UKAEA FUS 535, UKAEA, United Kingdom (2007).

[2] Ziegler J.F., J.P. Biersack, L. Haggmark, *The Stopping and Ranges of Ions in Solids*, Pergamon (1985), see *www.srim.org*.

[3] Experimental Nuclear Reaction Data (EXFOR), www-nds.iaea.org.

[4] Bém, P., *et al.*, "Low and medium energy deuteron-induced reactions on ^{27}Al", *Phys. Rev.* C **79**, 044610 (2009).

[5] Bém, P., *et al.*, "The activation of Cu and Al by deuterons at energies up to 20 MeV", *Proceedings of the International Conference on Nuclear Data for Science and Technology*, Nice, France, p. 1003 (2008).

[6] James, F., M. Foos, *Comp. Phys. Comm.* 10, 343 (1975).

[7] Sudár, S., S.M. Qaim, "Isomeric cross-section ratio for the formation of ^{58}Co^{m,g} in neutron, proton, deuteron, and alpha-particle induced reactions in energy region up to 25 MeV", *Phys. Rev.* C 53, 2885 (1996).

Cross-sections of neutron threshold reactions studied by activation method

J. Vrzalová,[1,2] **O. Svoboda,**[1,2] **A. Krása,**[1] **M. Majerle,**[1] **A. Kugler,**[1]
A. Laredo,[1] **M. Suchopár,**[1,2] **V. Wagner,**[12]
[1]Nuclear Physics Institute of the ASCR PRI, Řež, Czech Republic
[2]Faculty of Nuclear Sciences and Physical Engineering, Czech Technical University in Prague, Prague, Czech Republic

Abstract

The neutron cross-sections of various threshold reactions using different quasi-monoenergetic neutron sources based on proton reaction on ^{7}Li target were studied. The measurements were carried out in NPI ASCR in Řež near Prague and in TSL in Uppsala (Sweden) and neutron sources with energy range from 20 to 100 MeV were used. The last experiment was carried out in February 2010 in TSL Uppsala using proton beams with energies of 65, 70, 80, and 93 MeV. Cross-sections of (n,xn), (n,p) and (n,alpha) reactions in Au, Al, Ta, Bi, Y, In foils and iodine samples were determined. Activated foils and iodine samples were measured by the means of HPGe detectors and a wide range of spectroscopic corrections was applied. Our preliminary values of experimental cross-sections are compared with the results of TALYS code and also with data from EXFOR database. Many cross-sections were measured in the energy regions where no experimental data are available so far.

Motivation

Measurement of spatial distribution of neutrons is an important part of studies of spallation based experiments. The activation detectors are very useful tool for neutron field determination in this case. We use threshold reactions on gold, aluminium, bismuth, indium, tantalum, yttrium, and cobalt samples for neutron detection. Unfortunately, almost no experimental cross-section data for most of the observed threshold reactions are available above 30 MeV. Therefore, it is necessary to perform new cross-section measurements in this region.

Neutron sources

Our experiments relating to cross-section measurements took place in years 2008 and 2009 in the Nuclear Physics Institute (NPI) in Řež (four measurements) and in years 2008 and 2010 in The Svedberg Laboratory (TSL), Uppsala, Sweden (seven measurements). Proton beams of different energies were used (in TSL 25, 50, 62, 70, 80, 92 and 97 MeV, in NPI 20, 25, 32.5 and 37 MeV (Figure 1)). A high energy neutron source with well known monoenergetic spectrum is needed for cross-section studies. This source must be in addition high intensive in the case of measurements by means of activation method. Unfortunately, such an ideal source does not exist. The only available sources to use are quasi-monoenergetic, with not negligible continuum background. We used a neutron source based on the ^{7}Li(p,n)^{7}Be reaction. Approximately half of the neutrons were produced in the peak corresponding to the ground state and the first excited state at 0.43 MeV in ^{7}Be. The second half of the intensity was in the continuum in lower energies corresponding to higher excited states, multiple-particle emission etc.

In the NPI, the energy range of neutron source was between 10 and 37 MeV [1]. High energy protons from the cyclotron were lead to lithium target with carbon backing to stop protons. The thickness of the neutron source was 2 mm. The sample distances from the lithium target were 11 to 16 cm. The neutron flux density was 10^{8} cm^{-2}s^{-1}. The uncertainty of the neutron spectra determination was in this case 10 %. The uncertainty of the beam intensity determination was 5%. Time of single irradiation was about 20 hours and the process of irradiation was relatively stable. Neutron spectra are considered to be the same as in the work of Y. Uwamino [2].

Because of the relatively small source energy range in NPI (up to 37 MeV), the measurements were performed in TSL Uppsala. The energy range of TSL cyclotron is from 20 MeV to 180 MeV for protons [3]. The remaining part of proton beam behind the lithium target was deflected by a magnet and guided onto a graphite beam dump. The neutron beam was formed by 100 cm iron collimator and the maximum neutron flux density 10^{5} cm^{-2}s^{-1} was possible. Samples were located 373 cm from the lithium target. Time of single irradiation was about 8 hours. The uncertainty of the beam intensity determination was 10% and the uncertainty of the neutron spectra determination was also 10%. Our measurements in Uppsala were successful and confirmed the applicability of this source to such measurement of reactions used in our activation detectors.

Figure 1: Neutron spectra for different proton energies (NPI ASCR Řež)

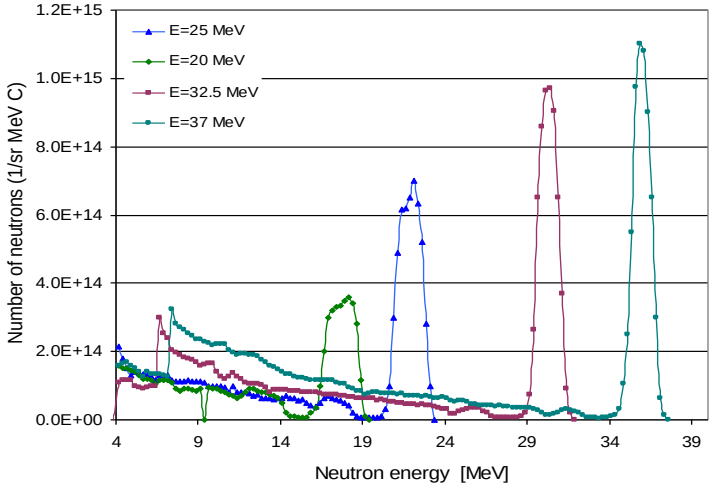

Cross-section measurements

Except the iodine the studied materials were in the form of foils of thickness ranging from 0.05 mm up to 1 mm. The weights of the foils were from 0.2 grams up to 7 grams. The foils were wrapped in paper, so the nuclide transport between the foils was minimized. The iodine samples were in the form of solid KIO_4 tablet packed hermetically in plastic. The samples were measured as soon as possible on the HPGe detectors. The uncertainty of the efficiency calibration of detectors was under 3%. Each foil was measured several times. The transport time of foils on HPGe detector lasted for two minutes in TSL and about 15 minutes in NPI.

Spectra from the HPGe detector were analyzed by the program DEIMOS32 after irradiation and measurement [4]. DEIMOS enables evaluation of the peak position and its area in defined part of the spectrum. The basic peak shape is Gaussian. The obtained areas of peaks contain information about detected photon numbers. Appropriate spectroscopic corrections have to be made during follow-up analysis. Among them are corrections on the decay during cooling, decay during irradiation and measurement, unstable irradiation, coincidences, non-point like emitter, detector dead time, detector efficiency, and self absorption. Spectroscopic corrections make about 1% uncertainty. Statistical uncertainty of the Gauss fit of the gamma peaks in the DEIMOS32 code depends on intensity and its value is usually between 1 % and 10%. Final uncertainty is set as a square root of the second powers of particular statistical and systematic uncertainties.

The total yield of observed radioactive nuclei per one gram of activated material and one neutron was calculated by Eq. (1):

$$N_{yield} = \frac{S_p \cdot C_{abs}(E)}{I_\gamma \cdot \varepsilon_p(E) \cdot COI \cdot C_{area}} \frac{t_{real}}{t_{live}} \frac{1}{m_{foil}} \frac{e^{(\lambda \cdot t_0)}}{1 - e^{(-\lambda \cdot t_{real})}} \frac{\lambda \cdot t_{irr}}{1 - e^{(-\lambda \cdot t_{irr})}}, \quad (1)$$

where S_p is the peak area, C_{abs} – self-absorption correction, I_γ – gamma line intensity, ε_p (E) – detector efficiency, COI – correction for real Coincidences, C_{area} – square-emitter correction, C_{abs} – self-absorption correction, t_{real}/t_{live} – dead time correction, m_{foil} – mass of foil and the last two fraction represents decay during cooling and measurement and decay during irradiation.

The yields calculated by the means of different gamma lines were used for mean value calculation. The cross-section value can be calculated with the knowledge of yield:

$$\sigma = \frac{N_{yield} \cdot S \cdot A}{N_n \cdot N_A}, \quad (2)$$

where S is the foil area, A – molar weight, Nn – number of neutrons in peak, NA – Avogadro's number.

To find gamma lines and half life of isotopes a database Lund/LBNL Nuclear Data Search was used [6].

Background subtraction

In the ideal case, the threshold energy of the observed reactions lied at the beginning of the neutron peak (*e.g.* ^{124}I in Figure 2). In real case radioisotope production by the background neutrons was mostly not negligible, as we can see in Figure 2 for other isotopes. This was solved by the subtraction of background contribution. Background contribution was determined by folding of the neutron source spectrum and calculated cross-sections. The cross-sections were calculated by means of the deterministic code TALYS 1.0. [5], basic setting of the code was used.

This procedure is insensitive to the absolute value of the TALYS cross-section, but sensitive to the shape of cross-section dependency on neutron energy. If we use models with different nuclear level density, the shapes of cross-section dependency on energy will change. Default model in code TALYS is Fermi, but also backshifted Fermi model, superfluid model, or Goriely or Hilaire tables can be used.

The ratio between cross-sections models with different nuclear level density and default Fermi model, reaction (n,3n) on bismuth, is represented in Figure 3. In some examples difference between Fermi model and others go up to 70%. It is necessary to analyze the influence of this factor on determination of radioactive nuclei number in the future.

Figure 2: Example of different influence of background (values in the parentheses are ratios between production in the peak and total production)

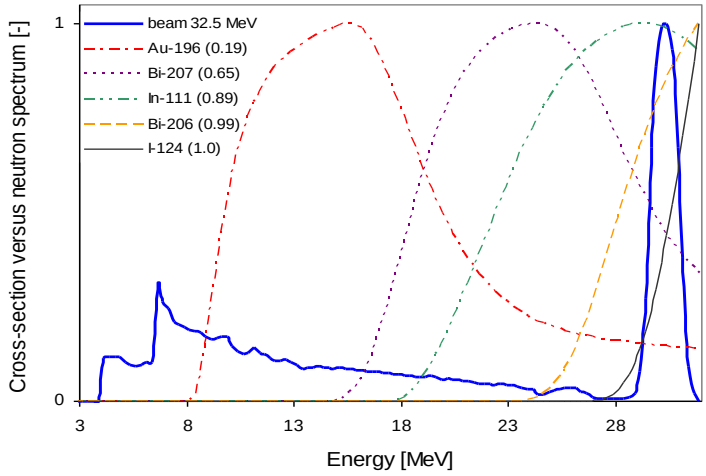

Results

Cross-section measurements in NPI and TSL cover a wide range of energies. A lot of new experimental data were measured. Products of (n,xn) threshold reactions were observed up to x = 10, for example ^{209}Bi(n,10n)^{200}Bi. The highest observed isotope in gold was ^{188}Au, ^{108}In in natural indium, ^{119}I in iodine and ^{176}Ta in tantalum.

Our results for well known cross-sections agree with experimental data found on EXFOR and it is possible to believe that also the first measured cross-section data are under control. Values of experimental cross-sections are compared with the results of TALYS code and also with data from EXFOR [7] database. Some examples are in Figure 4 – Figure 7.

Figure 3: Difference between cross-section models with different nuclear level density and default Fermi model, reaction ^{209}Bi (n,3n)^{207}Bi, TALYS 1.0

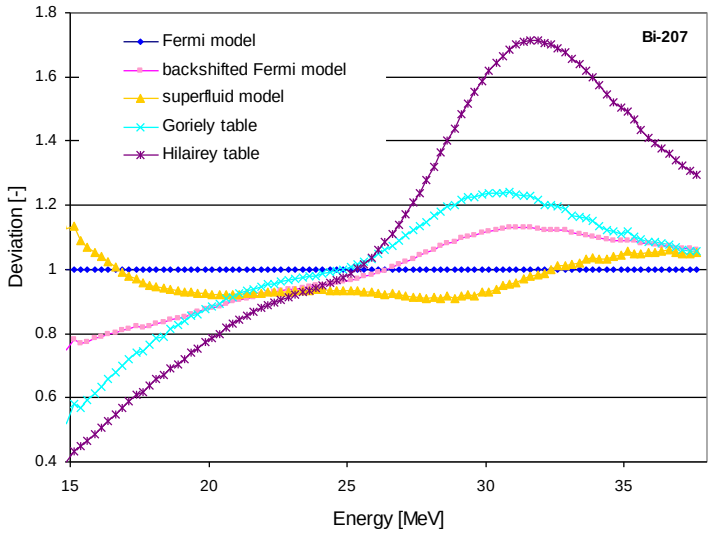

Figure 4: Comparison of experimental data from NPI and TSL with TALYS and EXFOR, ^{197}Au (n,2n)^{196}Au reaction

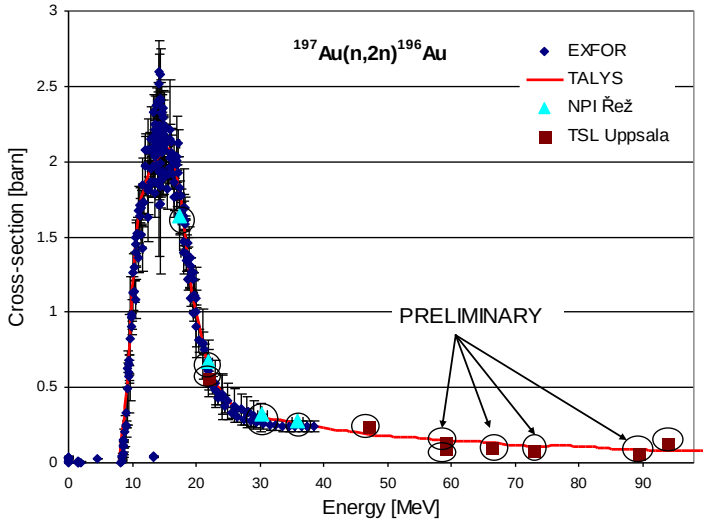

Figure 5: Comparison of experimental data from NPI and TSL with TALYS and EXFOR, ^{197}Au (n,4n)^{194}Au reaction

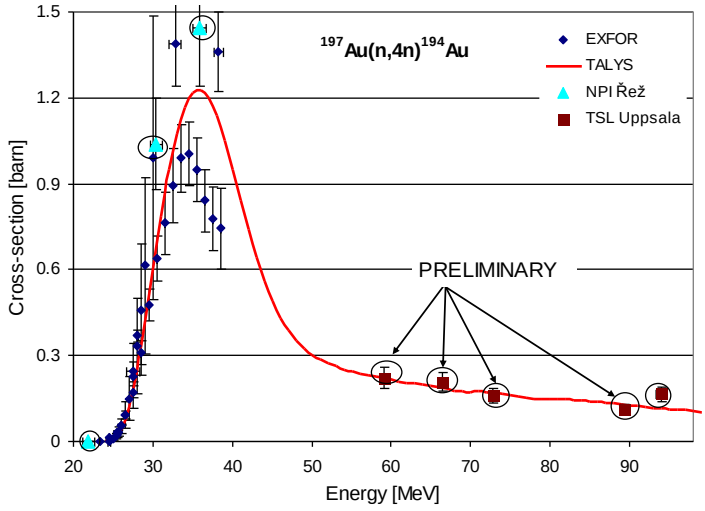

Figure 6: Comparison of experimental data from NPI and TSL with TALYS and EXFOR, ^{197}Au (n,6n)^{192}Au reaction

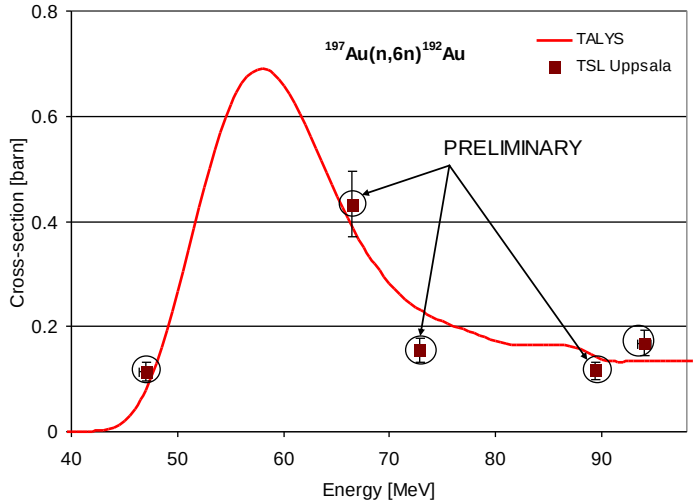

Figure 7: Comparison of experimental data from NPI and TSL with TALYS and EXFOR, ^{209}Bi (n,4n)^{206}Bi reaction

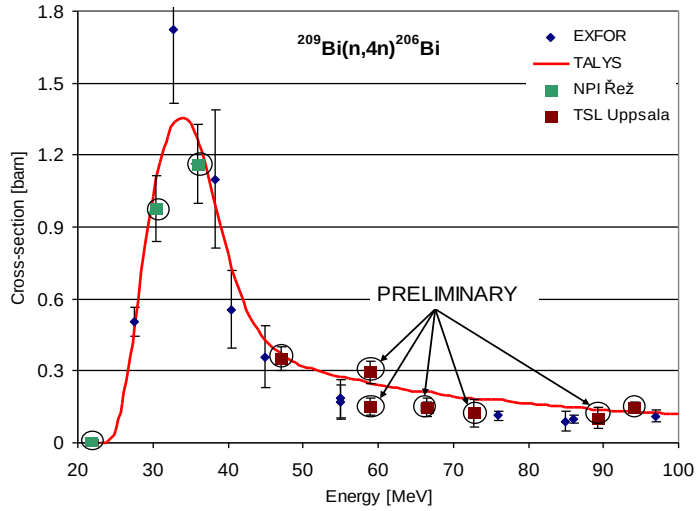

Conclusion

Eleven cross-section measurements were performed in years 2008 – 2010 in TSL Uppsala and NPI Řež. Quasi-monoenergetic neutron sources were used and energy region from 17 MeV to 94 MeV was covered. Our data were compared with data from EXFOR database and with code TALYS. Good agreement between our data and other experimental data and code TALYS was observed in many cases. Previous measurements in NPI and TSL are now completely processed and were published at scientific workshop EFNUDAT – Slow and Resonance neutrons in 2009 in Budapest [8] and at International Conference on Nuclear Data for Science and Technology in April 2010 in South Korea [9]. Results from the last measurement are still in processing and for this time just preliminary cross-sections data are presented. By the means of this new measurement we covered energy range 59 – 89 MeV, where no data were available so far.

Acknowledgements

We would like to thank the staff of TSL Uppsala (especially to Alexander Prokofiev and Torbjörn Hartman) and the staff of the cyclotron in NPI Řež for great support and excellent beams. Our special thanks belong to Marek Fikrle for the help with the set up of iodine samples. We would also like to thank Pavel Bém, Eva Šimečková and Milan Honusek for the possibility of joining their irradiations.

This work was supported by the EFNUDAT program [10], grant number CTU0808214 and by the F4E program of the Nuclear Reaction Department (NPI), F4E-2008-GRT-014.

References

[1] Bém, P., *et al.*, "The NPI cyclotron-based fast neutron facility", *Proceedings of the International Conference on Nuclear Data for Science and Technology – ND 2007*, Nice, France, p. 555-558 (2007).

[2] Uwamino, Y., *et al.*, "High energy p/Li neutron field for activation experiment", *Nucl. Instr. and Meth. in Phys. Res.* A, 389, 463-473 (1997) and Honusek, M., E. Šimečková, priv. comm.

[3] Prokofiev, A.V., *et al.*, "The TSL Neutron Beam Facility", *Rad. Prot. Dos.*, 126, 18-22 (2007).

[4] Frána, J., "Program DEIMOS32 for Gamma-Ray Spectra Evaluation", *J. Rad. Nucl. Chem.*, V.257, No.3, 583-587 (2003).

[5] Koning, A.J., *et al.*, "TALYS-1.0.", *Proceedings of the International Conference on Nuclear Data for Science and Technology – ND 2007*, Nice, France, p. 211-214 (2007).

[6] Chu, S.Y.F., *et al.*, The Lund/LBNL Nuclear Data Search web, *http://nucleardata.nuclear.lu.se/nucleardata/toi*, September 20 (2010).

[7] Experimental Nuclear Reaction Data (EXFOR/CSISRS), *www.nndc.bnl.gov/exfor*, September 20 (2010).

[8] Svoboda, O., *et al.*, *Proceedings of the 2nd EFNUDAT scientific workshop on Neutron Measurements, Theory and Applications, EFNUDAT – Slow and Resonance Neutrons*, Budapest, Hungary, p. 155-161 (2009).

[9] Svoboda, O., *et al.*, *Proceedings of the International Conference on Nuclear Data for Science and Technology – ND2010*, Jeju Island, Korea, forthcoming.

[10] European Facilities for Nuclear Data Measurements, *www.efnudat.eu*, September 20 (2010).

Neutron-induced fission studies at the IGISOL facility

M. Lantz,[1] **D. Gorelov,**[2] **B. Lourdel,**[1] **H. Penttilä,**[2] **S. Pomp,**[1]
D. Rados,[1] **I. Ryzhov,**[3] **V. Simutkin,**[1] **E. Tengborn**[1]
[1]Uppsala University, Uppsala, Sweden
[2]Department of Physics, University of Jyväskylä, Finland
[3]Khlopin Radium Institute, St Petersburg, Russia

Abstract

For a sustainable development of nuclear energy the handling of radioactive waste is a key issue. Innovative fuel cycles are developed for the transmutation of minor actinides and long-lived fission products and therefore accurate knowledge of the fuel inventory is necessary. The IGISOL facility with JYFLTRAP at the accelerator laboratory of the University of Jyväskylä will be used for measuring independent fission yield distributions from neutron induced fission. The facility has a well demonstrated ability for such measurements in proton induced fission. Currently, the facility is moving to a new location next to the recently installed MCC30/15 high intensity cyclotron. A neutron converter target is planned which will make use of the intense proton and deuteron beams. We plan to build a water-cooled tungsten target similar to the white neutron source at TSL. The converted neutrons allow independent fission yield studies of key actinides in a simulated fast reactor neutron field. In addition a thermal neutron field can be produced using a water sphere around the converter target. This will allow studies of the fission products of minor actinides which will become more important in today's light water reactors due to increased burn-up. The neutron source target will be realised in collaboration with the AlFONS (Accurate FissiOn data for Nuclear Safety) project of Uppsala University, financed by the Swedish Radiation Safety Authority and the Swedish Nuclear Fuel and Waste Management Co. The prospects of neutron-induced fission at the renovated IGISOL facility will be discussed.

Introduction

Nuclear power in the near future will go through some changes of importance from a nuclear physics point of view. The ageing Light Water Reactors (LWR) of today will be either upgraded or replaced with new ones that allow longer use of the fuel, which implies higher burn-up. Most likely there will also be the introduction of new reactor concepts belonging to Generation IV, including Fast Breeder Reactors (FBR), with the aim of more efficient use of the fuel, and the possibility to transmute long lived fission products and actinides. In both cases there will be a need for better knowledge of the fuel inventory.

The IGISOL mass separator, coupled to the penning traps of JYFLTRAP, at the University of Jyväskylä, has been used successfully during a number of years for the identification of different properties of exotic nuclei, including measurements of masses, proton separation energies, and decay spectroscopy [1]. Recently it has also proven its capability for high precision measurements of proton-induced fission products from ^{238}U [2,3]. It is therefore natural to use this facility also for high-precision measurements of neutron-induced fission yields of interest for innovative nuclear fuel cycles.

This report presents our intention, within the AlFONS (Accurate FissiOn data for Nuclear Safety) project of Uppsala University, to design a neutron source for such measurements, and a few preliminary conclusions from our initial studies.

The IGISOL facility

IGISOL stands for Ion Guide Separator On-line and is a successful method, developed at the accelerator facility of University of Jyväskylä, for mass separation of short-lived nuclides [4]. The mass separation resolution is of the order of $m/\Delta m \approx 300$ or better, which is enough for an unambiguous mass identification over the entire isotopic chart. Ions entering the IGISOL mass separator origin from thin targets that have been bombarded by a suitable accelerator beam. In the present scenario the idea is to bombard fissile actinides with fast or thermal neutrons, and to use IGISOL for mass separation of the fission fragments.

Following radio-frequency quadrupole cooling and bunching, the beam with the selected mass is sent to the JYFLTRAP, which contains two cylindrical Penning traps. The Penning traps identify isotopes with respect to their mass-to-charge ratio, m/q, by determining the cyclotron frequency, f_c, of each ion in a strong magnetic field, B, according to the relation $f_c = 1/(2\pi) \times q/m \times B$. The first Penning trap purifies the beam and the second one is used for the actual measurement. The combined effect is a mass resolution of $\Delta m/m \approx 10^{-7}$ or better, enabling high precision mass measurements of exotic nuclei and isomeric states [5].

The IGISOL facility has a proven capability for high quality measurements of proton-induced fission yields [2,3]. This ability will now be used for measurements of neutron-induced fission yields. The high precision of the IGISOL-JYFLTRAP setup will improve the quality of the existing fission yields, and extend them with data for fission fragments that have not been included so far and that may be of importance in reactors with higher burn-up. In an initial stage ^{235}U would be measured for calibration purposes, followed by measurements of ^{238}U, ^{239}Pu and ^{240}Pu. Furthermore, the facility can be used for systematic measurements on potential actinides of relevance in various Generation IV scenarios, such as ^{232}Th, ^{233}U, ^{237}Np, and ^{243}Am. More detailed information about the IGISOL facility and its capabilities is given by Penttilä *et al.,* in recently published work [3] and in another talk at this workshop [6].

Initial studies for the design of a neutron source

During the fall of 2010 the IGISOL-JYFLTRAP facility is being moved to a new location next to the recently installed MCC30/15 high intensity cyclotron, which enables proton beams of 18-30 MeV with a current of 100 μA, and deuterons of half the energy and current [7]. To fully utilize the intense proton and deuteron beams, a neutron converter target is being planned. The converter targets should be able to simulate both thermal and fast reactor neutron fields in order to perform studies of relevance for reactor applications.

The initial studies within the AlFONS project have been performed mainly with the Monte Carlo code MCNPX [8], and a few independent double checks with FLUKA [9,10]. Our approach has been to utilize the local experience with the ANITA white neutron source [11], which is being used at the The Svedberg Laboratory for studies of Single Event Effects (SEE) with atmospheric-like neutrons. Due to the different energies (the ANITA target is exposed to proton energies up to 175 MeV), as well as purposes, a straightforward application to the IGISOL facility is not feasible. In any case, the initial approach is to use a thick tungsten target of similar dimensions as the ANITA target and produce neutrons through the W(p,n) reaction. There is plenty of experience with tungsten as neutron converter, and, besides being a heavy, neutron rich nuclide, it has a high melting point, high thermal conductivity, and does not produce much residual radioactivity.

In the present work, there are no surrounding material except for the target itself and eventual moderator material, and the surrounding is treated as vacuum. All results with neutron flux are calculated in the unit neutrons per square centimetre per initial proton, at a distance of 100 cm from the centre of the neutron production target. The actual distance between the neutron source and the fission target will be 20-50 cm, resulting in a higher neutron flux, but for the initial studies a larger distance is selected in order to reduce geometrical effects. The initial calculations were performed with 30 MeV protons impinging on a cylindrical tungsten target with 2.5 cm thickness and 2.5 cm radius. This is an ongoing work that was recently started, so all results and conclusions below are preliminary and subject to change.

Investigations of different target geometries

During our initial investigation we (re)discovered that neutrons at energies below 10 MeV are sensitive to the geometry of the production target. For 30 MeV protons the neutrons are produced, mainly through the W(p,n) reaction, within 0.1 cm from the surface of the target. The mean free path for neutrons in the target matter is relatively low, so targets thicker than 1 cm give a substantial shielding effect in the forward direction. Therefore the neutron flux is higher in the backwards direction, and we have made a naive test in order to see if it is possible to use this effect in order to increase the neutron flux onto the fission target. Figure 1 shows a few examples of the study. In all plots the incident proton beam is directed towards the angle 0 degrees. For all cases the neutron flux has been measured 100 cm away from the target centre. The black curve is the “normal” case with the original tungsten target. Besides a slight forward peaking due to high energy neutrons, there is a substantial increase in the neutron flux in the backwards directions. In Figure 2 the corresponding energy spectra is show for 0, 90, and 180 degrees scattering angle. The blue curve shows the neutron spectra for a small cylindrical target, 0.2 cm thick and with 0.1 cm radius. In this case we get, as expected, the opposite effect, with a forward peaked neutron flux which is of the same magnitude

Figure 1: The left part shows a radar plot of the simulated neutron flux versus scattering angle for different target geometries. The gray shaded area in the centre shows the geometry of a semi-spherical target that is tilted 45 degrees with respect to the proton beam (incident from below). The right part shows the neutron flux for the different geometries in a regular diagram.

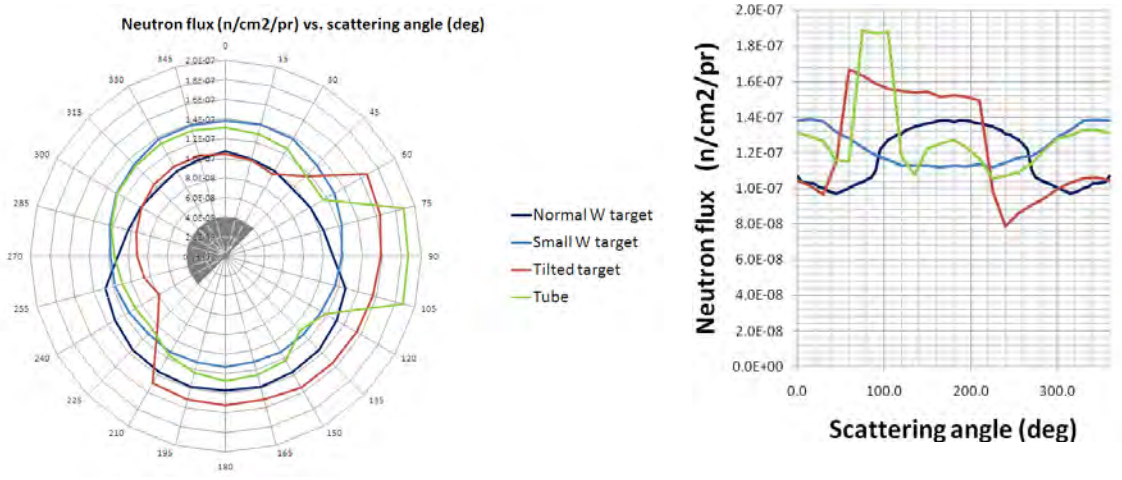

as the backwards neutron spectra for a thick target. A third option that was looked into was to use a half-sphere with radius 2.5 cm, which has the flat surface tilted 45 degrees with respect to the incident proton beam. In the left part of Figure 1, the shape is outlined as a grey shadow. The resulting neutron flux is show as red lines in Figure 1. A fourth option that was investigated was to add a cylindrical tungsten tube with thick walls, facing towards the angle 90 degrees. As expected, the tube enhances the neutron flux at the scattering angle 90 degrees.

From the four cases displayed in Figure 1, we see that it is in principle possible to enhance the neutron flux in a given direction, thereby increasing the fission yield. It should be noted, however, that no clear conclusions can be drawn before a more thorough investigation of the neutron fluxes are done. The relative increase in neutron flux is less than a factor of two, so the more complex geometry of the neutron source will probably discourage further investigations, though there are positive aspects with respect to higher fission yield, activation issues, and target cooling that need to be considered. Furthermore, the gain will most likely only be of interest for a fast neutron spectrum, while the same geometry may become problematic for a thermal spectrum.

Figure 2: The left part shows the simulated neutron spectra for the "normal" target at the scattering angles 0, 90 and 180 degrees. The right part shows the corresponding neutron spectra for a small target. The error bars show the statistical uncertainty due to limited statistics in the Monte Carlo simulation.

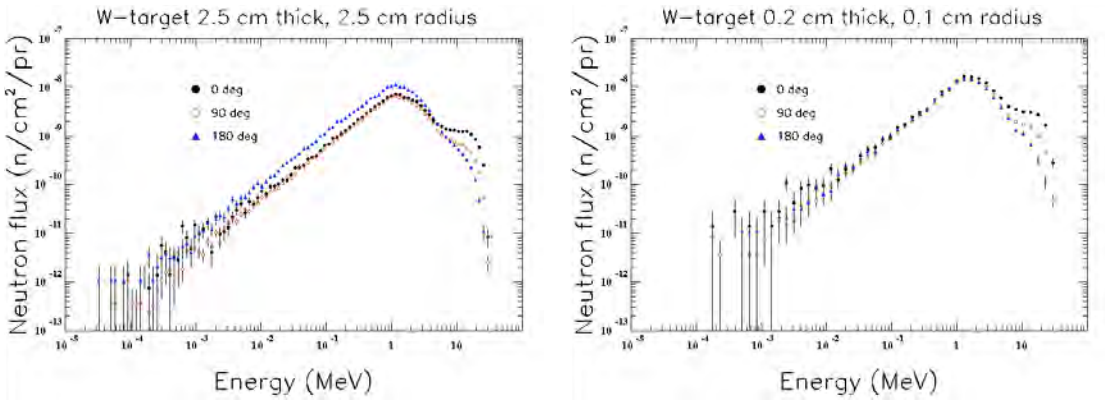

Investigations of different moderator geometries

We have made some basic comparisons of the neutron flux with different water moderator thickness. Shown in Figure 3 is a comparison of neutron spectra without moderator, and with two different moderator thicknesses, assuming a setup where the moderator is sphere of water that completely surrounds the target. As before, the neutron flux is determined at a distance of 100 cm from the centre of the target. The spectra are also compared with typical neutron fields for LWR and fast reactors [12]. The intensity of the reactor spectra have been renormalized arbitrarily.

As seen it is quite easy to obtain a neutron spectrum that is similar to the one in a LWR. For the fast reactor spectra it seems that it may be possible to improve from the un-moderated spectra by introducing a little bit of a moderator material in order to make the spectra somewhat softer. Another approach may be to reduce the proton beam energy, or consider other neutron sources.

Plans for the near future

As mentioned above the studies mentioned are so far very rudimentary and need to be extended in a more systematic manner. Producing a suitable neutron flux in order to obtain fission fragments of relevance is of course the main objective, but there are a number of practical considerations that need to be addressed. Below is a list of studies that are planned in the near future:

- Optimize neutron spectra with respect to energy and intensity in order to make them as similar as possible to LWR and FR spectra, by modifying the target geometry and moderator thickness. Besides water, other moderator materials may be considered. The selected

moderator needs to be easy to remove or modify when fast neutron spectra will be used. Reductions of the incident proton energy will also be considered.

- Due to the intense proton beam, up to 100 μA, we need to consider different options for cooling of the neutron source, and how this may affect the target geometry. The power released in the target is 3 kW, to be compared with the ANITA target at TSL, where the power is less than 100 W.
- The target area needs to be accessed on a regular basis, so activation of material need to be investigated, both with respect to the immediate radiation field from the activated neutron source assembly, as well as secondary activation due to neutron leakage into surrounding material. The possibility of moving the target assembly into a shielded area should be considered.
- Other kinds of neutron sources should be considered, for instance the available deuteron beam. Mono-energetic neutron sources such as portable D-T or D-D generators are relatively easy to handle, but they give lower neutron yields than the proton beam. On the other hand they have the advantage of giving neutrons at a well defined energy. In the case of limited accelerator access it could be worth consideration.

Figure 3: Simulated neutron spectra for a "normal" target without moderator (black circles), surrounded by 5 cm water moderator (red circles), and with 10 cm water moderator (blue triangles). The spectra are shown for the scattering angle 0 degrees, *i.e.* along the proton beam axis. Typical fast breeder and LWR spectra are shown as dashed and dash-dotted lines, respectively. The error bars show the statistical uncertainty due to limited statistics in the Monte Carlo simulation.

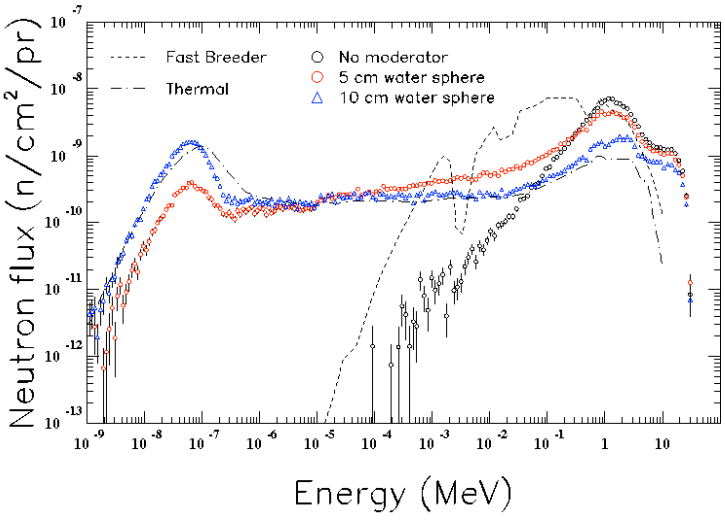

Conclusions

The IGISOL-JYFLTRAP facility is moving to a new location, and one of the future tasks will be high precision measurements of neutron-induced fission yields in view of novel nuclear fuel cycles. Our initial studies of the design of a neutron production target shows that it is possible to imitate a thermal neutron spectrum, and there are also possibilities for improvements on the un-moderated spectra in order to make it more similar a fast reactor spectrum. It is possible to increase the neutron flux in arbitrary directions, but because the gain is within a factor of two it is probably not worth any further investigations. The design study continues and will soon move from pure nuclear physics considerations to more practical issues such as cooling, activation of target and surrounding material, and easy handling.

Acknowledgements

This work is based on the MSc. thesis work of Daniel Rados at Uppsala University. The AlFONS project is funded by the Swedish Radiation Safety Authority (Strålsäkerhetsmyndigheten, SSM), and the Swedish Nuclear Fuel and Waste Management Co. (Svensk Kärnbränslehantering AB, SKB). We would like to thank Peter Wolniewicz and Johan Simu for fruitful discussions about fast reactors.

References

[1] Äystö, J., and the JYFLTRAP collaboration, "Ion-Trap Spectrometry for Exotic Nuclei", *Nucl. Phys.* A 834, 724c-729c (2010).

[2] Hager, U., *et al.*, "First Precision Mass Measurements of Refractory Fission Fragments", *Phys. Rev. Lett.* 96, 042504 (2006).

[3] Penttilä, H., *et al.*, "Determining isotopic distributions of fission products with a Penning trap", *Eur. Phys. J.* 44, 147-168 (2010).

[4] Karvonen, P., *et al.*, "Upgrade and yields of the IGISOL facility", *Nucl. Instrum. Methods B* 266, 4454-4459 (2008).

[5] Kolhinen, V.S., *et al.*, "JYFLTRAP: A Cylindrical Penning Trap for Isobaric Beam Purification at IGISOL", *Nucl. Instrum. Methods* A 528, 776-787 (2004).

[6] Penttilä, H., *et al.*, "Fission studies at the renovated IGISOL facility", these proceedings.

[7] Heikkinen, P., "New MCC30/15 Cyclotron for the JYFL Accelerator Laboratory", *Proc. 18th Conf. Cyclotrons and their Applications*, Giardini Naxos, Italy (2007).

[8] Pelowitz, D.B., *MCNPX User's Manual Version 2.6.0*, Los Alamos National Laboratory report, LA-CP-07-1473 (2008).

[9] Battistoni, G., *et al.*, "The FLUKA code: Description and benchmarking", *Proc. Hadronic Shower Simulation Workshop 2006*, AIP Conf. Proc. 896, 31-49 (2007).

[10] Fassò, A., *et al.*, *FLUKA: a multi-particle transport code*, CERN-2005-10 (2005), INFN/TC_05/11, SLAC-R-773.

[11] Naitou, Y., *et al.*, "Measurement of the spectral neutron flux at the ANITA facility at TSL", *Proceedings of the 2009 Annual Symposium on Nuclear Data*, Ricotti, Tokai, Japan (2009).

[12] U.S. Department of Energy (DOE), *Nuclear Physics and Reactor Theory*, Volume 1 of 2, DOE-HDBK-1019/1-93, FSC-6910, Washington, D.C. 20585 (1993).

The double fission-fragment time-of-flight spectrometer VERDI

R. Borcea,[1] F.-J. Hambsch,[1] S. Oberstedt,[1] Sh. Zeynalov,[1*] A. Göök,[2,3] A. Oberstedt,[2,4] T. Belgya,[5] Z. Kis,[5] L. Szentmiklosi,[5] K. Takáks ,[5] T. Martínez-Perez[6]
[1]EC-JRC Institute for Reference Materials and Measurements, Geel, Belgium
[2]School of Science and Technology, Örebro University, Örebro, Sweden
[3]Present address: Institute for Nuclear Physics,
University of Technology Darmstadt, Darmstadt, Germany
[4]Fundamental Fysik – Chalmers Tekniska Högskola, Göteborg, Sweden
[5]Institute of Isotopes, Hungarian Academy of Sciences, Budapest, Hungary
[6]Nuclear Innovation Group, Department of Energy, CIEMAT, Madrid, Spain

Abstract

The investigation of correlated fission characteristics like fragment mass- and energy-distributions is usually based on the double-energy technique using twin Frisch-grid ionisation chambers (IC). Providing the existence of prompt-neutron emission data the pre-neutron fission fragment mass and energy distributions may be obtained in an iterative process. However, those input data do not exist for isotopes other than ^{233,235}U and ^{239}Pu at sufficient detail, and extrapolation methods have to be applied when analysing neighbouring compound nuclear systems. The double fission-fragment time-of-flight spectrometer VERDI aims at investigating the neutron-induced fission fragment characteristics Measuring fragment velocity and kinetic energy for both fission fragments simultaneously allows obtaining mass and kinetic energy distributions without introducing a-priori information about prompt neutron emission. In addition, the measurement of pre- and post-neutron fission-fragment data provide prompt neutron multiplicity data as a function of fragment mass and total kinetic energy. In order to achieve a mass resolution $\Delta A < 2$, ultra-fast time pick-up detectors based on artificial diamond material are used. The spectrometer in its present single (v, E) version was tested for the first time in an experiment performed at the Budapest Research Reactor. The results of this experiment, the performance of the diamond detectors with fission fragments, time-of flight spectra and post-neutron mass distributions are presented and discussed.

[*] Present address: Joint Institute for Nuclear Research, Dubna, Moscow Region, Russia.

Introduction

Reliable predictions on fission product yields are relevant in modern nuclear applications such as GEN-IV reactors or ADS, for the estimation of radio-toxicity of nuclear waste, safety of reactor operation, decay heat calculations etc. These data can be also used for the modelling of fission-fragment mass and kinetic energy distributions of minor actinides (^{237}Np, ^{241,243}Am, $^{242\text{-}248}$Cm), for obtaining the emission spectrum and multiplicity (as a function of fragment mass) of prompt γ-rays and neutrons and the delayed neutron emission pre-cursor yields. In order to determine this information, it is necessary to measure accurately the fission fragment yield as a function of fragment mass and kinetic energy.

Within the concept of a double velocity measurement together with a subsequent measurement of both fragment energies pre- and post-neutron fragment mass and energy distributions may be obtained. These data then contain information about the number of prompt neutrons emitted as a function of fragment mass and excitation energy. The time-of-flight spectrometer VERDI is based on the concept of a simultaneous measurement of both fission fragment velocity and energy. This principle has been used previously in the case of the Cosi-Fan-Tutte spectrometer which was operated at ILL Grenoble (France) [1]. Despite the excellent mass resolution the spectrometer suffered from a very small geometrical efficiency and was shut down after a view years of operation. The VERDI spectrometer is presently being developed at IRMM with the goal to overcome the limited geometrical efficiency in conjunction with sufficient mass resolving power.

Design and detectors

The VERDI spectrometer consists of two symmetric time-of-flight sections with a length of 50 cm each, as it can be seen in Figure 1.

At the end of each time-of-flight section an array of silicon-detectors in PIPS design [2] are placed, each array containing up to 19 detectors with an area of 4.5 cm^2. This gives an overall geometrical efficiency of 0.5%, which is 100 times higher than in the case of Cosi-Fan-Tutte.

The set-up is handled using standard NIM electronics, an ASR (analogue signal router) and a tag-word module for detector identification, both modules developed in our research group for the VERDI project.

As VERDI aims at achieving a mass resolution better than 2 m. u., it is essential to use a very fast fission trigger. In the former Cosi-Fan-Tutte spectrometer micro-channel plate detectors were used as fission trigger. This type of detectors, while providing indeed an excellent timing resolution, is very delicate in operation and may suffer from radiation damage.

In the case of the VERDI spectrometer, the artificial diamond material was investigated as a possible choice for a transmission detector. In a first phase, a thick (non-transmission) detector made of artificial polycrystalline diamond material by means of chemical vapour deposition (pcCVD diamond detector) was used, and the spectrometer was operated in a single (v, E) configuration.

Figure 1: Schematic view of the double time-of-flight VERDI spectrometer

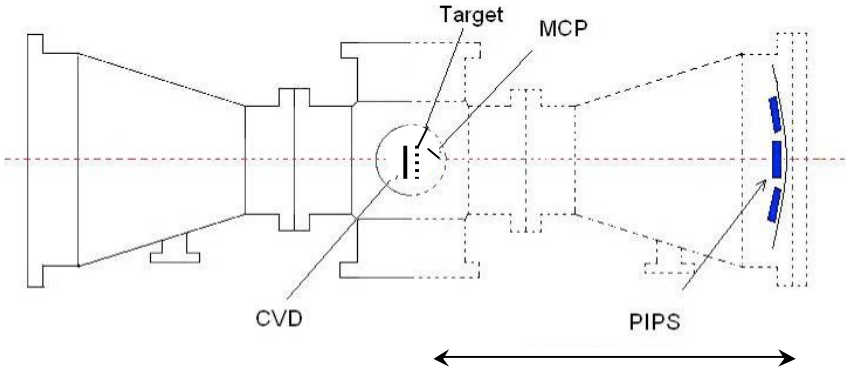

Characteristics of the pcCVD diamond detector

In nuclear physics diamond detectors are used mainly in high-energy heavy ion experiments as beam monitors and tracking devices, replacing the traditionally employed silicon detectors. The advantages of diamond detectors are an easy operation, because they are robust and do not need cooling or very high vacuum, a low leakage current and high resistance to radiation [3]. For these reasons we tested the response of diamond detectors, for the first time, to low-energy heavy ions, *i.e.* fission fragments. A 100 µm thick pcCVD diamond detector with an active area of 1 cm × 1 cm was exposed to fission fragments. The detector is shown in Figure 2.

Figure 2: Photo of the pcCVD diamond detector used as fission trigger in the single (v, E)-version of the VERDI spectrometer

For the investigation of the timing resolution of the diamond detector, two identical pcCVD diamond detectors were placed in a test vacuum chamber, at a distance of 9.5 cm from each other, with a spontaneous fission ^{252}Cf source attached to one of them.

Since the time-of-flight spectrum is composed of a large variety of particles, with different energies and masses, timing properties had to be deduced from simulations. For that purpose Monte-Carlo simulations have been performed on the basis of experimental mass and kinetic-energy yield data [4-6] and taking the geometry of the set-up into account. The free parameter in such a simulation is the width of the total resolution function, which was varied until the best description of the experimental time-of-flight spectrum was achieved. The time-of flight spectrum thus obtained is presented in Figure 3 together with results of Monte Carlo simulations assuming different values for intrinsic timing resolution.

Figure 3: Time-of-flight spectrum obtained using a ^{252}Cf spontaneous fission source (symbols); the data are compared with results from Monte Carlo simulation results assuming different values for the intrinsic timing resolution

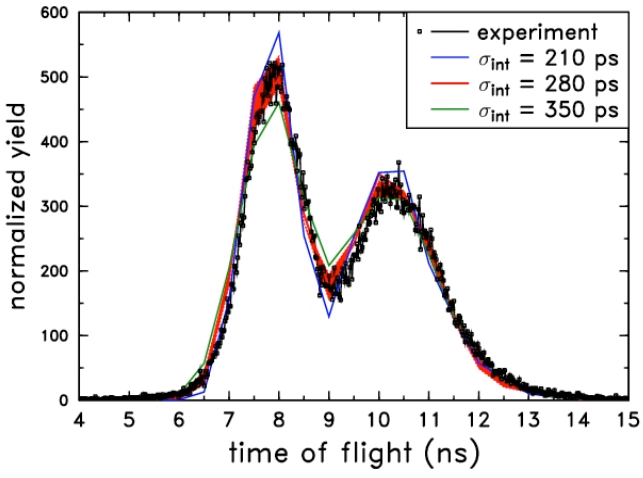

The intrinsic timing resolution of the pcCVD diamond detector inferred from the comparison of the measured with simulated spectra is (285 ± 15) ps.

The overall time-of-flight resolution of the system pcCVD diamond detector and silicon detector was determined using the same procedure and was found to be as good as 400 ps.

During the test measurements the detector was exposed to a total fission-fragment dose of at least 1.2×10^9 including a corresponding α-particle dose of 4×10^{10} and a fast neutron dose of about 5×10^9 without any deterioration of the output signal due to possible radiation damage.

First measurements on the reaction ^{235}U(n, f)

A first test experiment was performed at the Budapest research reactor in the framework of the EFNUDAT programme of the European Commission using VERDI in its one-arm configuration. VERDI was installed in front of the exit of the cold-neutron beam facility of the reactor. The spectrometer was equipped with 10 silicon detectors.

A 113 µg ^{235}U target was mounted on top of the diamond detector in the centre of VERDI.

Attached to the ^{235}U source, a thin ^{6}LiF source was mounted. From the two-body reaction ^{6}Li(n, α)^{3}H mono-energetic alphas and tritons are emitted with well known energies; they can, therefore, be conveniently used for time calibration. The set-up was irradiated with cold neutrons with a thermal equivalent flux of 5×10^7/s/cm^2. The counting rate was 2 fission events/s per detector. The experiment took place during 5 days.

In the process of data analysis a pulse-height defect correction according to Schmitt and Neiler [7] was applied. The post-neutron mass and kinetic energy distributions for ^{235}U were calculated and compared to experimental data measured with the 2E technique [8, 9]. The mass distributions for 8 detectors are shown in Figure 4 (lines) together with the experimental data (symbols) from ref. [10,11]. The distributions obtained with VERDI compare well with that from obtained with the 2E technique. From the width of the present distributions we may infer a mass resolution of the VERDI spectrometer in its present configuration is of about 3-4 m. u. In order to achieve a better performance several improvements were already implemented.

Figure 4. Mass distributions from the reaction ^{235}U(n, f) obtained for 8 silicon detectors (lines) the data measured using the 2E technique are represented by symbols

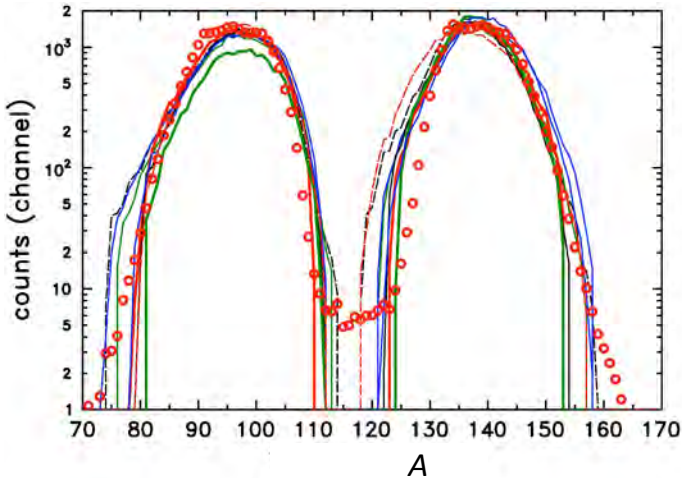

Recent improvements and perspectives

As the mass resolution is directly related to the timing resolution of the detector system, efforts have been made to improve this parameter. Firstly, we implemented a new broadband preamplifier of the DBA-IV-type which was developed at GSI (Germany) in particular for the use with diamond detectors [12]. As a result the output signal of the large pcCVD diamond detector was much faster

showing a rise-time below 1 ns and an improved signal-to-noise ratio. Secondly, we adapted the design of our diamond detectors. As shown in Figure 5 a 4-fold segmentation has been imposed. Together with a larger thickness (180 mm) the detector capacitance is reduced by a factor of about 7. This again led to much shorter signals with a rise time well below 700 ps, and a further improved signal-to-noise ratio.

Figure 5. The segmented pc CVD diamond detector currently used in the VERDI spectrometer

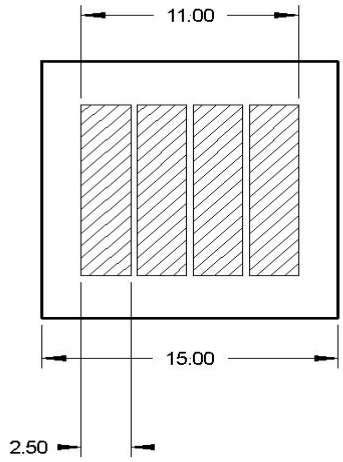

Tests are presently being conducted using a ^{252}Cf source. The first mass and kinetic energy distributions show already a qualitative improvement compared to the previous ones; a detailed analysis of the data is in progress.

At the same time, a thin (5 µm) pcCVD diamond detector is tested in view of its possible use as a transmission detector in the VERDI spectrometer, in its final two-arm configuration. The transmission detector has a 8-fold strip design, for which the capacitance corresponds to that of the large-area detector.

Conclusions and outlook

The time-of-flight spectrometer VERDI is operational in its single (v, E) version. It is a compact device with large geometrical acceptance and is easy to operate despite the large number of energy detectors. The instrument is mobile and can be transported and coupled to any available neutron source. In addition, VERDI can also be combined with an array of γ-ray and/or neutron detectors to perform correlation measurements.

In its final configuration, the VERDI spectrometer will be a useful tool for obtaining fission data with high accuracy.

Acknowledgements

This work was supported in part by the EFNUDAT programme (agreement number 31027)

References

[1] Oed, A., *et al.*, *Nucl. Inst. Meth. in Phys. Res.* 219, 569 (1984).

[2] PIPS® (Silicon) Detectors, TMPD series, CANBERRA Industries, *www.canberra.com/pdf/Products/Detectors_pdf/C36115-PIPS-SS.pdf*.

[3] Berdermann, E., *et al.*, "Diamond Detectors for Heavy-Ion Measurements", *Proc. XXXVI Int. Winter Meeting on Nuclear Physics*, Bormio (1998).

[4] Hambsch, F.-J., S. Oberstedt, *Nucl. Phys.* A617, 347-355 (1997).

[5] Hambsch, F.-J., private communication (2004).

[6] Birgersson, E., *et al.*, *Nucl. Phys.* A 791, 1-23 (2007).

[7] Schmitt, H.W., *et al.*, *Physics and chemistry of fission*, International Atomic Energy Agency, Vienna, p. 531 (1965).

[8] Al-Adili, A., private communication (2010).

[9] Gönnenwein, F., *The Nuclear Fission Process*, ed. C. Wagemans, CRC PRESS (1991).

[10] Budtz-Jørgensen, C., *et al.*, *Nucl. Inst. Meth.* A258, 209 (1987).

[11] Vives, F., *et al.*, *Nucl. Phys.* A662, 63 (2000).

[12] Moritz, P., *et al.*, *Proc. ICNDST-7*, Hong Kong (2000).

Three-nucleon system dynamics studied via deuteron-proton breakup

Stanisław Kistryn
Institute of Physics, Jagiellonian University Krakow, Poland

Abstract

Nucleon-nucleon (NN) interaction is a basis for vast fields of fundamental nuclear physics and its application, therefore a detailed knowledge of the dynamics of few-nucleon systems has been a subject of intensive quest over several decades. Modern NN potential models can be probed quantitatively in the three-nucleon environment by comparing predictions based on rigorous solutions of the Faddeev equations with the measured observables. Proper description of the experimental data can be achieved only if the dynamical models include subtle effects of suppressed degrees of freedom, effectively introduced by means of genuine three-nucleon forces. A large set of high precision, exclusive cross-section data for the ^{1}H(d,pp)n breakup reaction at 130 MeV, acquired in a first new-generation experiment at KVI Groningen, contributes significantly to constrain the physical assumptions underlying the theoretical interaction models. Comparison of nearly 1800 cross-section data points with the predictions using nuclear interactions generated in various ways, allowed to establish for the first time a clear evidence of importance of the three-nucleon forces in the breakup process. Moreover, the results, supplemented by a set of cross-sections from another dedicated experiment at FZ Juelich, confirmed predictions of sizable Coulomb force influences in this reaction. Following further, comparably rich and precise data sets, encompassing also polarization observables, will form a database to validate the theoretical models of few-nucleon system dynamics.

Introduction

Precise knowledge of the nucleon-nucleon (NN) interaction is one of the most demanded pieces of information in the field of nuclear physics. Understanding the details of few-nucleon system dynamics is of crucial importance not only for the fundamental nuclear physics, but also for several fields of its application. They comprise, for instance, optimization of radiation shielding design for various installations, predicting performance of targets and guides of spallation neutron sources, evaluation of irradiation dose in nuclear medicine, planning the future energy amplifiers and nuclear waste transmutation plants. The codes used in simulating the reactions relay on accurate modelling of two-nucleon (2N) and three-nucleon (3N) dynamics, and since this information enters at the very beginning (fast, direct stage of the process in Intra-Nuclear Cascade or Quantum Molecular Dynamics), possible inaccuracies in the models can be easily a cause of severe flaws of the global predictions.

In general, the desired exact understanding of all features of the few-nucleon system dynamics would provide a natural basis for description of properties and interactions of nuclei. The 2N system has been intensively studied over last decades and resulted in forming a solid database, on which modern models of NN potentials have been founded. Thus, one is tended to assume that the basic NN force is well under control. This optimistic presumption has to be verified by applying models of the NN interaction to reproduce properties of many-nucleon systems with increasing complexity. Obviously, the least complicated non-trivial environment is the one composed of three nucleons.

Dynamics of the three-nucleon system can be comprehensively studied by means of the nucleon-deuteron (Nd) breakup reaction. Its final state, constrained by only general conservation laws, provides a rich source of information to test the 3N Hamiltonian details. It is of particular importance when components of the models which account for subtle effects, like three-nucleon force (3NF) contributions to the potential energy of the 3N system, are under investigation. Nowadays precise predictions for observables in the 3N system can be obtained via exact solutions of the 3N Faddeev equations for any nucleon-nucleon interaction, even with the inclusion of a 3NF model [1,2].

The most widely used in few-nucleon studies, so called realistic NN potentials (RP) are Argonne v_{18} (AV18), charge dependent Bonn (CD Bonn) or Nijmegen I and II forces. Extension of that picture is provided by the baryon coupled-channel potential (CCP), in which one Δ-isobar degrees of freedom are allowed on top of purely nucleonic ones [3-5]. The most basic approach, however, stems from the effective field theory applied to the NN system. The resulting expansion scheme for nuclear systems is called chiral perturbation theory (ChPT). For the 3N system it is numerically developed in full at the next-to-next-to-leading (NNLO) order [6-9]. All the above approaches can also be supplemented by model 3NF's. In the RP case semi-phenomenological 3NF's are used, most commonly the Tucson-Melbourne (TM99) or Urbana IX (UIX) models. In the CCP and ChPT frameworks this additional dynamics is generated naturally, together with the NN interactions. The predicted effects are, however, smaller than for the TM99 or UIX forces.

There are additional difficulties in interpretation of the experimental results by means of theoretical calculations. The most important, until recently missing feature, is the Coulomb interaction: The experiments are performed mainly for the deuteron-proton system while all calculations used to strictly neglect any long-range forces. Only in the last years a significant step forward has been made in including the Coulomb force effects for the breakup reaction. It was first tried within the coupled-channels approach [10,11] and recently applied also for the AV18+UIX potential [12]. Contrary to the former expectations, the influence of the Coulomb force on the breakup observables can be quite significant, as will be demonstrated below.

New generation breakup experiment

To allow for conclusive comparisons between the experimental data and theoretical predictions large sets of data are required. Unfortunately, precise measurements of the breakup reaction are very demanding. The experimental coverage is concentrated at lower energies, below 30 MeV nucleon energy – see [2,13] for references. In the recent years some revival of the activity can be noticed (see [14] for the listing of papers), but again, only few kinematical configurations are usually studied.

Our new approach to the breakup research assumed a simultaneous measurement in a large part of the phase space by using high acceptance position-sensitive detection system. Measurements

of the ^{1}H(d,pp)n reaction were carried out at KVI Groningen, The Netherlands, at 130 MeV beam energy, providing worldwide first extensive set of the breakup cross-section data, spanned on a systematic grid of kinematical variables. Cross-section values were extracted for about 80 kinematical configurations [15,16], defined by the polar angles of the two outgoing protons, θ_1, θ_2, and their relative azimuthal angle ϕ_{12}, and presented as functions of the arc-length variable S, giving in total nearly 1800 experimental points. The data covered a substantial fraction of the phase-space and allowed to conclude on importance of the 3NF effects for the breakup reaction – only inclusion of this additional dynamics in the calculations leads generally to a much better description of the cross-sections.

The role of additional dynamics in the breakup cross-section is recapitulated in a global approach to the KVI data in Figure 1. The relative difference of the experimental and theoretical cross-sections, $(\sigma_{exp}-\sigma_{th})/\sigma_{exp}$, was determined and plotted as a function of E_{rel}, the kinetic energy of the relative motion of the two breakup protons. Combining the AV18 potential with the UIX 3NF (left panel) significantly improves the data description in almost the whole range of E_{rel} but the smallest relative energies, where it drives the predictions away from the data. The overall improvement of the data description due to inclusion of the TM99 3NF in the calculations (compared to the ones with the pure CD Bonn NN potential) is expressed by a reduction of the global χ^2 by about 40% [16].

In comparisons of our results we were faced with quite substantial disagreements at low values of E_{rel}. Only with the inclusion of the Coulomb force into the calculations in the coupled-channels approach they were mostly explained and removed [17]. A consistent theoretical treatment of phenomenological 3NF and the Coulomb force has been achieved only very recently [12] and allows to scrutinize both these effects at the same level of accuracy. Middle panel of Figure 1 shows the impact of the Coulomb force effects on our cross-section data. While at larger values of E_{rel} the influence of the long-range electromagnetic interaction is negligible, it strongly reduces the disagreements at small E_{rel}. Only with such a large set of the breakup data significance of the Coulomb effects could have been proved and their behaviour traced over the phase space [17]. It has been also established that even after including the Coulomb force there is still room for 3NF effects. The resulting total action of both dynamical ingredients supplementing the pure NN interaction can be seen in Figure 1, right panel. One observes that at small E_{rel} values to strong action of the Coulomb force is compensated by 3NF effects, leading to a nearly perfect agreement between the data and the theoretical cross-sections. The discrepancies remaining at large E_{rel} values hint at some still unresolved problems in our understanding of 3N system dynamics, *e.g.* non-complete model of 3NF.

Figure 1: Relative discrepancies between the experimental KVI data and the theoretical predictions of the breakup cross-sections as a function of the relative energy of the two breakup protons.
***Left panel:* Action of UIX 3NF with respect to the pure NN AV18 potential.**
***Middle panel:* Action of the Coulomb force, when combined with the AV18.**
***Right panel:* Combined action of the above two effects together.**

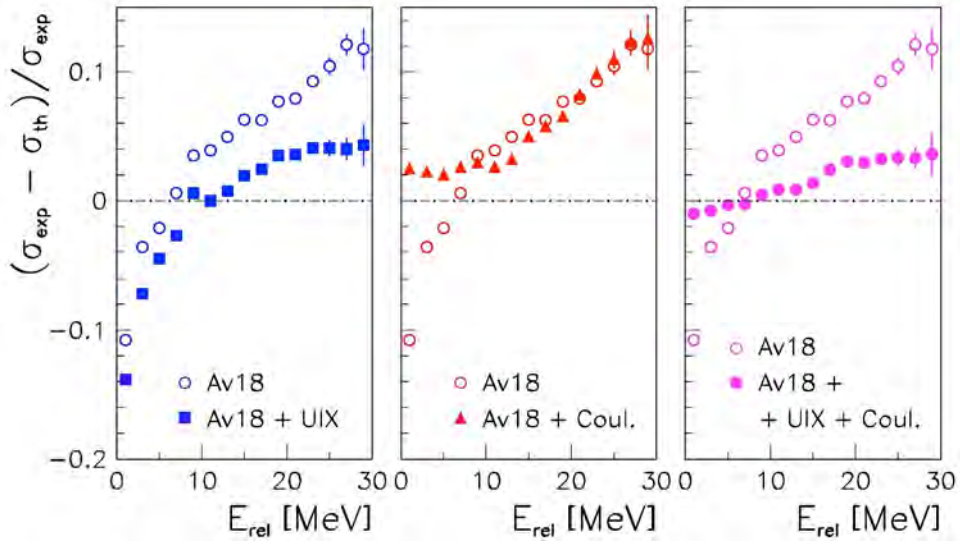

Breakup experiment at forward angles

The first calculations of the Coulomb force influences for the breakup reaction pointed to some quite spectacular effects for small emission angles of the two protons. The cross-section is not only strongly suppressed but its distribution is distorted, with a local minimum enforced in the middle of the S-range. This behaviour has been confirmed by a subset of KVI data, for configurations at the acceptance edge of the detection system [17].

To study this effects in some depth, a new experiment has been performed at the Research Center Jülich (FZJ), Germany, using the deuteron beam of 130 MeV extracted from the COSY synchrotron and the detection system covering the range of very forward polar angles. An example of the cross-section data for one of the kinematical configurations common to both experiments is shown in Figure 2. An excellent agreement between the two data sets is visible – it should be mentioned that both distributions have been normalized independently. This agreement proves certain stage of maturity of including the Coulomb force effects in the theoretical calculations [18].

It should be noted that for relatively sharp structures in the cross-section, the theoretical calculations have to be appropriately averaged over the angular and energy regions, corresponding to the ones used in the data evaluation procedure. Only then they can be confronted with the experimental data – the size of the effect can be inspected in Figure 2. A larger sample of the FZJ results showing the distortion effect of the cross-section distribution due to the Coulomb force is presented in Figure 3.

Also the FZJ experiment provided a rich data set for the ^{1}H(d,pp)n breakup cross-section at 130 MeV, which has been used for global comparisons with various theories. The data have been acquired and analyzed for the forward angular range of proton polar emission angles, providing in total nearly 2400 data points. As an example, Figure 4 presents a global comparison of all these data with eight theoretical approaches (see legend of the Figure). The comparison is expressed in terms of "χ^2-like" value – one should consider only the relative differences between its values obtained when using different theoretical predictions, without attributing a strict statistical meaning to the absolute values of the parameter. Comparisons are again made in function of the energy of the

Figure 2: Cross-section distribution as a function of arc-length S for one kinematical configuration (specified in the panel). Dashed line represents calculations without the Coulomb force. Dotted line shows the results of calculations including the Coulomb force, for point-like geometry (central angles). Averaged calculations are shown as the solid line. Data measured at KVI are shown as red dots (with small errors). Cross-section results obtained in the FZJ experiment (for a fraction of the collected data) are shown as green dots. The E_{rel} dependence on S is shown by the dash-dotted line.

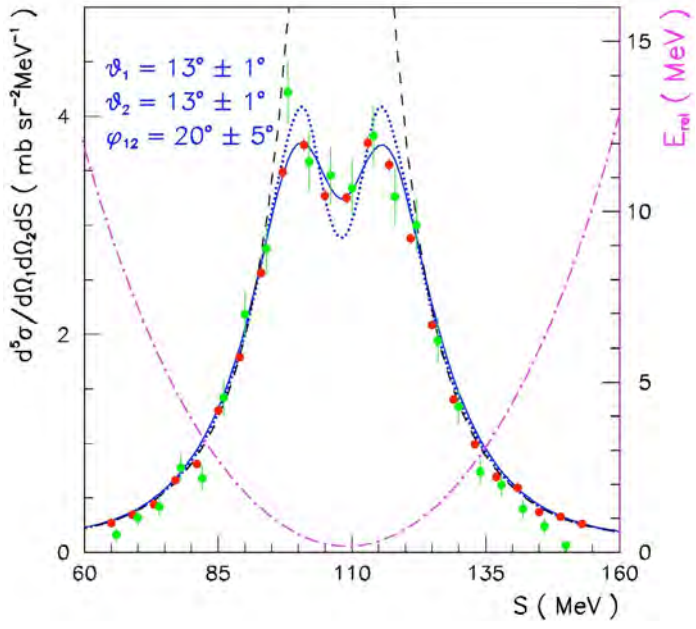

Figure 3: Cross-section data for the breakup reaction measured at FZJ for six kinematical configurations specified in the panels. The lines show the results of the appropriately averaged calculations of CCP with the Coulomb force included.

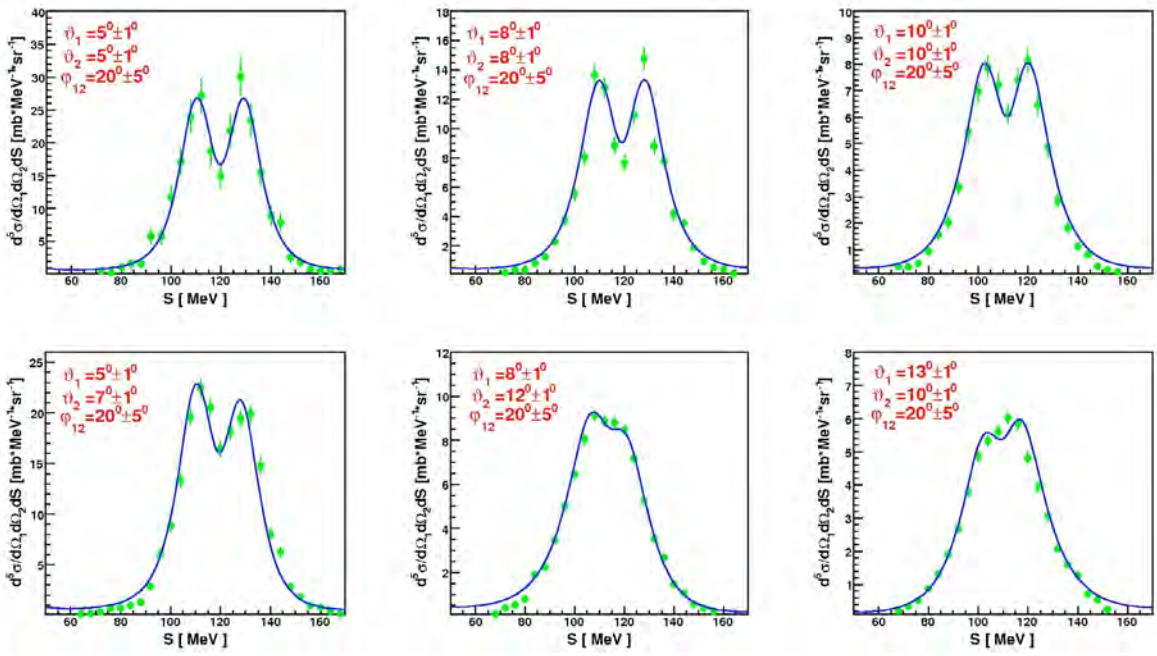

Figure 4: Quality of reproducing of the experimental FZJ breakup cross-sections data by the theoretical predictions as a function of the relative energy of the two breakup protons. Data description quality is quantified by chi-square per degree-of-freedom values, without a strict statistical meaning, rather as a relatively comparable parameter only.

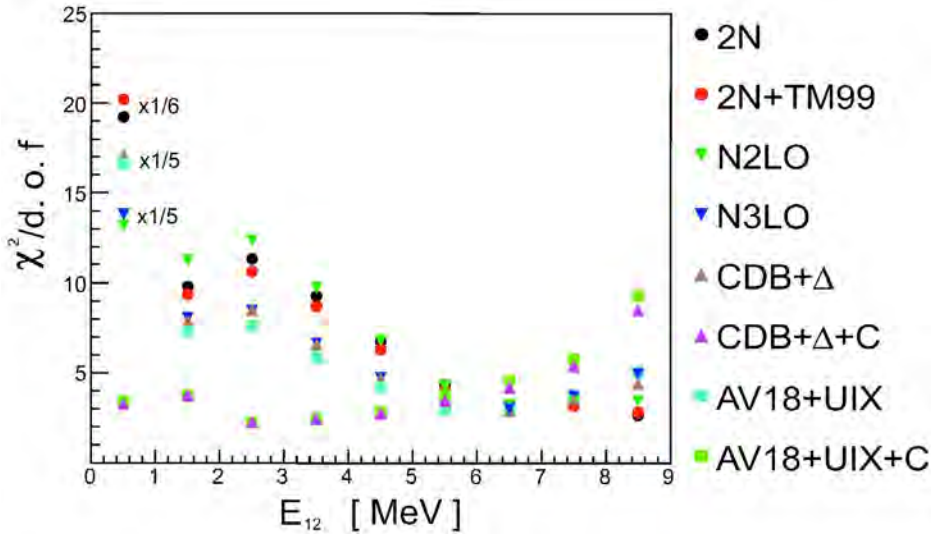

relative motion of the two breakup protons (here denoted as E_{12}). One can clearly recognize that only the theoretical approaches including the Coulomb interaction are able to much better reproduce the bulk of data at small E_{12} values. Worth noting is also the fact that for relative energies larger than about 5 MeV the net role of the Coulomb force is no longer important.

Summary

Studies of the breakup reaction performed in a large part of the phase space are shedding light on the role of various aspects of the 3N system dynamics. After the pioneering experiments, further data sets are being acquired at several beam energies [19,20]. They present a general success of the modern calculations in describing the data, however, possibly complete theoretical treatments, including all important ingredients (3NF, Coulomb interaction, relativistic effects), as well as developments in ChPT are very important for better understanding of the three-nucleon system dynamics.

The cross-section data are supplemented with equally large sets of various analyzing powers and measurements of even higher-order polarization observables (see Refs.[21,22] and references therein). Certain discrepancies observed in those observables are a hint of problems in the spin part of the current models of 3NF. More experiments to study 3N system dynamics are planned at several laboratories, including the next step – continuation of the few-body system studies in the four-body environment.

Acknowledgements

This report is given on behalf of the whole Collaboration working on the described projects. Indispensable contributions from all experimentalists and theoreticians are sincerely acknowledged, as well as the help of KVI and FZJ technical staff. Financial support for the project has been provided in parts by several Polish, Dutch, German and European Institutions. Thanks are due to the NEMEA-6 Organizers for kind invitation.

References

[1] Glöckle, W., *The Quantum Mechanical Few-Body Problem*, Berlin Heidelberg: Springer-Verlag (1983).

[2] Glöckle, W., *et al.*, J., *Phys. Rep.* 274, 107 (1996).

[3] Chmielewski, K., *et al.*, *Phys. Rev. C* 67, 014002 (2003).

[4] Deltuva, A., K. Chmielewski, P.U. Sauer, *Phys. Rev. C* 67, 034001 (2003).

[5] Deltuva, A., R. Machleidt, P.U. Sauer, *Phys. Rev. C* 68, 024005 (2003).

[6] Epelbaum, E., *et al.*, *Phys. Rev. C* 66, 064001 (2002).

[7] Entem, D.R., R. Machleidt, *Phys. Lett. B* 524, 93 (2002).

[8] Epelbaum, E., W. Glöckle, U.-G. Meissner, *Eur. Phys. J. A* 19, 125 and 401 (2004).

[9] Epelbaum, E., *Rep. Prog. Nucl. Phys.* 57, 654 (2006).

[10] Deltuva, A., A.C. Fonseca, P.U. Sauer, *Phys. Rev. Lett.* 95, 092301 (2005).

[11] Deltuva, A., A.C. Fonseca, P.U. Sauer, *Phys. Rev. C* 73, 057001 (2006).

[12] Deltuva, A., *Phys. Rev. C* 80, 064002 (2009).

[13] Kuroś-Żołnierczuk, J., *et al.*, *Phys. Rev. C* 66, 024004 (2002).

[14] Kistryn, St., *Three-Nucleon Force Effects in the Deuteron-Proton Breakup Reaction*, Habilitation Thesis, DjaF Krakow, ISBN 83-86774-42-8 (2005).

[15] Kistryn, St., *et al.*, *Phys. Rev. C* 68, 054004 (2003).

[16] Kistryn, St., *et al.*, *Phys. Rev. C* 72, 044006 (2005).

[17] Kistryn, St., *et al.*, *Phys. Lett. B* 641, 23 (2006).

[18] Stephan, E., *et al.*, *Eur. Phys. J. A* 24, 515 (2009).

[19] Mardanpour, H., *et al.*, *Nucl. Phys. A* 790, 426c (2007).

[20] Eslami-Kalantari, M., *et al.*, Mod. *Phys. Lett. A* 24, 839 (2009).

[21] Sekiguchi, K., *et al.*, *Phys. Rev. C* 79, 054008 (2009).

[22] Stephan, E., *et al.*, *Phys. Rev. C* 82, 014003 (2010).

Experimental study of the (n,alpha) reaction on a set of light nuclei

V.A. Khryachkov,[1] **I.P. Bondarenko,**[1] **B.D. Kuzminov,**[1] **N.N. Semenova,**[1] **A.I. Sergachev,**[1] **G. Giorginis**[2]
[1]IPPE Obninsk, Russia
[2]EC-JRC-IRMM Geel, Belgium

Abstract

An experimental setup based on an ionization chamber with Frisch grid and waveform digitizer was used for (n,α) cross-section measurements. Use of digital signal processing allowed us to select a gaseous cell inside the sensitive area of the ionisation chamber with high accuracy. This kind of approach provides a powerful method to suppress background from detector components and parasitic reactions on the working gas. The new method is especially interesting for the study of reactions on elements for which solid target preparation is difficult (e.g. noble gases). Additionally it has the advantage of an accurate determination of the number of nonradioactive nuclei in the selected gas cell. In the present experiments a set of working gases was used, which contained admixtures of nitrogen, oxygen, neon, argon and boron. Fission of ^{238}U was used as neutron flux monitor. The cross-section of the (n,α) reaction for ^{16}O, ^{14}N, ^{20}Ne, ^{36}Ar, ^{40}Ar and the branching ratio α_0/α_1 of the $^{10}B(n,\alpha_0)$ to $^{10}B(n,\alpha_1)$ reactions were measured for neutron energies between 1.5 and 7 MeV.

Experimental set up

A new spectrometer based on an ionization chamber with Frisch grid and digital signal processing [1] and a fast neutron beam profiling technique [2] were developed at IRMM in collaboration with IPPE. It allows to measure the cross-section of the (n,α) reaction on constituents of the working gas with high precision [3]. This type of set up was later also built at IPPE and in comparison with the IRMM spectrometer a set of improvements were achieved. Specifically the new setup allows to reliably suppress background of recoil protons in hydrogenous working gases, determine the directionality of α particle emission (in or opposite to the neutron beam direction), work with electronegative detector gases maintaining the possibility of good energy resolution, measure for a series of light gases the pulse height defect (PHD) which can be quite large. A new method for PHD compensation was also developed. Additionally the new setup allows the development of a novel method for the measurement of the angular distribution of the reaction products. All these improvements allowed us to extend the range of working gases and increase the number of elements which were successfully investigated at IPPE.

The block diagram of the new setup, shown in Figure 1, and the working principle of signal digitisation and storage are identical to those of the IRMM setup [1, 3]. They are presented here again taking into account that some hardware components are different in the two setups. The detector consists of two ionisation chambers. The main ionization chamber with Frisch grid (GIC) was used as detector for (n,α) reaction products. A parallel plate chamber which contains a thin solid ^{238}U layer was used as neutron flux monitor. The uranium sample was installed on the common cathode of the two chambers in a back-to-back geometry to the main chamber. In this way the neutron flux was measured very close to the position of the gas target simultaneously with the reaction under investigation.

Figure 1: Block diagram of the experimental setup.
PA – preamplifier, TFA – Timing filter amplifier, D – discriminator, SA – spectroscopy amplifier, DLA – Delay line amplifier, WFD – Waveform digitizer, PC – Personal computer.

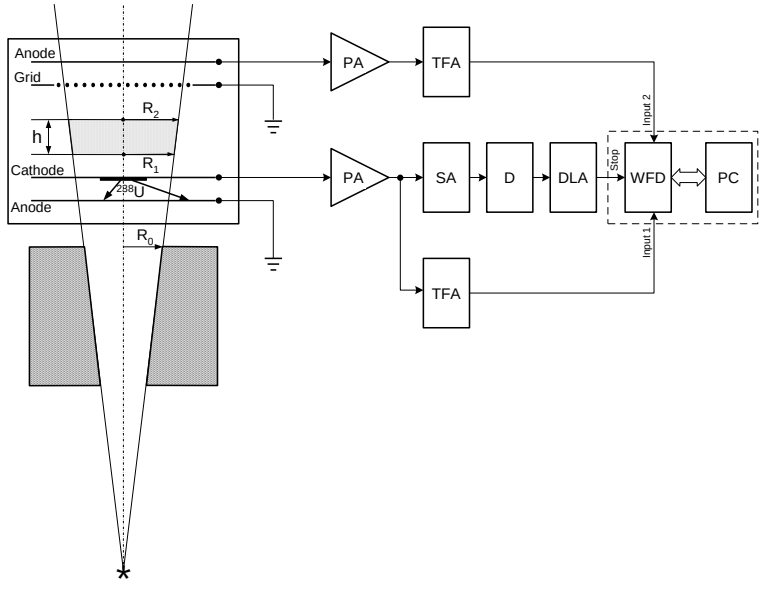

The diameter of the electrodes was 12 cm, the distances cathode-to-grid and grid-to-anode were 40 and 3 mm, respectively. The axis of the neutron beam coincided with the symmetry axis of the GIC. Different isotopes existing in the working gas of the ionisation chamber can contribute to the anode and cathode signals. The anode signal of the GIC and the common cathode signal at the exit of the corresponding charge sensitive preamplifiers were linearly amplified (without shaping) and fed to the inputs of a two channel waveform digitiser (WFD, LeCroy 2262, 10 bit). The digitisation rate was 80 MHz or equivalently a signal sample was taken ever. 12.5 ns. The required trigger for the WFD operation was obtained by splitting the cathode signal after the preamplifier. The WFD was operated in the so called pre-trigger mode. Digitization was started by the DAQ (data acquisition

programme) and the WFD memory was continuously filled till a trigger occurred. At this moment the memory contents were frozen and sent for storage to the PC hard disk. Typical digitised signals of an α particle and a fission fragment can be seen in Figure 2. They contain all needed information for the production of clean α particle and ^{238}U fission fragment signatures, which is a condition for accurate cross-section measurements.

Figure 2: Examples of signals of the main and monitor chambers

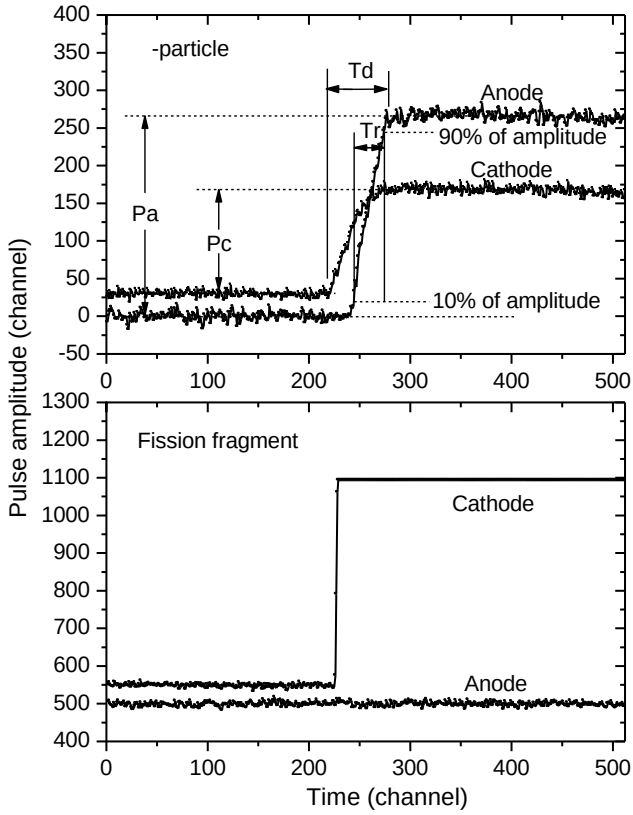

Digital signal processing of the recorded anode and cathode waveforms event-by-event provides information about amplitude, starting point, and end point for each signal. Joint analysis of this parameters allows to determine the following physical parameters for each event: total kinetic energy of the reaction products; full electron drift time (T_d) which can be transformed to a spatial coordinate in the interelectrode space where the reaction took place; anode signal rise time (T_r) which can be used to obtain the emission angle of the light charged particle in the lab coordinate system; particle type and emission directionality from the shape of the anode signal. The above information allows to localise the birth place of the detected particles and effectively suppress background from the surrounding detector components (electrodes and chamber wall). Additionally corrections can be made to the measured energy of the reaction products in order to compensate for electron loss on electronegative atoms and pulse height defect.

There are a number of advantages using gas targets in cross-section measurements instead of solid ones. The number of target atoms can be quite large. For 3% admixture of the concerned isotope in the working gas a 100 times larger number of atoms can be obtained in comparison with a conventional solid target situated on cathode d. There is freedom in the determination of an isolated target volume inside the detector's sensitive volume. This allows to achieve effective suppression of background from the surrounding detector components (electrodes and chamber wall) as mentioned above. Most of the light gases are not radioactive and the determination of the number of atoms is difficult. For a series of elements (*e.g.* the noble gases Ne, Ar and other) solid target preparation is not an easy task due to their physical and chemical properties. Use of gaseous targets solves

this problem. The number of atoms in a gaseous target can be determined using simple laws for ideal gases. In a gaseous target with suitable pressure both reaction products are stopped within the effective volume and the sum of their kinetic energy is measured. Under these conditions the problems of passive energy loss in the target material and the particle leaking effect [4] are eliminated. Furthermore the energy deposited in the working gas does not depend on the emission angle of the detected particles so that the response function is linear to a good approximation. The detector registers particles in the full 4π solid angle and cross-sections can be measured in one experiment without any event losses for emission close to 90°. For solid targets two measurements are needed, one for forward and one for backward particle emission with the additional requirement for corrections near 90°.

Fast neutrons were produced via the T(p.n) and D(d,n) reactions at the IPPE EG-1 accelerator. Solid deuterium and tritium targets with thicknesses from 1 mg/cm^2 to 2 mg/cm^2 were used.

The digitised fission fragment signals were used to generate a pulse height spectrum with a clean separation between neutron induced fission and natural α particle decay. The settings of the cathode amplifier were optimised for α particle detection in the GIC chamber. With these amplifier settings the fission fragment signals were saturated. This was not a problem because the purpose of the neutron monitor was to record only the number of fission events and not their real energy distribution. The total number of fission events was obtained by properly extrapolating the fission fragment spectrum to zero pulse height.

Results

a) Experimental investigation of the ^{16}O(n,α) cross-section

In this experiment 96.84%Kr+3.16%CO_2 gas mixture was used. The gas manufacturer (Linde) guaranteed the number of oxygen atoms with a precision of better than 3%. Oxygen was as target for the (n,α) reaction study. Specifically the cross-section of the ^{16}O(n,α_0) reaction channel in the neutron energy range 1.7 – 7 MeV was measured. The result is shown in Figure 3. The IPPE data set is in good agreement with the earlier measurement at IRMM [3] and the Harissopulos et al. data [5] below approximately 5.5 MeV.

In the present work the energy region 5.2-6.2 MeV was investigated in more detail than in the earlier work [3]. Particularly the new data show a neutron energy point to the left of which there is good agreement between our experiment and the ENDF B VII evaluation and to the right of it the existence of a large, 180% discrepancy.

Figure 3: Energy dependence of 16O(n,α0) cross-section

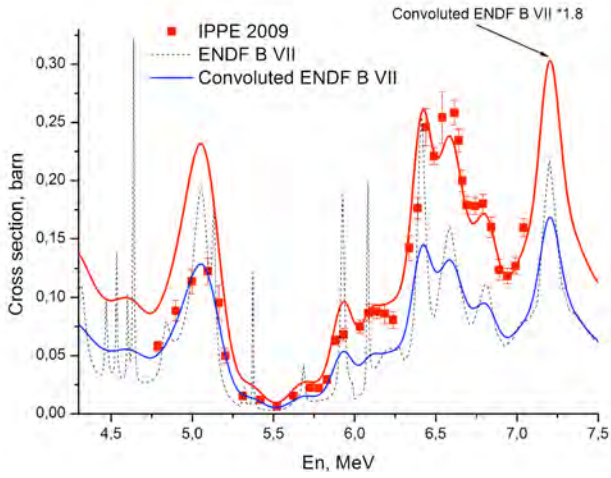

b) Experimental investigation of the $^{14}N(n,\alpha)$ cross-section

In this measurement a 97%Kr+3%N_2 gas mixture was used. The precision for the number of nitrogen atoms (3%) was taken from the specifications of the gas producer. Nitrogen present in the working gas was the target for the (n,α) reaction. It was also assumed that nitrogen as small detector gas admixture increases the electron drift velocity. Investigation of the $^{14}N(n,\alpha_0)$ $^{14}N(n,\alpha_1)$ and $^{14}N(n,\alpha_2)$ reaction channels in the neutron energy region 1.7 – 7 MeV was performed. The result is shown in Figure 4. Our results are in good agreement with the ENDF VII evaluation and the Gabbard et al. data [6] in the energy regions 1.7-3 MeV and 6-7 MeV , but there is a large discrepancy in the energy region 4-6 MeV which can reach a factor of 3 and more . A possible explanation of this discrepancy could be found by analysis of the energy spectra. In the energy region of the discrepancy the cross-section rises steeply from low values above 5 MeV to large values down to 4 MeV. Under these conditions a small number of background neutrons can produce a lot of α particles. If the detector energy resolution is not sufficiently high this background component can contribute to the real events produced by the main group of neutrons so that larger cross-sections than the real values can be obtained.

c) Experimental investigation of $^{20}Ne(n,\alpha)$ cross-section

In this measurement a 73.72%Kr+22.3%Ne+3.98%CO_2 gas mixture was used. The gas manufacturer (Linde) guaranteed the number of neon atoms with a precision better than 3%. Neon was the target for the (n,α) reaction. Carbonic acid was added to increase the electron drift velocity. Cross-section data for the $^{20}Ne(n,\alpha_0)$, $^{20}Ne(n,\alpha_1)$, $^{20}Ne(n,\alpha_2)$ and $^{20}Ne(n,\alpha_3)$ reaction channels in the neutron energy

Figure 4: Energy dependence of $^{14}N(n,\alpha_0)$ cross-section

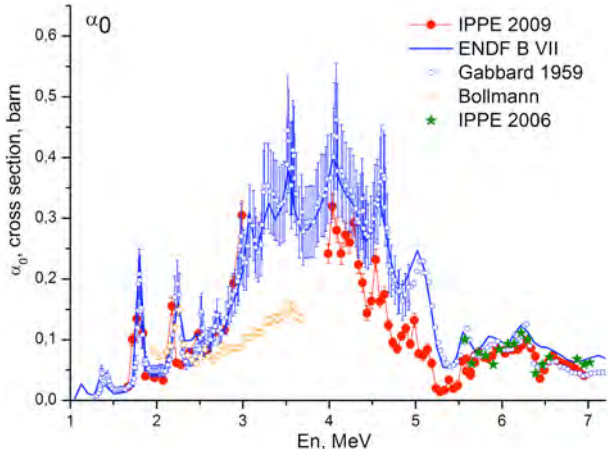

Figure 5: Energy dependence of $^{20}Ne(n, \alpha_0+\alpha_1)$ cross-section

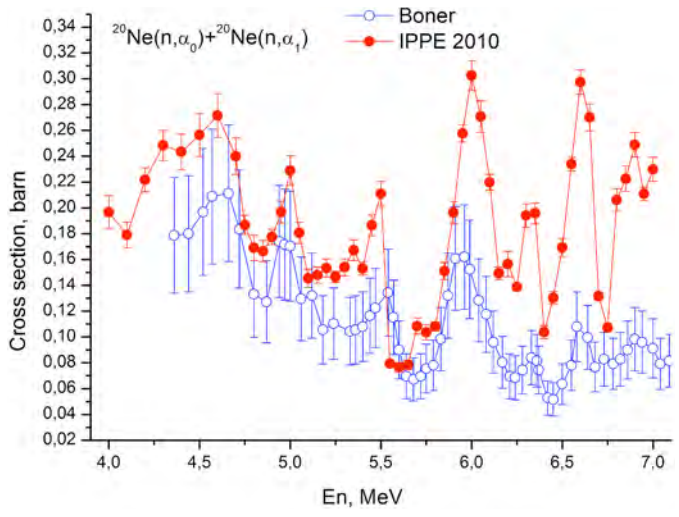

range 4–7 MeV were produced. Partial cross-sections for the $^{20}Ne(n,\alpha_0)$, $^{20}Ne(n,\alpha_1)$, $^{20}Ne(n,\alpha_2)$ and $^{20}Ne(n,\alpha_3)$ cannels were measured for the first time. A large pulse height defect was observed. The response function has "V type" shape. The right branch corresponds to α particles emitted in the neutron beam direction. The left branch corresponds to α particles emitted in opposite direction to the neutron beam. A similar effect was found in the work of Bell et al. [7]. They only measured the sum of the cross-sections of the (n,α_0) and (n,α_1) channels. To make a comparison we added the partial cross-sections for the (n,α_0) and (n,α_1) channels as shown in Figure 5 together with the data of Bell et al. [7]. There is a large discrepancy between the latter [7] and our data of up to a factor of 3.

d) Experimental investigation of $^{36}Ar(n,\alpha)$ u $^{40}Ar(n,\alpha)$ cross-section

In this measurement a P10 (90%Ar+10%CH_4) gas mixture was used. The gas manufacturer (Linde) guaranteed the number of argon atoms with a precision better than 3%. Argon in the working gas was assumed to be the target in which the investigated (n,α) reaction took place. In this experiment we could not use carbonic acid to increase the electron drift velocity because the Q-value of the

Figure 6: Energy dependence of $^{36}Ar(n,\alpha_0)$ cross-section

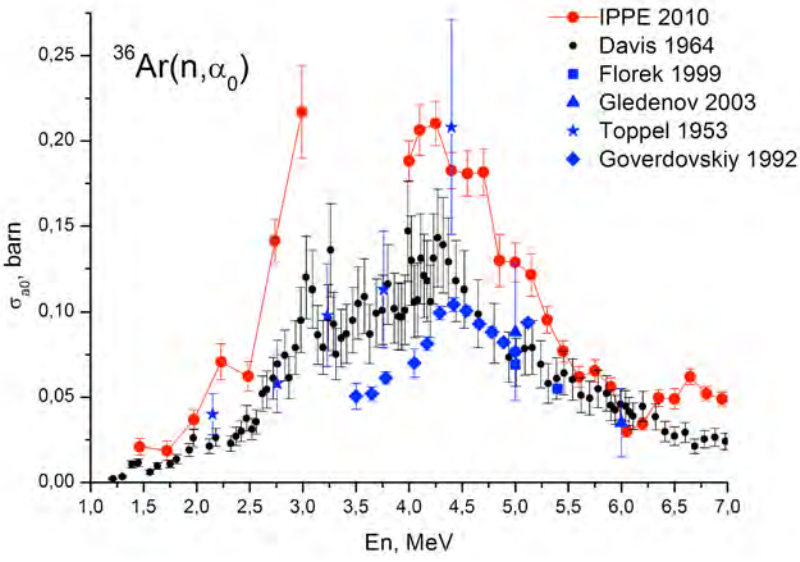

Figure 7: Energy dependence of $^{40}Ar(n,\alpha_0)$ cross-section

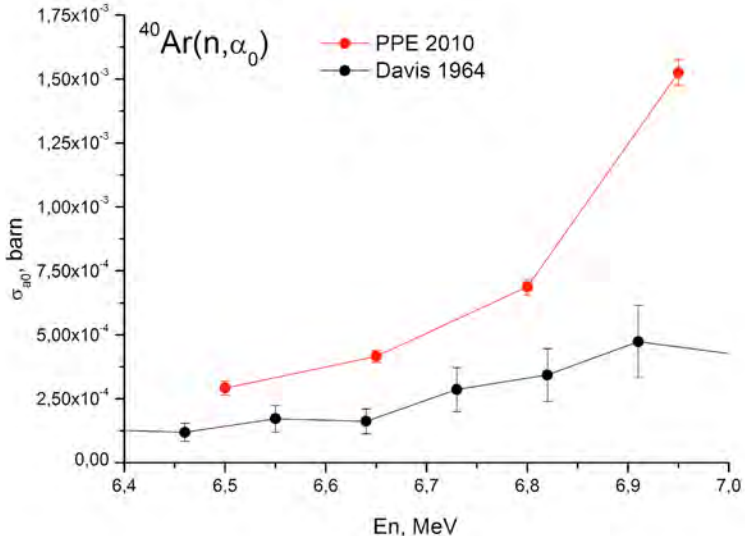

$^{16}O(n,\alpha_0)$ reaction is close to that of $^{40}Ar(n,\alpha_0)$. We used methane instead but in this case there were a lot of recoil protons inside the working gas. Using digital methods for pulse shape analysis allowed us to separate proton and α particle signals. Investigation of the $^{36}Ar(n,\alpha_0)$, $^{36}Ar(n,\alpha_1)$ and $^{40}Ar(n,\alpha_0)$ reactions in the neutron energy region 1.5–7 MeV was made. Some of the results are shown in Figures 6 and 7 for the full and high energy ranges, respectively.

In the full energy region we observed a large discrepancy (up to a factor of 2) between our cross-sections and the data of Davis et al. [8]. In contrast to other reactions which were investigated by the latter $^{36}Ar(n,\alpha_0)$ has a large positive Q-value. For this reaction the wall effect is much larger than it was for the other reactions studied by Davis et al. It seems that the theoretical calculation of the wall effect correction [8] was not precise enough.

f) Experimental investigation of branching ratio α_0/α_1 for the $^{10}B(n,\alpha)$ reaction

In this measurement a Kr+10%BF3 gas mixture was used. Boron trifluoride is a pungent, toxic and strong electronegative gas. One gram (1 ml) water at 0°C and 762 mm Hg absorbs 3.76 g BF_3 or equivalently 1 ml H_2O absorbs 1242 ml of gaseous BF_3. In order to make work with this gas possible the chamber and gas system were fully reconstructed using BF3 compatible materials. Furthermore a special algorithm was added in the evaluation software which makes corrections for electron capture in the working gas. All these improvements allowed us to work safely with boron trifluoride and to obtain a reasonable energy resolution. It is necessary to notice that measurements of the yield ratio using gaseous targets are practically free from systematic uncertainties.

This is because the yield ratio does not depend on the working gas pressure, number of boron atoms and its isotopic composition. There is also no need for the determination of an effective gaseous target inside of GIC sensitive volume as is the case in absolute cross-section measurements. The results of our measurement together with different evaluations and the Davis et al. data [9] are shown in Figure 8. Our data are in good agreement with data of the latter [9] but there is a significant discrepancy between the ENDF B VII and JENDL evaluations. The IPPE data clearly support the JENDL and disapprove the ENDF B VI evaluation in the energy range of our measurement.

Figure 8: Energy dependence of the branching ratio α_0/α_1 for the $^{10}B(n,\alpha)$ reaction

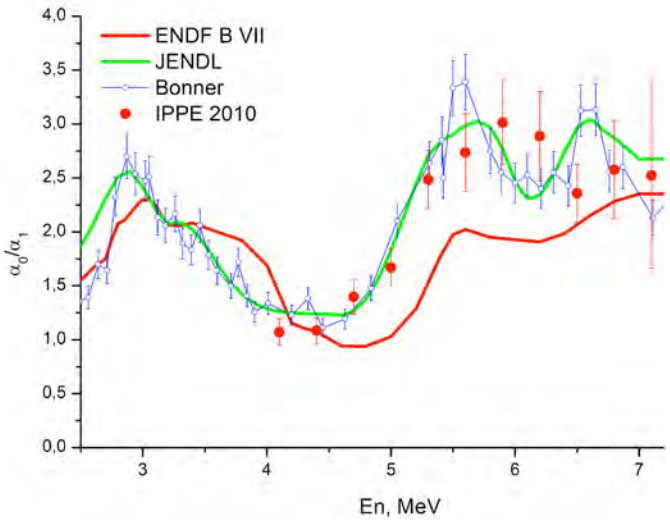

Future plans

Presently we continue the boron measurement with lower neutron energy. In the nearest future we plan to measure the $^{19}F(n,\alpha)$ and $^{12}C(n,\alpha)$ cross-sections. Furthermore we have developed and now are completing the manufacturing of a new low background spectrometer which allows the investigation of (n,α) reactions on solid targets for Li and elements of structural materials (*e.g.* Fe, Ni, Cr, V and others).

Conclusion

It was demonstrated that a new digital spectrometer with gaseous target allows to measure (n,α) cross-sections with high precision. Measurement results show that in spite of a long time history of investigation of light elements the uncertainty of the cross-section is currently of the order of few ten or hundred percent.

Common conclusion of this work is that existing evaluations for (n,α) cross-sections cannot describe the real situation. To solve this problem there is a real need for new experimental data and new evaluations.

References

[1] Giorginis, G., *et al.*, "A Time Projection Chamber (TPC) for cross-section measurements of (n, charged particle) reactions using gas targets", to be submitted to *Nucl. Instr. and Meth. A*.

[2] Giorginis, G., *et al.*, "Fast Neutron Beam Profiling (FNBP) using neutron activation", to be submitted to *Nucl. Instr. and Meth. A*.

[3] Giorginis, G., *et al.*, "The cross-section of the $^{16}O(n,\alpha)^{13}C$ reaction in the MeV energy range", *Proc. of Int. Conf. NDST 2007.* Nice, France (2007).

[4] Giorginis, G., V. Khryachkov, "The effect of particle leaking and its implications for measurements of the (n,α) reaction on light elements by using ionisation chambers", *Nucl. Instr. and Meth. A* 538 (2005).

[5] Harissopulos, S., *et al.*, "Cross-section of the $^{13}C(\alpha,n)^{16}O$ reaction: A background for the measurement of geo-neutrons", *Physical Review C* 72 (2005).

[6] Gabbard, F., H. Bichsel, T.W. Bonner, "The disintegration of nitrogen by fast neutrons", *Nucl. Physics* 14 (1959/60).

[7] Bell, R.J., T.W. Bonner, F. Gabbard, "The disintegration of ^{20}Ne by fast neutrons", *Nucl. Physics* 14 (1959/60).

[8] Davis, E.A., *et al.*, "The disintegration of ^{36}Ar and ^{40}Ar by neutrons", *Nucl. Physics* 55 (1964).

[9] Davis, E.A., *et al.*, "The disintegration of ^{10}B and ^{19}F by fast neutrons", *Nucl. Physics* 27 (1961).

Prompt fission neutron multiplicity investigation in spontaneous fission of ^{252}Cf

Sh. Zeynalov,[1] **O. Zeynalova,**[1] **F.-J. Hambsch,**[2] **S. Oberstedt**[2]
[1]JINR-Joint Institute for Nuclear Research, Dubna, Russia
[2]EC JRC Institute for Reference Materials and Measurements, Geel, Belgium

Abstract

The present work focuses on investigating the non-linear dependence of the average prompt fission neutron (PFN) multiplicity as a function of the total kinetic energy (TKE) of the fission fragments (FF) by using modern digital signal processing (DSP). A twin Frisch-grid ionization chamber (TGIC) was used for FF mass and kinetic energy spectroscopy. A fast NE213 equivalent liquid scintillation neutron detector (ND) was used for the PFN time-of-flight measurement. About 10^7 fission events coincident with PFN detection were acquired in the experiment. Correlated FF kinetic energies, the angle between the fission axis and the PFN and the PFN velocity were measured with an eight channel waveform digitizers (WFD) system, having 100 MHz sampling frequency and 12 bit pulse height resolution. Analysis of the acquired data revealed effects, causing distortion of the measured angular distribution of PFN and the dependence of their average number on TKE of the FF. Special modification of the experiment and respective modifications in the data analysis procedure has resulted in a reasonable agreement between experimental results and theoretical calculations. For the first time a linear dependence of the PFN multiplicity on TKE in the range of (140 – 220) MeV is demonstrated. A new measurement set-up in experiments with actinide targets like ^{235}U, ^{239}Pu, etc. is proposed.

Introduction

The purpose of the present experiment was to study the details of prompt fission neutron (PFN) emission in spontaneous fission of ^{252}Cf. The experimental method was adopted from Ref. [1] replacing the analogue electronics with modern digital pulse processing hardware/software. The measurement of correlated fission fragment (FF) kinetic energies by a double ionization chamber allowed the determination of FF masses, velocities and angles between FF and the PFN, coinciding with FF detection. In the current experiment the reconstruction of PFN emission kinematics was done carefully taking into account corrections due to various effects distorting the results of the measurement. The advantage provided by the digital pulse processing allowed to resolve some longstanding contradictions between theoretical calculations and experimental results.

Experimental setup

The anode current caused by a fission fragment (FF) in the TGIC was amplified by a charge-sensitive pre-amplifier and sampled with a 12 bit, 100 Ms/sec waveform digitizer (WFD). The step-like long anode signals were software-wise transformed into short current pulses, which allowed effective pulse pile-up elimination. The anode current pulses were used to determine the fission fragment angle with respect to the cathode-plane normal. Prompt fission neutron (PFN) time-of-flight (TOF) spectroscopy was performed after passing the neutron detector (ND) pulse, digitized with a 12 bit WFD and a rate of 100 Ms/sec, through a 12th order digital low pass filter. The ND pulse shape discrimination was implemented using raw-signal waveforms. The measurement of the FF characteristics, both in coincidence and non-coincidence with the PFN, was done without re-adjusting the apparatus. A Cf-sample with an activity of about 500 fission/sec, deposited on a 100 μg/cm^2 thick Ni foil was mounted on the common cathode of the twin Frisch-grid ionization chamber (TGIC), which operated with P-10 under atmospheric pressure as working gas at a constant flow between 50 and 100 ml/min. About 1.2×10^7 coincidences between FF and PFN signals were acquired in the measurement, which is comparable to the statistics reported in Ref. [1].

Experimental method and results

The detailed information on PFN emission in fission is available from the measured dependence of the average PFN multiplicity on the mass number A and the TKE of the fissile nucleus – $\bar{\nu}(A,TKE)$. Averaged characteristics on $\bar{\nu}(A)$ or $\bar{\nu}(TKE)$ by integrating over respective variable are obtained, if the FF mass yield matrix - $Y(A,TKE)$ is known, for example:

$$\bar{\nu}(A) = \frac{\int_0^{\infty} \bar{\nu}(A,TKE)Y(A,TKE)dTKE}{\int_0^{\infty} Y(A,TKE)dTKE}, \quad (1).$$

$$\bar{\nu} = \int_0^{\infty} \bar{\nu}(A,TKE)Y(A,TKE)dTKEdA, \;\; 200 = \int_0^{\infty} Y(A,TKE)dTKEdA$$

Similar relations can be written for averaging over A:

$$\bar{\nu}(TKE) = \frac{\int_0^{\infty} \bar{\nu}(A,TKE)Y(A,TKE)dA}{\int_0^{\infty} Y(A,TKE)dA}, \quad (2).$$

$$\bar{\nu} = \int_0^{\infty} \bar{\nu}(A,TKE)Y(A,TKE)dTKEdA, \;\; 200 = \int_0^{\infty} Y(A,TKE)dTKEdA$$

$\nu(A)$, $\nu(TKE)$ can be easily determined if the distributions of $\nu(A,TKE)$ and $Y(A,TKE)$ are known. To do so for each fission event the FF and PFN kinetic energies, FF masses along with the angle between PFN and FF motion should be determined. All this information can then be used to reconstruct the PFN emission kinematics both in the laboratory (LF) and in the centre of mass (CMF) frames. Possible explanations of the discrepancies in the results of experiments from refs. [2-6] might stem from

significant systematic errors in the kinematic parameters of the FF. In the measurement method of FF mass and kinematic parameters we carefully verified the data analysis procedure taking into account the new possibilities provided by the digital signal processing. The measurements were carried out using the experimental setup presented in Figure 1.

Figure 1: Experimental setup

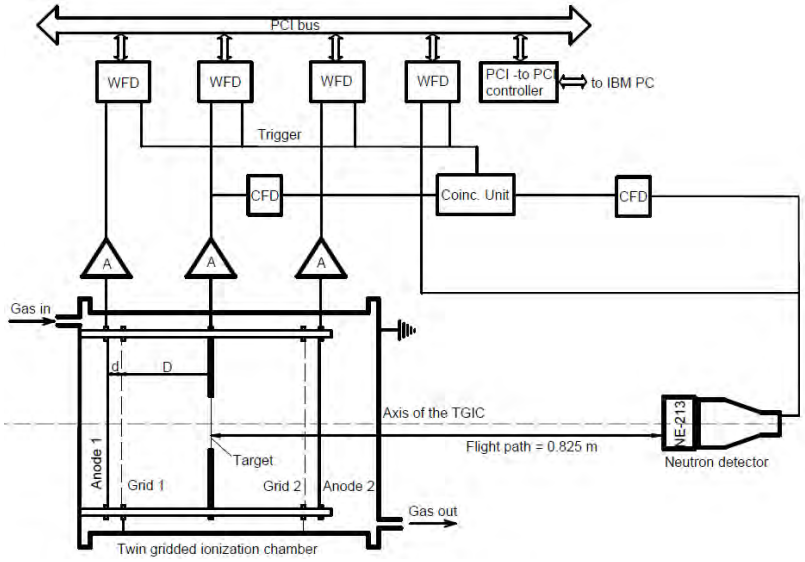

The two angular distributions of correlated FF, measured in the LF are presented in Figure 2a. The angle between the FF and the PFN was measured using half of the TGIC from the layer side in one of the measurements and from the target backing side in the other measurement. Comparison of the curves in Figure 2a (obtained after energy loss and grid inefficiency corrections were applied) demonstrates a significant difference, increasing for the angles close to 90°. Apparently, the observed anisotropy distortion in the LF is due to energy losses in the target backing. After transformation to the CMF during data analysis this effect might cause systematic errors, distorting the reaction kinematics.

Figure 2: a) FF angular distribution measured for the ^{252}Cf(sf) reaction within half of the TGIC from the layer side (solid line) and from the backing side (dashed line) in LF. b) ^{252}Cf(sf) reaction kinematics.

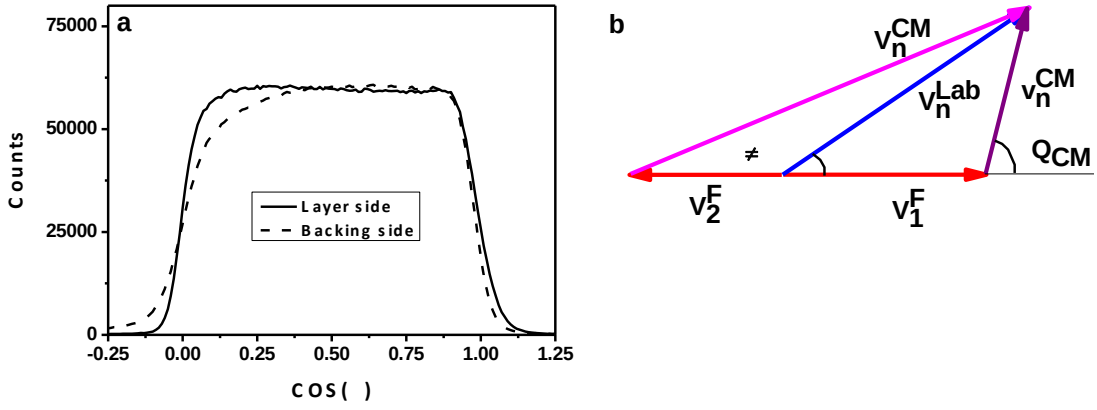

The background created by the second FF to the PFN emission of the first one was investigated in Ref. [1] and was modified in our approach. According to the reaction kinematics depicted in Figure 2b, the kinetic energy of the second FF in the CMF, must be much higher than the kinetic

energy of the first FF. Bearing in mind the exponential drop of the PFN energy spectrum in the CMF, the contribution to the PFN from both FFs could be evaluated using the probabilities defined as:

$$W_1 = \frac{1}{N}\exp(\frac{-E_1}{N}),\ W_2 = \frac{1}{N}\exp(\frac{-E_2}{N}),\ W_1 + W_2 = 1 \quad (3),$$

where W_1/W_2 - are probabilities of PFN emission and E_1/E_2 - are the kinetic energies of first and second FF respectively, the parameter N is a normalization factor. A comparison of the mass distributions plotted using measured data and probabilities, defined by eq. (3) are presented in Figure 3a. Results are in agreement with ref. [1], where the background from the complementary fragments was found to be small. The transformation of the measured angular distribution of the FF in the CMF, where the cos(Θ) was measured in the target layer half of the TGIC is plotted in Figure 3b, proving that more than 99% of the PFN are emitted from fully accelerated FFs. The transformation from LF to CMF was done using the following formula:

$$\Omega_{CM}(\nu_{CM},\Theta_{CM})d\nu_{CM}d\cos(\Theta_{CM}) = \frac{\nu_{CM}}{\nu_{lab}}\Omega_{lab}(\nu_{lab}(\nu_{CM},\Theta_{CM}),\ \Theta_{lab}(\nu_{CM},\Theta_{CM})) \quad (4)$$

Figure 3: a) Relative contribution to the PFN of investigated FF from the complementary FF as a function of the mass split. b) PFN angular distribution in the CMF after correction for background neutrons from the correlated FF along with a fit with Legendre polynomials

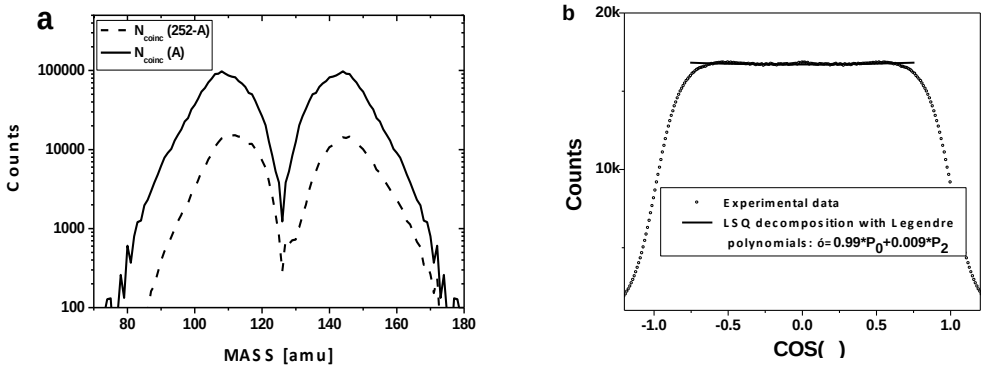

The average PFN multiplicity as a function of FF mass number, evaluated from the experiment based on the described method above is presented in Figure 4a in comparison with literature data [1, 7]. The saw-tooth like shape of the PFN distribution is explained in a model proposed by Brosa et al. [8] making two main assumptions: multi-modal fission and random neck rupture (MM-RNR).

Figure 4: a) Dependence of average PFN multiplicity on FF mass in comparison with literature [1, 7]. b) Dependence of average PFN multiplicity on TKE in comparison with literature and theoretical calculations [9].

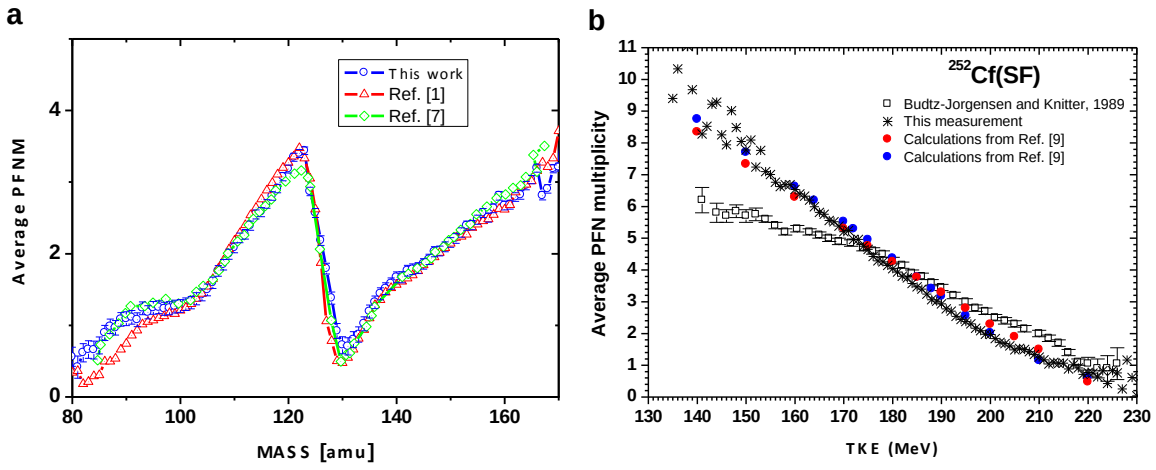

The model provides the link between the experimentally measured configuration, asymmetry and neck shape of the fissile nucleus. In addition, the distribution $\bar{\nu}(A,TKE)$ contains information on neck elasticity as well as on the partition of the excitation energy between both FFs. The dependence of the PFN multiplicity as a function of TKE is presented in Figure 4b in comparison with data from Ref. [1] and theoretical calculations from Ref. [9].

Outlook and conclusion

A modification of the TGIC made recently provides the possibility of the measurement of the FF axis orientation in 3D. The anodes of the TGIC are made position sensitive thanks to splitting them into two electrically isolated parts as shown in the left part of Figure 5 (backgammon method). The motion of the electrons in the grid-anode space induces an electric current shared by the two parts of the anode. The difference between instant currents is zero when the electrons are close to the line dividing the anode into two symmetric parts (ML-middle line). Deviation from this line to any direction perpendicular to the ML increases the current in the corresponding half of the electrode. This fact was, provides position sensitivity along a chosen direction. When anode of one half of TGIC is oriented along the X axis of the coordinate frame in the right side of Figure 5 and anode of the other side is oriented along the Y axis, the fission axis orientation in space can be measured. Let the Z axis in Figure 5 be stretched along the TGIC axis, then the ionization chamber part of the experimental setup was modified as shown in Figure 6 leaving ND part unchanged. The charge sensitive preamplifiers in each anode circuit were replaced by two wideband current preamplifiers. Considering drift of electrons created during FF deceleration inside the TGIC, the electric pulses at the preamplifier output can be used to evaluate the fission axis orientation in the coordinate frame of Figure 5 using the following approach. To measure the cosine of the angle Θ between the FF and the TGIC's axis the drift time method, utilizing the drift time dependence on Θ of electrons released by the FF, was implemented: $T[L] = \frac{\sum_{k=Tg}^{Tg+L} k*(I_1[k]+I_2[k])}{\sum_{k=Tg}^{Tg+L}(I_1[k]+I_2[k])} - Tg$, where Tg is the trigger signal leading edge position, $I_1[k]$ and $I_2[k]$ are the sampled current pulses from the respective half of the anode. The trigger signal was obtained from the common cathode pulse and referred to as the time instant of the fission event. The dependence of cos(Θ) on the drift time can be found using the following formulae:

$T_{90} = \frac{D+0.5*d}{W}$, $T_{90} - T(E) = (T_{90} - T_0(E))*\cos(\Theta)$, $P^C = \frac{P^O*T_{90}}{T_{90}+\sigma*T}$, where D and d are the cathode-grid and grid-anode distances, respectively, W is the free electron drift velocity, T_0, T_{90} are the drift times for FF having Θ equal to 0° and 90°, respectively, σ is the grid inefficiency, P^C, P^O are the grid inefficiency corrected and uncorrected total charges collected on the anodes and T is the drift time for the

Figure 5: The anode of the position sensitive TGIC (left). Illustration of fission axis orientation evaluation in the coordinate frame with the z-axis directed along the TGIC axis (right).

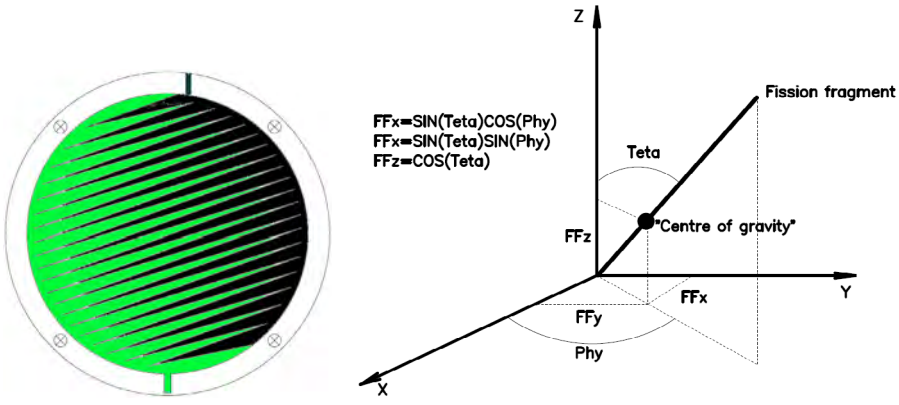

considered FF. The X_C coordinate of the FF "centre of gravity" was found using the following equation $X_C = \frac{\sum_{k=Tg}^{Tg+L} k*(I_1[k] + I_2[k])}{\sum_{k=Tg}^{Tg+L} (I_1[k] + I_2[k])}$. In a similar way the Y_C coordinate of the correlated FF, detected in the other half of the TGIC, was found. The angles between the fission axis and the coordinate axis were then found using the following equations:

$$X_C = R1*SIN(\Theta)*COS(\Phi)$$
$$Y_C = R2*SIN(\Theta)*COS(\Phi) \quad (5),$$

where R1, R2 are the average range of the FF, having known kinetic energies E1, E2, respectively. The ranges were supposed to be proportional to the maximum drift time known for each half of the chamber from a cos(Θ) calibration procedure similar to one used in ref. [1]. Finally the three cosines between the FF axis and the coordinate axis in Figure 5 were found:

$$COS(X) = SIN(\Theta)*COS(\Phi) = \frac{X_C}{R1},\ COS(Y) = SIN(\Theta)*COS(\Phi) = \frac{Y_C}{R2},\ COS(Z) = COS(\Theta) \quad (6)$$

Figure 6: Modified experimental setup of the time position sensitive TGIC

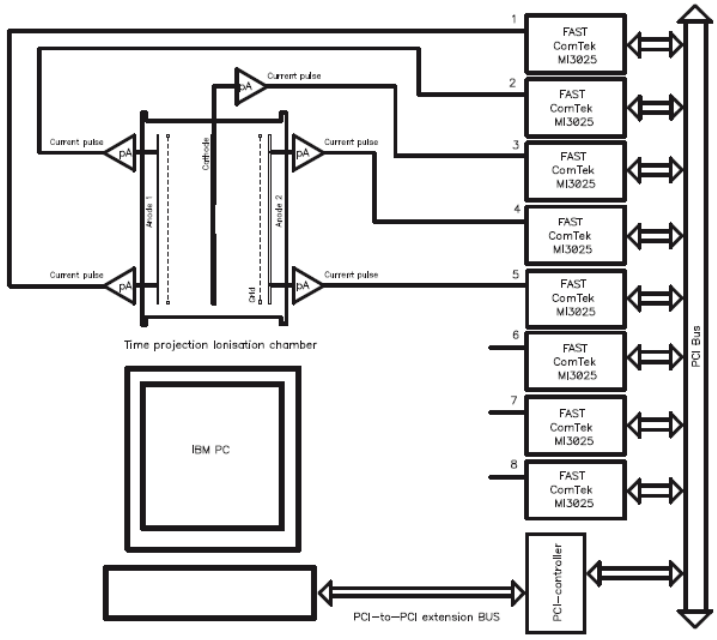

Figure 7: FF angular distributions measured for different fixed intervals in COS(Z)

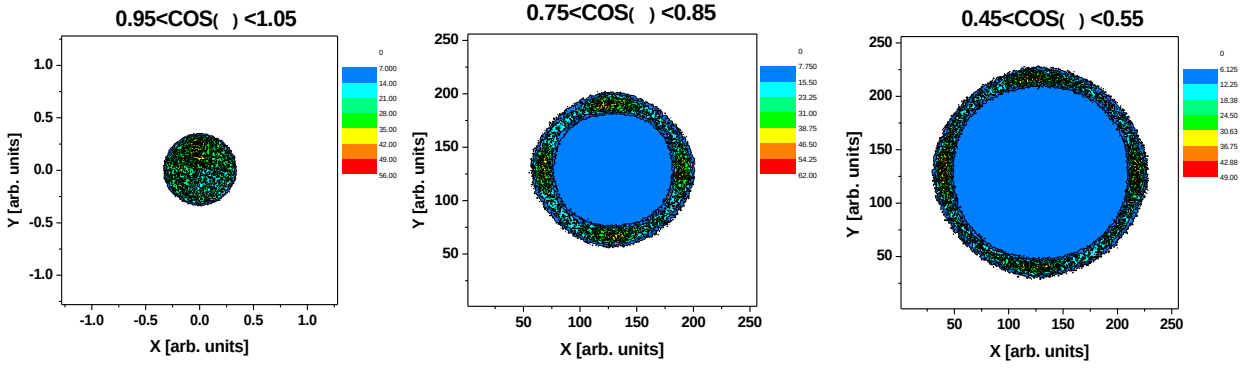

The modified experimental setup was used in a measurement of the spontaneous fission of ^{252}Cf to prove the above claimed properties of the TGIC. The angular distribution of FF measured for fixed intervals in COS(Θ) are plotted in Figure 7, demonstrating the angular sensitivity of the method. A preliminary evaluation of precision of the method gives about 0.1 as the averaged between the three cosine values. A more detailed evaluation is underway and should be done in the near future, but, nevertheless, the preliminary result is already quite promising. The position sensitive TGIC developed in this work opens a new perspective for future PFN investigation, especially for actinide targets like ^{235}U and ^{239}Pu.

Apparently targets from these nuclei cannot be made of negligible thickness, like for ^{252}Cf. Still the PFN investigation should be done in the full solid angle. Hence, positioning of an ND along the TGICs axis to simplify the measuring procedure does not work anymore. Here, our position-sensitive TGIC will allow to place additional ND off-axis, increasing considerably the experimental efficiency.

References

[1] Budtz-Jorgensen, C., H.-H. Knitter, *Nucl. Phys. A* 490, 307 (1988).

[2] Bowman, H.R., *et al.*, *Phys. Rev.* 129, 2133 (1963).

[3] Skarsvag, K., I. Singstad, *Nucl. Phys.* 62, 103 (1965).

[4] Vorobyev, A.S., *et al.*, *Nucl. Instr. Meth. A* 598, 795 (2009).

[5] Kapoor, S.S., R. Ramanna, P.N. Rama Rao, *Phys. Rev.* 131, 283 (1963).

[6] Samant, M.S., *et al.*, *Phys. Rev. C* 51, 3127 (1995).

[7] Nifenecker, H., *et al.*, *Symposium on Physics and Chemistry of Fission*, Rochester, N.Y., USA, Vol. 2, p. 117-178 (1974).

[8] Brosa, U., S. Grossmann, A. Mũller, *Phys. Report* 197, 167 (1990).

[9] Tudora, A., *Ann. Nucl. Energy* 35, 1 (2008).